HELMHOLTZ ZENTRUM MÜNCHEN
ABTEILUNG FÜR APOPTOSE IN HÄMATOPOIETISCHEN STAMMZELLEN
LEITUNG: PROF. DR. IRMELA JEREMIAS

Characterization of ADAM10 as a vulnerability and novel potential therapy target of acute leukemia

Dissertation zur Erlangung des Doktorgrades der Fakultät für Biologie
der Ludwig-Maximilians-Universität München

vorgelegt von
Jan Philipp Schmid
aus Stuttgart

München, Juli 2024

Prüfungskommission

Diese Dissertation wurde angefertigt
unter der Leitung von Prof. Dr. Heinrich Leonhardt
im Bereich für Human Biology & BioImaging
an der Ludwig-Maximilians-Universität München

Erstgutachter/in:	Prof. Dr. Heinrich Leonhardt
Zweitgutachter/in:	Prof. Dr. Irmela Jeremias
Tag der Abgabe:	18.03.2024
Tag der mündlichen Prüfung:	08.07.2024

Eidesstattliche Erklärung

Ich versichere hiermit an Eides statt, dass die vorgelegte Dissertation mit dem Titel

“Characterization of ADAM10 as a vulnerability and novel potential therapy target of acute leukemia”

von mir selbständig und ohne unerlaubte Hilfe angefertigt ist.

Hiermit erkläre ich, dass die Dissertation nicht ganz oder in wesentlichen Teilen einer anderen Prüfungskommission vorgelegt worden ist.

Außerdem erkläre ich, dass ich mich anderweitig einer Doktorprüfung ohne Erfolg nicht unterzogen habe.

München, den 18.03.2024

_____

Jan Philipp Schmid

Table of Contents

Abstract

The interaction of leukemic cells with their surrounding bone marrow (BM) microenvironment is crucial for leukemia formation and maintenance. Especially dormant leukemia stem cells (LSCs) reside in this protective niche, allowing them to evade chemotherapy. As LSCs are main drivers of relapse development in leukemia patients, it is of high clinical relevance to efficiently eradicate them. We aimed at identifying surface molecules which can be targeted to disrupt the interaction between leukemic cells and the BM microenvironment, thereby releasing leukemia cells from their niche and re-sensitizing them towards chemotherapeutic agents.

We employed our recently established pipeline for functional *in vivo* CRISPR/Cas9 knockout (KO) screens to test a customized surface molecule library comprising candidates from the lab's own previous proteome and secretome analysis of LSC-resembling cells, complemented with candidates from the literature. While performing screens in two B-ALL patient-derived xenograft (PDX) models, we discovered both commonly depleted genes, including the positive controls *CXCR4* and *ITGB1,* but also PDX model specific dropouts. We selected *ADAM10* as our candidate gene because it was depleted in both tested PDX models and showed increased expression in primary leukemia cells from patients of diverse subgroups of acute leukemias, which correlated with poorer overall survival in these patients.

We confirmed ADAM10 as a broad vulnerability in numerous ALL and AML PDX models *in vivo*, independently from underlying driver mutations and genetic alterations. In contrast, *in vitro* most PDX models were insensitive to loss of ADAM10. We could confirm the specificity of the observed phenotype of the KO through *in vivo* reconstitution assays, which further elucidated ADAM10's catalytically active metalloproteinase domain to be mainly responsible for its role in leukemic cells. Multi-omics analysis revealed that ADAM10 KO affected diverse biological processes, such as cell cycle, cell death, metabolism including OXPHOS as well as membrane and adhesion associated processes. Proof-of-concept experiments functionally confirmed the effect on the first two pathways. Additional functional characterization of PDX cells subjected to chemical inhibition or genetic KO of ADAM10 found the early engraftment and homing capacity, the frequency of leukemia-initiating cells and the CFU potential to be diminished upon ADAM10 reduction or loss, respectively. Moreover, performing *in vivo* and *in vitro* chemotherapy trials in ALL and AML PDX models, using a mixture of PDX cells with and without ADAM10 KO competitively growing within the same mouse, we showed that loss of ADAM10 sensitized the cells towards routinely used chemotherapeutic agents.

In summary, we propose ADAM10 as a potential novel target for the treatment of leukemia patients in the future.

Zusammenfassung

Die Interaktion leukämischer Zellen mit ihrer Mikroumgebung im Knochenmark ist essenziell für die Entstehung und das Fortbestehen von Leukämie. Vor allem ruhende Leukämiestammzellen (LSCs) halten sich in dieser schützenden Nische auf und können so der Chemotherapie entgehen. Da LSCs hauptursächlich für die Entstehung von Rückfällen bei Leukämiepatienten sind, ist es von großer klinischer Bedeutung, diese effizient zu beseitigen. Unser Ziel war die Identifizierung von Oberflächenmolekülen mit dem Potenzial, die Interaktion zwischen leukämischen Zellen und der Mikroumgebung im Knochenmark zu stören, sie dadurch aus ihrer Nische zu lösen und sie gegenüber Chemotherapeutika zu re-sensibilisieren.

Hierfür setzten wir unseren kürzlich etablierten Arbeitsablauf für funktionelle *in vivo* CRISPR/Cas9-KO-Screens ein und verwendeten eine maßgeschneiderte Oberflächenmolekül-Bibliothek, die Kandidaten aus vorangegangenen Proteom- und Sekretomanalysen unseres Labors von LSC-ähnlichen Zellen sowie ergänzend Kandidaten aus der Literatur umfasste. Während der Durchführung von Screens in zwei Xenotransplantationsmodellen (PDX), die von Patienten mit B-Zell akuter lymphatischer Leukämie stammten, entdeckten wir allgemeine Dropouts, darunter die Positivkontrollen CXCR4 und ITGB1, aber auch PDX-Modell spezifische Dropouts. Wir untersuchten ADAM10 im Detail, da es in beiden getesteten PDX-Modellen reduziert war. Darüber hinaus war ADAM10s mRNA-Spiegel in primären Leukämiezellen von Patienten verschiedener Untergruppen akuter Leukämien erhöht, was mit einer geringeren Überlebenswahrscheinlichkeit dieser Patienten korrelierte.

Wir konnten bestätigen, dass ADAM10 in zahlreichen ALL- und AML-PDX-Modellen unabhängig von zugrundeliegenden Treibermutationen und genetischen Veränderungen *in vivo* eine genetische Schwachstelle darstellt, im Gegensatz zu einer Unempfindlichkeit der meisten ALL-PDX-Modelle *in vitro*. Die Spezifität des beobachteten Phänotyps des KOs bestätigten wir durch *in vivo* Rekonstitutionsversuche, die darüber hinaus aufdeckten, dass die katalytisch aktive Metalloproteinase-Domäne von ADAM10 hauptverantwortlich für dessen Rolle in den leukämischen Zellen ist. Multi-omics-Analysen ergaben, dass durch den ADAM10 KO verschiedene biologische Prozesse wie Zellzyklus, Zelltod, Stoffwechsel inklusive OXPHOS sowie membran- und adhäsionsassoziierte Prozesse betroffen sind, wobei die ersten beiden durch weitere Experimente funktionell bestätigt werden konnten. Zusätzliche funktionelle Charakterisierungen nach chemischer Inhibition oder genetischem ADAM10 KO in PDX-Zellen ergab, dass die Fähigkeit zum erfolgreichen Anwachsen und Finden der Nische, die Häufigkeit von Leukämie-initiierenden Zellen sowie das CFU-Potenzial nach einer

ADAM10-Reduktion bzw. einem ADAM10-Verlust vermindert sind. Darüber hinaus konnten wir in *in vivo*- und *in vitro*-Studien in Kombination mit der Gabe von Chemotherapeutika in ALL- und AML-PDX-Modellen, in welchen wir eine Mischung aus PDX-Zellen mit und ohne ADAM10 KO verwendeten und diese kompetitiv in derselben Maus wachsen ließen, feststellen, dass der Verlust von ADAM10 die Zellen gegenüber routinemäßig eingesetzten Chemotherapeutika sensibilisiert.

Zusammenfassend schlagen wir ADAM10 als mögliches neues Therapieziel für die zukünftige Behandlung von Leukämiepatienten vor.

List of Abbreviations

∆MP	Metalloproteinase lacking ADAM10 variant
ABL1	ABL proto-oncogene 1, non-receptor tyrosine kinase
ACT	Catalytically active ADAM10 variant
AD	Alzheimer's disease
ADAM10	A Disintegrin and metalloproteinase domain-containing protein 10
ADAM17	A Disintegrin and metalloproteinase domain-containing protein 17
ADC	Antibody drug conjugate
Ader	Aderbasib
AL	Acute leukemias
ALL	Acute lymphoblastic leukemia
AML	Acute myeloid leukemia
APP	Amyloid-beta precursor protein
AraC	Cytarabine
ASXL1	Additional sex combs like transcriptional regulator 1
B-ALL	B-cell acute lymphoblastic leukemia
BCL2	B-Cell lymphoma 2 protein
BCL6	B-Cell lymphoma 6 protein
BCOR	BCL6 corepressor
BCP	B-cell precursor
BCR	Breakpoint cluster region
BFP	Blue fluorescent protein
BIFC	Bimolecular fluorescence complementation
BLIMP1	B lymphocyte-induced maturation protein-1
BM	Bone marrow
C8 family	Tetraspanin family with eight conserved cysteines in the large extracellular loop
cAMP	Cyclic adenosine monophosphate
CAR-T	Chimeric antigen receptor T cells
Cas9	CRISPR associated protein 9
CBFB	Core-Binding Factor Subunit Beta
CD	Cluster of Differentiation
CD19	B-lymphocyte antigen CD19
CD79A	B-cell antigen receptor complex-associated protein alpha chain
CD81	Tetraspanin-28, alias: TSPAN28

CFU	Colony forming unit
CI	Confidence interval
CN	Cytogenetically normal
CP domain	Cytoplasmic domain
CR	Complete remission
CR domain	Cysteine-rich domain
CREB	cAMP response element-binding protein
CREBBP	CREB binding protein
CRISPR	Clustered Regularly Interspaced Short Palindromic Repeats
crRNA	CRISPR ribonucleic acid
CT	Cycle Threshold
CTRL	Control
CX_3CL1	C-X3-C motif chemokine ligand 1
CXCL16	C-X-C motif chemokine ligand 16
CXCR4	C-X-C motif chemokine receptor type 4
Cyclo	Cyclophosphamide
DAPI	4′,6-Diamidin-2-phenylindol
Dauno	Daunorubicine
DEK	DEK Proto-Oncogene
DI domain	Disintegrin domain
diaPASEF	Data-independent acquisition method using a parallel accumulation–serial fragmentation
DLG1	Discs large MAGUK scaffold Protein 1
DLL1	Delta-like ligand 1
DMSO	Dimethyl sulfoxide
DNA	Deoxyribonucleic acid
dNTP	Deoxynucleotide triphosphates
Doxo	Doxorubicine
DSB	Double-strand break
DUX4	Double Homeobox 4
EF1α	human elongation factor-1 alpha promoter
eFFly	Enhanced firefly luciferase
ELDA	Extreme Limiting Dilution Analysis
ER	Endoplasmic reticulum
ERG	ETS Transcription Factor ERG
ERK	Extracellular-signal regulated kinases
ETV6	ETS Variant Transcription Factor 6

EVE-1	SH3 domain containing 19, alias: SH3D19
EZH2	Enhancer of zeste 2 polycomb repressive complex 2 subunit
F11R	Junctional adhesion molecule A
FACS	Fluorescence Activated Cell Sorting
FDA	Food and drug administration
FDR	False discovery rate
FLT3	Fms-like tyrosine kinase 3
FLT3-ITD	Fms-like tyrosine kinase 3 (Internal tandem duplications)
FSC	Forward scatter
FYN	FYN proto-oncogene, Src family tyrosine kinase
G1	Gap phase 1
G2/M	Gap phase 2 / mitosis
GAPDH	Glyceraldehyde 3-phosphate dehydrogenase
GC	Germinal center
gDNA	genomic DNA
GEPDX	Genetically engineered patient-derived xenograft
GFP	Green fluorescent protein
GGH	Gamma-glutamyl hydrolase
GLuc	Gaussia luciferase
GO	Gene ontology
GOI	Gene of interest
GRB2	Growth factor receptor bound protein 2
GSEA	Gene Set Enrichment analysis
H-2K^k	H-2K^k antigen is expressed on mouse MHC class I–positive cells
H1	Human type 3 RNA Pol III promoter H1
H2AFX	H2A histone family member X
H2AFY	H2A histone family member Y
HDR	Homology directed repair
HER2	Human Epidermal Growth Factor Receptor 2, Erb-B2 Receptor Tyrosine Kinase 2
HIST1H4A	Histone 4
HSCT	Hematopoietic stem cell transplantation
HSP90α	Heat shock protein 90 α (family class A member 1)
i.p.	intraperitoneal
i.v.	intravenous
ICE	Inference of CRISPR edits
IDH	Isocitrate Dehydrogenase 1

InDel	Insertion and deletion
IQR	Inter-quartile distance
IRF4	Interferon regulatory factor 4
iRFP	Near-infrared fluorescent protein
ITGA4	Integrin alpha 4
ITGA7	Integrin alpha 7
ITGB1	Integrin beta 1
ITGB2	Integrin beta 2
ITK	Interleukin-2-inducible T cell kinase
IVC	Individually ventilated cages
KAT6A	Lysine Acetyltransferase 6A
KEGG	Kyoto Encyclopedia of Genes and Genomes
KMT2A	Lysine Methyltransferase 2A, alias: MLL
KO	Knockout
LDTA	Limiting dilution transplantation assay
L-Zip	Leucine zipper motif
L1-CAM	L1 Cell Adhesion Molecule
LAT1	Large neutral amino acid transporter 1
LCK	Lymphocyte cell-specific protein-tyrosine kinase
LIC	Leukemia-initiating cells
LRC	Label-retaining cells
LSC	Leukemia stem cells
MACS	Magnetic-activated cell sorting
MAD2	Mitotic arrest deficient 2
MAGeCK	Model-based Analysis of Genome-wide CRISPR/Cas9 Knockout
MAML1	Mastermind like transcriptional coactivator 1
MAP kinase	Mitogen-activated protein kinase
MECOM(EVI1)	MDS1 and EVI1 complex locus
membr.	Membrane
MEF2D	Myocyte enhancer factor 2D
Min	minute
MLL	Mixed lineage leukemia, alias: KMT2A
MLLT3	Mixed-lineage leukemia translocated to chromosome 3 Protein
MOI	Multiplicity of infection
mRNA	Messenger ribonucleic acid
MS	Mass spectrometry
mTagBFP	Monomeric blue fluorescent protein

MYH11	Myosin heavy chain 11
NCK	Non-catalytic region of tyrosine kinase adaptor protein 1
NCSTN	Nicastrin
nd	Not determined
NF- κB	Nuclear factor kappa-light-chain-enhancer of activated B cells
NGS	Next generation sequencing
NHEJ	Non-homologous end joining
NICD	Notch intracellular domain
NK cell	Natural killer cell
NKG2D	Killer cell lectin like receptor K1, alias: KLRK1
NOD	Non-obese diabetic
NOTCH1	Neurogenic locus notch homolog protein 1
ns	Not significant
NSG	NOD.Cg-Prkdc^{scid}Il2rg^{tm1Wjl}/SzJ
NUP214	Nucleoporin 214
OXPHOS	Oxidative phosphorylation
OS	Overall survival
P2A	Porcine teschovirus-1 2A peptide
p300	E1A binding protein P300
PACSIN3	Protein kinase C and casein kinase substrate in neurons 3
PAM	Protospacer adjacent motif
pB	Peripheral blood
PBS	Phosphate Buffered Saline
PBX1	Pre-B-Cell Leukemia Homeobox 1
PC7	Pro-domain convertase protein 7
PCR	Polymerase chain reaction
PDX	Patient-derived xenograft
Ph-pos	Philadelphia chromosome positive
Ph-like	Philadelphia chromosome positive like
POTEI	POTE ankyrin domain family member I
PRO	Pro-domain
Protease site 1	S1
Protease site 2	S2
Protease site 3	S3
qRT-PCR	Quantitative real-time polymerase chain reaction
RBP*jκ*	Recombination signal binding protein for immunoglobulin kappa J region

RNA	Ribonucleic acid
RNP	Ribonucleoprotein
RRA	Robust ranking algorithm
RT	Room temperature
RUNX	Runt-related transcription factor
RUNX1	RUNX Family Transcription Factor 1
RUNX1T1	RUNX1 Partner Transcriptional Co-Repressor 1
S	Synthesis phase
SCID	Severe combined immunodeficiency
SF3B1	Splicing factor 3b subunit 1
SFFV	Spleen focus-forming virus
sgRNA	Short guide RNA
SIRPα	Signal regulatory protein alpha
SLC	Solute carrier
SLC19A1	Folate transporter 1
SLC3A2	4F2 cell-surface antigen heavy chain
SOT	Start of therapy
SP	Signal peptide
SPF	Specified pathogen-free
SRSF2	Serine and arginine rich splicing factor 2
SSC	Side scatter
STAG2	Stromal antigen 2 cohesin complex component
STAT1	Signal transducer and activator of transcription 1
Syntaxin 4	Membrane integrated Q-SNARE proteins participating in exocytosis family member 4
T-ALL	T-lymphoblastic leukemia
T2A	Thosea asigna virus 2A peptide
TCF3	Transcription Factor 3
TCGA	The Cancer Genome Atlas
Thr719	Threonine residue 719
Thr725	Threonine residue 725
TFRC	Transferrin receptor protein 1
TIMS	Thermal ionization mass spectrometry
TM	Transmembrane domain
TP53	Tumor protein P53
TRPM7	Transient receptor potential cation channel subfamily m member 7
TSPAN5	Tetraspanin 5

TSPAN10	Tetraspanin 10
TSPAN14	Tetraspanin 14
TSPAN15	Tetraspanin 15
TSPAN17	Tetraspanin 17
TSPAN33	Tetraspanin 33
U2AF1	U2 small nuclear RNA auxiliary factor 1
VE-cadherin	Vascular endothelial cadherin
VCR	vincristine
WT	Wild-type
XBP1	X-box binding protein 1
β-Actin	Beta-actin

List of Figures

List of Tables

1 Introduction

1.1. Acute leukemias

Leukemias are hematologic malignancies occurring in children and adults initiated by malignant transformation of cells of the hematopoietic system (**Figure 1**). In general, leukemias can be divided into acute and chronic depending on the growth kinetics and into lymphoblastic or myeloid based on the lineage of origin. In acute leukemias (AL), myeloid or lymphoid progenitor cells are blocked in their differentiation, followed by excessive proliferation, leading to the accumulation of leukemic blasts in the bone marrow (BM), the peripheral blood as well as in extramedullary sites. This eventually results in the disruption of healthy hematopoiesis and BM failure (De Kouchkovsky & Abdul-Hay, 2016; Terwilliger & Abdul-Hay, 2017). Typical symptoms of acute leukemias are rather unspecific, including pale skin, weight loss, fever, fatigue, shortness of breath, more frequent infections and bruises and bleeding (De Kouchkovsky & Abdul-Hay, 2016; Khwaja et al., 2016; Terwilliger & Abdul-Hay, 2017). Diagnosis of ALL and AML relies on the detection of more than 20% leukemic blasts of the respective lineage in the BM (Arber et al., 2016; Brown et al., 2020).

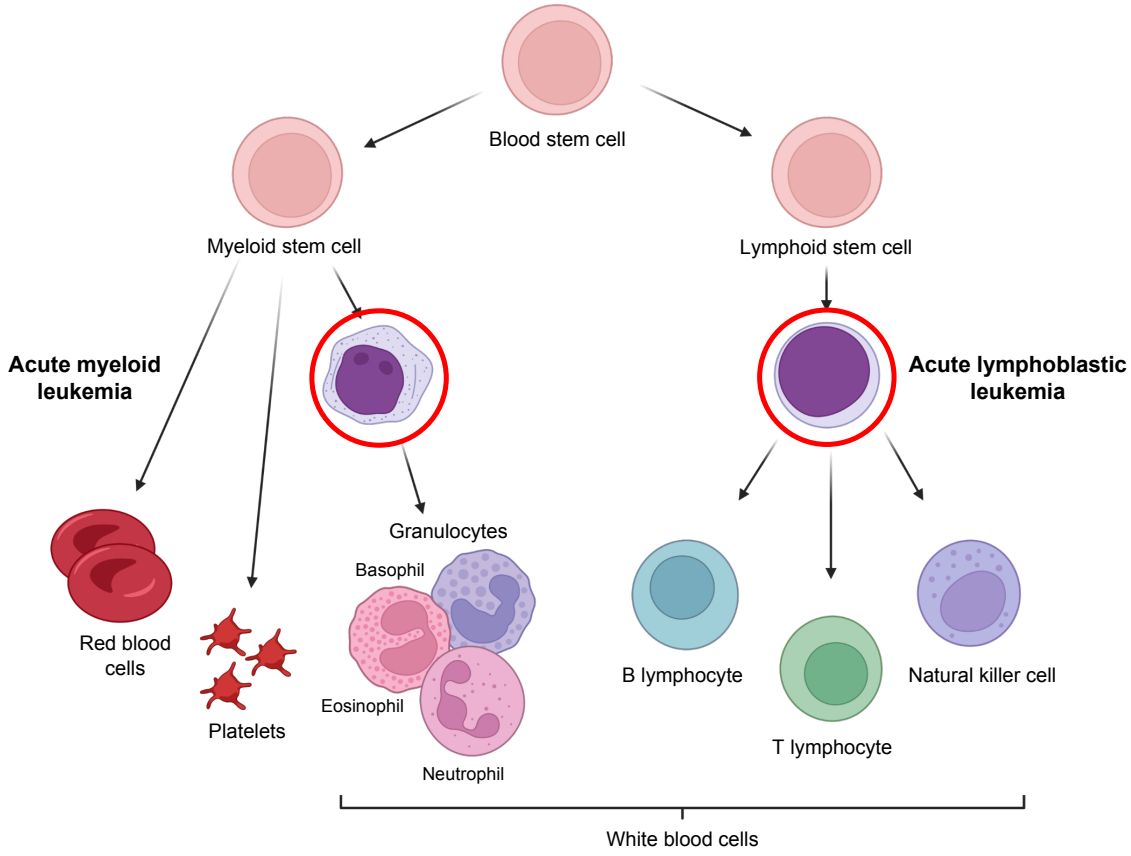

Figure 1: Scheme of the origin of acute leukemias. Following a malignant transformation of myeloid or lymphoblastic progenitor cells, healthy blood cell differentiation is blocked, leading to proliferation and subsequent accumulation of leukemic blast cells.

1.1.1 Acute lymphoblastic leukemia:

Acute lymphoblastic leukemia (ALL) is a disease found in both children and adults. The incidence is the highest in small children below the age of five, drops throughout childhood, reaching the lowest incidence between 25 and 45, before rising slowly in individuals above the age of 50 (Malard & Mohty, 2020). The American Cancer Society's estimate for 2023 are 6.540 new ALL cases and 1.390 deaths in the US, which are responsible for roughly 0.3% of all predicted cancer cases and 0.2% of all cancer-related deaths, respectively. Of note, it is the single most common type of cancer in children below 15 years of age (Siegel et al., 2023). Treatment of ALL patients has drastically improved in the last decades reaching a five-year overall survival of 90% in children (Pulte et al., 2009). Nevertheless, while 60% of patients are younger than 20 years, four out of five deaths occur in adults. From the patients above 50 only one fourth survives for more than five years post diagnosis, underlining the need for further therapy improvements (Malard & Mohty, 2020; Pulte et al., 2014).

1.1.1.1 Classification, risk stratification and treatment

ALL is classified by cytogenetic analysis identifying existent chromosomal aberrations and immunophenotyping using surface markers. It can be generally divided into B-lymphoblastic leukemia (B-ALL) with and without recurrent genetic abnormalities and T-lymphoblastic leukemia (T-ALL) with three out of four cases being B-ALL (Terwilliger & Abdul-Hay, 2017). Recurrent genetic abnormalities are aneuploidy and chromosomal rearrangements. High hyperdiploidy is most frequent in pediatric B-ALL. These can lead to the activation of oncogenes or induce the formation and expression of fusion transcripts. Based on these genetic alterations, patients are stratified into different risk groups and treated accordingly. While Philadelphia chromosome-positive (Ph-pos), Ph-like, *MLL* or *MEF2D* rearrangements and hypodiploid B-ALLs are associated with poor outcomes, patients with the TCF3-PBX1 or EVT6-RUNX1 fusion, deregulated *ERG* and *DUX4* as well as hyperdiploid B-ALLs have favorable prognoses (Malard & Mohty, 2020; Roberts & Mullighan, 2015). Current treatment for ALL consists of four phases over a period of two to three years. During the initial induction phase a combination of glucocorticoids such as prednisolone, prednisone or dexamethasone, anthracyclines such as dauno- and doxorubicin, anti-mitotic agents such as the vinca alkaloid vincristine (VCR), enzymes such as L-asparaginase, purine analogues such as 6-mercaptopurine, antifolates such as methotrexate or alkylating agents such as cyclophosphamide (Cyclo) are used in order to eradicate ALL cells as rapidly and efficiently as possible (Bukowski et al., 2020; Malard & Mohty, 2020). During the consolidation phase the pyrimidine antagonists cytarabine (AraC) together with VCR, methotrexate, asparaginase, glucocorticoids and mercaptopurines are utilized to eliminate remaining leukemia cells, followed by the intensification phase, in which a similar regimen as during the induction phase is used. Maintenance is the last phase of routine treatment, during which methotrexate and mercaptopurine is either given alone or in combination with glucocorticoids and AraC to prevent disease relapse (Brown et al., 2020; Bukowski et al., 2020; Malard & Mohty, 2020).

1.1.2 Acute myeloid leukemia:

Unlike ALL, AML is predominantly found in the elderly with 68 being the average age of initial diagnosis. Out of the 59.610 new leukemia cases and 23.710 deaths from leukemia as estimated by the American Cancer Society, AML accounts for one third of the cases (20.380) and half of the deaths (11.310) (Siegel et al., 2023). Although survival rates have drastically improved over the last decades, five-year overall survival rates remain low at 28% in patients above 20 years of age compared to 69% for patients below the age of 20, clearly indicating

the necessity to enhance available treatment options and therefore improve patient survival (Siegel et al., 2023).

1.1.2.1 Classification, risk stratification and treatment

Classification and risk assessment of AML is based on immunophenotyping and cytogenetics evaluating the present genetic alterations. While mutations of *CEBPA* and *NPM1* (without FLT3-ITD) and the fusions RUNX1::RUNX1T1 and CBFB::MYH11 are considered favorable, FLT3-ITD with or without *NPM1* mutation and MLLT3::KMT2A fusion belong to the intermediate risk group. In contrast, AML with the fusions DEK::NUP214, BCR::ABL1, KAT6A::CREBBP, *MLL* or *MECOM(EVI1)* re-arrangements, complex karyotypes or mutations in *ASXL1*, *EZH2*, *RUNX1*, *BCOR*, *STAG2*, *SF3B1*, *U2AF1*, *SRSF2* or *TP53* belong to the adverse risk group (De Kouchkovsky & Abdul-Hay, 2016; Döhner et al., 2022; Khwaja et al., 2016). Although AML patients can be stratified to different risk groups, the routine treatment has been constant over decades. During induction therapy the so-called '7 + 3' regimen is applied, combining the administration of AraC for seven days with anthracyclines such as daunorubicin or idarubicin for three days (Döhner et al., 2022). While anthracyclines inhibit topoisomerase II and therefore DNA synthesis, AraC is a cytosine analogue inhibiting both DNA and RNA synthesis resulting in cell cycle arrest and apoptosis in the highly proliferating AML cells (Galmarini et al., 2001; Hortobagyi, 1997). This induction period is followed by consolidation treatment with an intermediate dose of AraC, leading to a complete remission (CR) in more than 80% of the patients in favorable, 50-70% in intermediate and below 50% in adverse prognostic risk groups. CR is defined by the presence of less than 5% leukemic blast cells in the BM (Döhner et al., 2022; Estey, 2016). Low toxicity maintenance therapy is not generally required, but can be employed in order to reduce the risk of disease relapse. Lately, more individualized therapies have entered clinical trials and some of them have been approved by the FDA. For patients suffering from AML with FLT3 mutation, midostaurin is routinely included into the induction therapy (Döhner et al., 2022). Further agents, such as the antibody drug conjugate (ADC) gemtuzumab ozogamicin, the hypomethylating agents decitabine and azacytidine, the BCL2 inhibitor venetoclax or the IDH inhibitor ivosidenib, have been tested in clinical trials and are now implemented in routine therapy to enable the treatment of patients not eligible for intensive therapy (Baron & Wang, 2018; Castaigne et al., 2012; De Kouchkovsky & Abdul-Hay, 2016; DiNardo et al., 2018; Döhner et al., 2022; Estey, 2020; Stone et al., 2017; Wang et al., 2015; Wei et al., 2018). Still, most AML patients in the adverse risk group eventually relapse, while only 35-40% of the favorable risk group experiences relapses. As treatment options in relapsed patients are very limited, allogeneic hematopoietic stem cell transplantation (HSCT) can be performed to achieve long-term

remission and survival, in case a fitting donor is available (De Kouchkovsky & Abdul-Hay, 2016; Döhner et al., 2022).

In summary, although treatment of AL patients has improved drastically during the last decades, still new therapies are urgently needed to especially address patients with AMLs in adverse risk groups or with relapsed disease (Döhner et al., 2022; Malard & Mohty, 2020). There is increasing evidence that the currently used approach to classify patients, which depends on cytogenetics, cell morphology, immunophenotyping and genetics of recurrent mutations, is not sufficient to find the optimal treatment strategy for each individual patient (Arber et al., 2016; Döhner et al., 2022; Khoury et al., 2022).

1.2. Patient-Derived Xenograft mouse models of acute leukemias

1.2.1 PDX and other available models to study acute leukemias

It is crucial for model systems of AL to resemble the characteristics of the patient's disease as closely as possible including potential heterogeneity to enable prediction of clinical outcomes from pre-clinical studies. Classically, primary patient material, mouse models and leukemic cell lines are utilized. Each of these systems harbors distinct benefits and constraints.

The patient's disease is certainly best represented by primary patient material. The analysis of large patient cohorts with state-of-the-art multi-omics approaches has provided a plethora of invaluable insights into leukemogenesis as well as mechanisms of relapse development and potential treatment options (Downing et al., 2012; Jayavelu et al., 2022; Ma et al., 2018; Mullighan et al., 2008; van Galen et al., 2019; Waanders et al., 2020). Still, studies with primary patient material are mainly limited to descriptive approaches. Functional studies are severely hampered by the limited availability of primary material, in addition to the difficulty to cultivate, amplify or genetically engineer primary material *in vitro*.

In stark contrast, the use of leukemic cell lines offers sheer limitless possibilities respecting genetic modification, *in vitro* cultivation or availability of sufficient cell material. Nevertheless, cell lines hardly reflect the patient's disease with regard to tumor heterogeneity or mutational background, with heterogeneity being lost and non-physiological mutations being frequently acquired (Ben-David et al., 2019; Ben-David et al., 2018; Liu et al., 2019; Pan et al., 2009). Therefore, while facilitating functional investigations, leukemic cell lines do not sufficiently mimic the patient's disease, restricting the predictive value of these studies for drug testing or the establishment of new treatment strategies (Gillet et al., 2011; Hidalgo et al., 2014; Holohan et al., 2013).

Patient-derived xenografts (PDX) represent a highly suitable compromise between primary patient material and cell lines. Here, primary patient-derived material is engrafted into immunocompromised mice. PDX models closely mimic the mutational landscape and heterogeneity of the patient's disease, while enabling amplification of PDX cells via serial re-transplantation and allowing both functional studies as well as approaches involving genetic engineering (Hidalgo et al., 2014; Kamel-Reid et al., 1991; Kamel-Reid et al., 1989; Townsend et al., 2016; Vick et al., 2015).

1.2.2. Development, characteristics and applications of PDX models

The first acute leukemia PDX model, in this case an ALL model, was successfully generated in the late 1980s using severe combined immunodeficiency (SCID) mice lacking functional B-

and T-lymphocytes (Bosma et al., 1983; Kamel-Reid et al., 1989). Since then, several different mouse models have been developed with even further reduced immune systems to increase leukemia engraftment rates. SCID mice were bred with non-obese diabetic (NOD) mice harboring impairment of macrophages, dendritic cells, natural killer (NK) cells and the complement system (Kikutani & Makino, 1992). Today the most commonly used recipient mouse strain for PDX models of leukemia is the NOD / SCID Interleukin-2 receptor γ chain mutated (NSG, NOD.Cg-Prkdc^{scid}Il2rg^{tm1Wjl}/SzJ) strain, which is additionally devoid of cytokine signaling (McDermott et al., 2010; Shultz et al., 2005; Shultz et al., 1995). NSG mice allow comparatively high rates of initial engraftment and improve engraftment rates of serial re-transplantations (Townsend et al., 2016; Vick et al., 2015).

New PDX models are established by transplanting primary patient material, either peripheral blood (pB) samples or BM aspirates, into NSG mice via intravenous (i.v.) injection. The leukemic cells home to the BM during the early engraftment phase. Upon successful engraftment, the cells proliferate within their orthotopic niche, mirroring the patient's disease. At advanced stages of leukemia, cells disseminate from the completely filled BM into the pB and infiltrate other organs, such as spleen, liver or lung (Ebinger et al., 2016; Townsend et al., 2016; Vick et al., 2015; Woiterski et al., 2013). At this timepoint, animals start to display clinical symptoms of leukemia including apathy, rough fur, hunched back or weight loss. Upon any of these signs, animals are sacrificed and the PDX cells retrieved from BM and spleen, if possible (Kamel-Reid et al., 1991; Kamel-Reid et al., 1989; Townsend et al., 2016; Vick et al., 2015). Freshly isolated PDX cells can be re-transplanted both for passaging and for various *in vivo* experiments.

Main limitations of the PDX model are: (1) not all primary samples engraft in mice with a bias towards relapsed and highly aggressive samples, (2) the presence of low-level background skewing of the clonal structure and (3) the compromised immune system of the recipient NSG mice (Clappier et al., 2011; Townsend et al., 2016). Nevertheless, PDX mouse models represent the current gold standard for modelling and functional analysis of acute leukemias with several groups and studies successfully demonstrating that AL PDX cells mimic the patient's disease to a high degree. Genomic, epigenetic and transcriptomic profiles along with the main clonal structure of PDX cells correspond closely to the related primary patient material (Borgmann et al., 2000; Cassidy et al., 2015; Townsend et al., 2016; Vick et al., 2015; Woiterski et al., 2013; Wong et al., 2014). Thus, AL PDX cells can be utilized for studies on leukemia stem cells, the interaction between leukemic cells and the BM niche or for testing of new drugs or drug combinations in a clinically relevant setting (Ebinger et al., 2016; Habringer et al., 2018; Hope et al., 2003; Patel et al., 2014; Townsend et al., 2016; Zong et al., 2016).

1.2.3 Genetically engineered PDX models

PDX models of acute leukemias harbor several benefits compared to primary patient's material. Most strikingly, the feasibility to genetically engineer PDX (GEPDX) models using lentiviral transduction allows the stable integration of transgenes. **Figure 2** gives an overview of the typical pipeline for generating GEPDX models. In general, stable expression of fluorescent proteins and molecular tags enables enrichment of PDX cells via Fluorescence-activated Cell Sorting (FACS) and magnetic activated cell sorting (MACS) or the distinction of different PDX populations within the same animal. Furthermore, the introduction of recombinant luciferases, such as the Gaussia luciferase (GLuc) or the enhanced firefly luciferase (eFFly), permit highly sensitive bioluminescence *in vivo* imaging of the PDX cells inside living animals (Barrett et al., 2011; Bomken et al., 2013; Terziyska et al., 2012; Vick et al., 2015). This, facilitates monitoring of the leukemic burden especially at early timepoints after injection, when only a low number of PDX cells is present, which cannot be detected in peripheral blood (Ebinger et al., 2016; Ebinger et al., 2020; Terziyska et al., 2012; Vick et al., 2015). In addition, manipulation of the expression levels of endogenous genes is feasible using for example overexpression or knockdown approaches, both in a constitutive and inducible fashion (Carlet et al., 2021; Liu et al., 2020). For this project, particularly the option to knock out genes via CRISPR/Cas9 in the PDX model was essential. This allowed us to perform functional CRISPR KO screens in patient-derived cells *in vivo* (Bahrami et al., 2023; Ghalandary et al., 2023). Hence, we were able to investigate the vulnerabilities of the patient's individual tumor cells within their corresponding microenvironment in the BM niche.

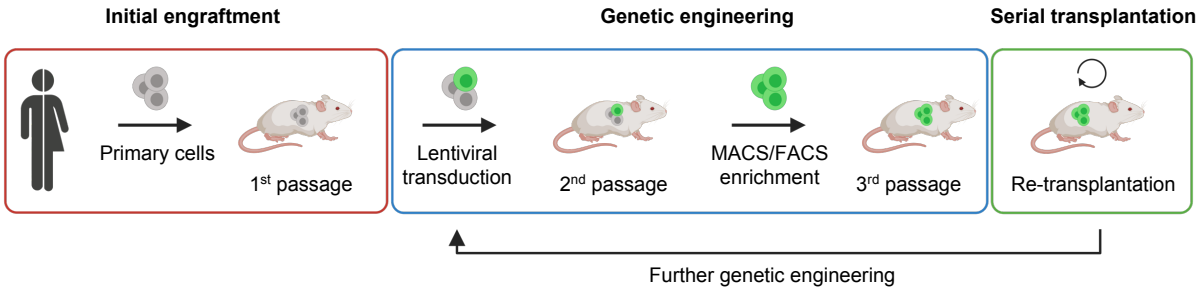

Figure 2: Overview of the GEPDX model. Primary patient's material is transplanted into NSG mice. Upon engraftment, PDX cells can be amplified, directly used for *in vivo* or *in vitro* experiments or genetically engineered via lentiviral transduction. Fluorochromes and molecular tags allow enrichment of transgene-positive PDX cells via FACS and MACS. GEPDX can be amplified, used for experiments or further genetically engineered.

1.3. CRISPR Cas9 enables functional dropout screens in the PDX model

1.3.1. Personalized medicine benefits from functional assays for improved understanding of disease biology

Conventional chemotherapy mainly targets proliferating cells in an unspecific fashion. Based on the underlying driver mutations and genetic alteration of the individual disease, interpatient response rates therefore vary considerably. Precision medicine aims at elucidating each patient's ideal treatment strategy, which is of high interest in the cancer field including acute leukemia (Burd et al., 2020; Dohner et al., 2021; Ho et al., 2020; Hunger & Mullighan, 2015; Kansal, 2016; Kirtonia et al., 2020; Malani et al., 2022; Pui, 2020; Tsimberidou et al., 2020). Improvements in sequencing technologies combined with ever decreasing costs have resulted in their broad application in cancer research and the development of diverse new techniques over the last years. Combined with other state-of-the-art technologies such as proteomics, these multi-omics approaches have significantly increased our understanding of disease biology. However, the vast majority of these studies is of mainly descriptive nature. Here, we aimed to acquire functional data on individual patient's tumor vulnerabilities.

1.3.2. Discovery of CRISPR/Cas systems revolutionized genetic engineering

Only three years ago, in 2020, Emmanuelle Charpentier and Jennifer Doudna received the nobel prize in chemistry for the discovery of the clustered regularly interspaced short palindromic repeats (CRISPR) / CRISPR-associated 9 (Cas9) system. In the short time since its introduction, CRISPR/Cas9 has revolutionized genetic engineering in medical, biotechnological as well as basic research. Due to its high specificity, broad applicability, ease of use and comparatively low costs, the CRISPR/Cas9 system rendered genome engineering feasible for almost any research laboratory around the world (Doudna & Charpentier, 2014; Moore, 2015). Since then, the Cas9 enzyme has been further modified to allow not only the cutting of DNA, but also the activation or repression of certain genes or genomics regions using a so-called 'dead' version of Cas9 fused to different activator or repressor proteins, respectively. Additionally, Cas proteins derived from different organisms have been utilized due to certain benefits, such as the enzyme size, the used protospacer adjacent motif (PAM) sequence, the produced cut or their preferential activity on DNA or RNA (Liu et al., 2022; Pickar-Oliver & Gersbach, 2019).

1.3.3. CRISPR/Cas9's mode of action

CRISPR/Cas9 derived from *Streptococcus pyogenes* is the most frequently used system. Here, the Cas9 acts as nuclease, producing blunt double-strand breaks (DSBs) in the DNA (**Figure 3**). The Cas9 enzyme is directed to the cleavage site by single guide RNAs (sgRNA), which are complementary to the targeted region of interest, thereby providing site-specificity. Cellular DNA damage repair mechanisms are activated by the introduced double-strand breaks. This repair can either occur via homology directed repair (HDR) if a compatible template is provided, or by the highly error-prone non-homologous end joining (NHEJ). NHEJ often results in the generation of small insertions and deletions (InDels). This can be exploited for the generation of gene knockouts. If DSBs are introduced into the coding region of the targeted protein, the formation of InDels frequently leads to frameshift mutations, resulting in premature stop codons and therefore truncated proteins or proteins with a complete loss-of-function (Doudna & Charpentier, 2014).

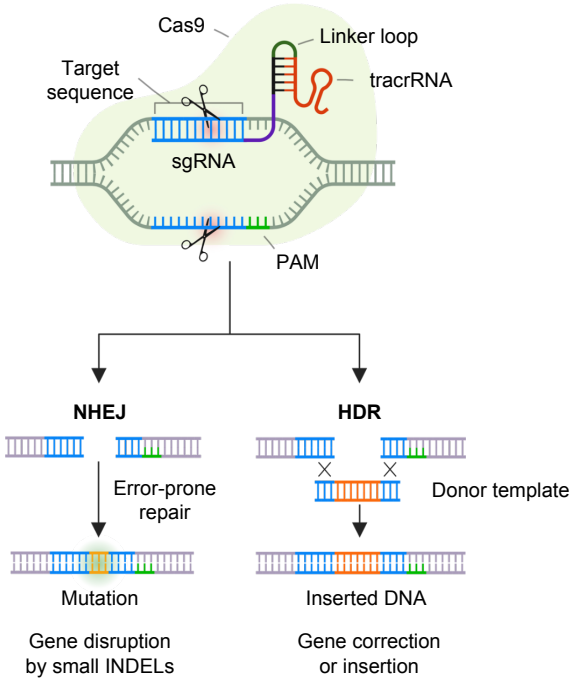

Figure 3: Scheme of CRISPR/Cas9's mode of action. Specific sgRNAs direct Cas9 to the cleavage site. Introduced double-strand breaks are repaired either via error-prone NHEJ or through HDR using a provided donor template.

1.3.4. Establishment of a pipeline for functional CRISPR/Cas9 KO screens in patient-derived xenograft models *in vivo*

In addition to the use of CRISPR/Cas9 for the generation of single gene knock-outs, the technique allows genetic screens with high-throughput. Functional *in vitro* CRISPR/Cas9 KO screens have been widely used in a plethora of studies in order to decipher essential and drug-resistance conferring genes or cancer-specific susceptibilities in cancer cell lines (Shalem et al., 2014; Wang et al., 2016; Wang et al., 2014; Yin et al., 2019). For this approach, sgRNAs targeting different genes are pooled to form a library. Integration of the sgRNAs is conducted at a low multiplicity of infection (MOI) in order to warrant predominantly single integrations and therefore single gene knock-outs. As readout, the sgRNA sequence is amplified from the DNA and sequenced via next-generation sequencing (NGS) comparing the abundance of each individual sgRNA in the input and output samples (Doench, 2018). While sgRNAs targeting genes essential for the tested PDX sample are depleted in the output compared to the input, the frequency of sgRNAs targeting non-essential genes is unaltered. While most studies use genome-wide screening libraries in cells lines, in our lab we started to use customized sub-libraries for the direct use in our patient-derived xenograft models, rendering the approach easier to translate to the clinical setting (Byrne et al., 2017; Guo et al., 2016; Hidalgo et al., 2014).

In order to enable functional CRISPR/Cas9 KO screens in the PDX model, several hurdles had to be overcome. Firstly, the introduction of Cas9 into the hard-to-transduce PDX cells is challenging due to its large size. Therefore, a former Postdoc in our lab, Martin Becker, developed a split-version of Cas9 combined with a split version of GFP (**Figure 4A**). While the Cas9 protein parts recombine via inteins, GFP re-assembles mediated by a leucine-zipper. This enabled us to reduce on the one side the plasmid size, while on the other side being able to track successful re-assembly of the two GFP parts by flow cytometry (Hu & Kerppola, 2003; Truong et al., 2015). Using lentiviral transduction of the two plasmids, each of which contains one part of Cas9 and GFP, PDX models stably expressing Cas9 were generated. A second technical challenge was the enrichment of sgRNA library-positive cells in a large scale for which enrichment via flow cytometry was not feasible. Ehsan Bahrami, also a former Postdoc in our lab and the person I collaborated with very closely for this project, generated a H-2K^k-BFP fusion protein (**Figure 4B**). This allowed both measurement and enrichment of BFP and therefore library-positive cells via flow cytometry as well as enrichment of large cell numbers using positive MACS selection for the H-2K^k molecular tag.

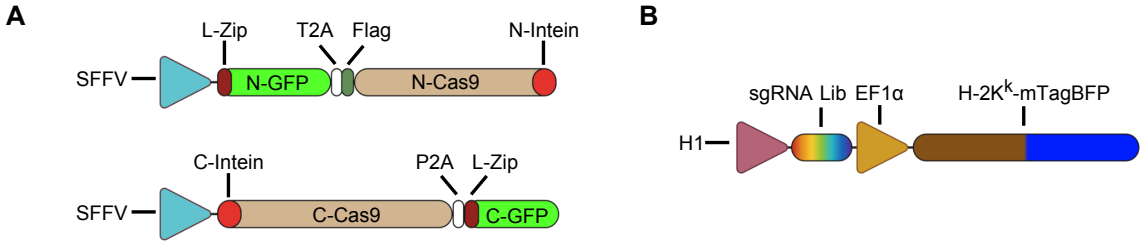

Figure 4: Technical improvements enabled *in vivo* customized CRISPR KO screens. A Schematic representation of the two lentiviral plasmids used for stable integration of Cas9 into PDX models. Each plasmid is expressed via the *spleen focus-forming virus* (SFFV) promoter. In the upper plasmid a leucine zipper motif (L-Zip) fused to the N-terminal GFP part is connected via a *Thosea asigna virus* 2A peptide (T2A) to a Flag tag, enabling protein detection and the N-terminal part of Cas9 fused to the N-Intein. In the lower plasmid, the C-Intein fused to the C-terminal part of Cas9 is connected via a *Porcine teschovirus-1* 2A peptide (P2A) to another L-Zip fused to the C-terminal part of GFP. The L-Zip motifs are used for bimolecular fluorescence complementation (BIFC) of GFP, while the two parts of Cas9 are fused mediated by the Inteins. **B** Schematic representation of the lentiviral plasmid used for stable integration of the sgRNA library into PDX models. Expression of the individual sgRNAs comprised within the library plasmid pool is driven by the human type 3 RNA Pol III promoter H1. The human elongation factor-1 alpha (EF1α) promoter drives expression of the H-2K^k-mTagBFP fusion protein, which enables analysis via flow cytometry and enrichment via both MACS and FACS. Adapted from (Bahrami, Schmid et al., 2023).

Based on previous experiments in the lab, performed by the former lab member Erbey Özdemir, which showed that roughly 1% of the transplanted cells engraft in the BM in the two ALL PDX models used for this project, we calculated the maximal feasible size of our customized sgRNA library. As the whole library should be represented within each individual animal and 10^7 is the highest number of cells which can be transplanted into a single mouse, we calculated a library size with ample safety margins. With 1% homing cells, five sgRNAs per gene and an average sgRNA coverage of at least 200 cells, we calculated 100 target genes to be included in our customized library. Moreover, both non-targeting sgRNAs as well as sgRNAs targeting known essential genes were included, serving as negative and positive controls, respectively. In conclusion, we were able to establish a pipeline for functional CRISPR/Cas9 KO screens using customized libraries in PDX models which highly resemble the individual patient's disease in the *in vivo* setting, enabling orthotopic growth in their respective niche and thereby interaction with the BM microenvironment, rendering our approach highly clinically relevant.

1.4. The surface molecule ADAM10

1.4.1. Importance of surface molecules for the interaction of leukemic cells with the BM microenvironment

Surface molecules play a crucial role for the interaction between leukemic cells and the microenvironment within the BM niche. We and others demonstrated, that this interaction can provide a protective environment, especially for leukemia stem cells (LSCs), rendering conventional chemotherapy ineffective in eliminating these cells (Delahaye et al., 2020; Ebinger et al., 2016; Menter & Tzankov, 2022; Phan & Croucher, 2020; Schepers et al., 2015; Zhou et al., 2016). LSCs are a rare and dormant subpopulation of cells with the ability to induce a relapse after remission. Thus, there is a high clinical need to efficiently target and, if feasible, eradicate LSCs (Bernt & Armstrong, 2009; Konopleva & Jordan, 2011; Misaghian et al., 2009; Pollyea & Jordan, 2017). Previously we found, that releasing the LSCs from the BM microenvironment renders them more sensitive towards routine chemotherapy (Ebinger et al., 2016; Ebinger et al., 2020).

One of the most studied molecule facilitating the interaction between LSCs and the BM niche is the CXC motif chemokine receptor type 4 (CXCR4). CXCR4 was shown to be crucially important for the early engraftment and homing to the BM, and its targeting via antagonists results in the release of leukemic cells into the peripheral blood along with their chemosensitization. (Habringer et al., 2018; Juarez et al., 2007; Nervi et al., 2009; Passaro et al., 2015; Petit et al., 2002; Tavor et al., 2004; Uy et al., 2012; Zeng et al., 2006). Therefore, disrupting the interaction between leukemic cells and the BM microenvironment clearly represents an attractive strategy to release LSCs from their sheltering niche and re-sensitize them towards routinely used chemotherapeutic agents.

1.4.2. ADAM10 is a member of the A disintegrin and metalloproteinase (ADAM) family

In humans, the ADAM family comprises 21 members of which 13 are proteolytically active (Edwards et al., 2008). ADAM proteins are enzymes anchored in the plasma membrane cleaving diverse transmembrane proteins, such as cytokine precursors, cytokine, phagocytic or Notch receptors as well as cell adhesion molecules (Lambrecht et al., 2018). Cleaving the ectodomains of these membrane-bound proteins can result in the release of soluble ectodomains, referred to as ectodomain shedding. The soluble ectodomains can harbor both activating and inhibiting functions on the surrounding proteins and cells (Lambrecht et al., 2018). Additionally, the residual protein part, which had been cleaved by an ADAM enzyme, is

often further processed by a γ-secretase in a process called regulated intra-membrane proteolysis (RIPping). This results in the production of a second cleaved molecule, which can either act as a transcription factor, be involved in cellular signaling or be designated for lysosomal degradation (Lambrecht et al., 2018; Murphy, 2008). Despite the common structure of the 13 proteolytically active ADAMs, there is no specific motif shared between potential substrates. This prevents *in silico* prediction and therefore renders the discovery of ADAM substrates cumbersome, limiting their identification to cleavage assays along with proteomic and secretomic approaches (Lambrecht et al., 2018).

1.4.3. Structure of ADAM10

ADAM10 is a multidomain protein, comprising several structurally and functionally distinct domains (**Figure 5**). Like all members of the ADAM family, ADAM10 carries a signaling sequence at the N-terminus crucial for trafficking from the ER to the plasma membrane via the secretory pathway (Edwards et al., 2008). The adjacent pro-domain has a dual role in inhibiting the enzymatic domain and safeguarding correct protein folding as intramolecular chaperone. During ADAM10's passage from the ER to the cell membrane, the pro-domain is removed by the pro-domain convertase protein PC7 and furin in a step-wise process. Thereby, ADAM10 gradually acquires its catalytical activity (Lambrecht et al., 2018). The pro-domain is followed by the metalloproteinase domain, which is the enzymatically active domain responsible for ADAM10's function as a sheddase. Intriguingly, ADAM10's enzymatic activity and metalloproteinase domain is crucial for maintaining its localization at the cell surface (Seifert et al., 2021). The neighboring disintegrin domain harbors an amino acid stretch called disintegrin loop, which suggests a potential interaction between ADAM10 and integrins (Edwards et al., 2008). Its name is derived from its initial discovery in snake venom, where its ability to bind integrin αIIbβIIIa disrupts platelet aggregation (Niewiarowski et al., 1994). Following the disintegrin domain, ADAM10 is comprised of the cysteine-rich domain, the stalk region, the transmembrane domain and the C-terminal domain. While the cysteine-rich domain is involved in the interaction with different substrates (Edwards et al., 2008), the cytoplasmic domain was described to be involved in signaling, interacting for example with DLG1, MAD2, PACSIN3 or the ADAM binding protein EVE-1, which was shown to be essential for cleaving of epidermal growth factor receptor ligands (Edwards et al., 2008; Tanaka et al., 2004). Furthermore, the interaction with non-receptor tyrosine kinases with SH3 domains, such as GRB2, FYN, ITK, LCK and NCK, was discovered (Ebsen et al., 2014; Lambrecht et al., 2018).

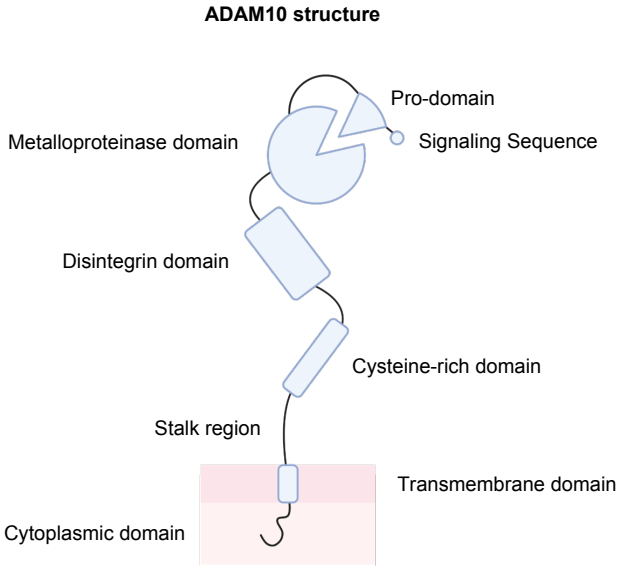

Figure 5: Structure of ADAM10. Schematic depiction of the individual domains of the ADAM10 protein. Starting from the N-terminus, ADAM10 is comprised of the signaling sequence, the pro-domain, the metalloproteinase domain, the disintegrin domain, the cysteine-rich domain, the stalk region, the transmembrane domain and the cytoplasmic domain at the C-terminus.

1.4.4. Regulation of ADAM10's activity

ADAM10 mediates an irreversible cleavage of its many substrates. Therefore, tight regulation of its enzymatic activity is crucial and occurs on several levels. The first mechanism is intracellular retention. Here, the correctly folded ADAM10 protein is restrained within the ER or Golgi via a so far not identified interaction of its cytoplasmic domain, whereas interaction with DLG1 promotes trafficking towards the cell membrane (Lambrecht et al., 2018). Secondly, ADAM10's activity is controlled at the cell surface. Both ADAM10 and ADAM17 tend to dimerize on the cell surface leading to an autoinhibitory conformation. MAP kinases of the p38 and ERK families were shown to phosphorylate both ADAM10 and ADAM17. The phosphorylation of certain key residues, e.g. Thr725 in ADAM17 and potentially Thr719 in ADAM10, diminishes dimerization and therefore results in activation of the ADAM's enzymatic activity (Cissé et al., 2011; Deng et al., 2014; Díaz-Rodríguez et al., 2002; Lambrecht et al., 2018; Soond et al., 2005; Xu et al., 2012). Another crucial mechanism of regulation of ADAM10's activity is its interaction with tetraspanins, a protein family comprising 33 members, each harboring four transmembrane domains. A subtype of these, the C8 family is defined by the presence of eight conserved cysteines within the larger loop on the extracellular side. ADAM10 is known to interact with the following six members of the C8 subgroup: TSPAN5, TSPAN10, TSPAN14, TSPAN15, TSPAN17 and TSPAN33. It is proposed and could partially be confirmed, that depending on the interacting tetraspanin and formation of the respective C8/ADAM10 complex, ADAM10's localization, enzymatic activity and possibly its preferred

substrates might be altered (Binger & Wright, 2022; Lambrecht et al., 2018; Matthews et al., 2017). Exemplary, the importance of TSPAN5 and TSPAN17 interaction with ADAM10 for the regulation of VE-Cadherin in transmigration of lymphocytes could be shown (Reyat et al., 2017). Additionally, TSPAN5 and TSPAN15 reciprocally regulate ADAM10's stability on the cell surface. TSPAN5 promotes faster endocytosis, while TSPAN15 stabilizes ADAM10 at the cell membrane (Eschenbrenner et al., 2020; Harrison et al., 2021).

1.4.5. ADAM10's role in normal hematopoiesis and disease

ADAM10 is involved in several processes during normal hematopoiesis. One of its best characterized roles is the activation of Notch, which is crucial for both the development and the correct functioning of immune cells. During Notch activation furin-like convertases cleave Notch at the protease site 1 (S1), resulting in an inactive heterodimer. Upon binding of its ligand, delta-like ligand 1 (DLL1), the Notch receptor changes its conformation enabling its cleavage by ADAM10 directly next to the cell membrane at the S2 site. This Notch external truncation (NEXT) is subsequently cleaved by a γ-secretase complex at the S3 site, releasing the Notch intracellular domain (NICD), which translocates into the nucleus and subsequently induces the transcription of Notch regulated genes, such as *MAML1*, *p300* and *RBPjκ* (Lambrecht et al., 2018).

In normal T cell biology, ADAM proteins exert important functions through the cleavage of cytokines, growth factors and receptors. During T cell development a dominant negative form of ADAM10 suppresses T cell development and ADAM10-deficient T cells are blocked in their differentiation, phenocopying Notch-1 loss (Lambrecht et al., 2018; Tian et al., 2008). Furthermore, the combined recruitment of ADAM10 and Notch1 to immunological synapses between dendritic cells and peripheral cells is crucial for T cell proliferation as well as for inducing the differentiation of T helper cells (Lambrecht et al., 2018). ADAM10 is also involved in the migration of T cells. CD44 is an adhesion molecule expressed by T cells binding both vascular endothelium and hyaluronic acid in the extracellular matrix. CD44's cleavage by ADAM10 results in disruption of the adhesive function and the release of intracellular domain CD44-ICD, which was connected to transformation in cancer (Lambrecht et al., 2018; Miletti-González et al., 2012; Nagano & Saya, 2004). Additionally, ADAM10 promotes transendothelial migration of T cells via cleavage of VE-cadherin and the chemokine ligands CXCL16 and CX_3CL1 (Hundhausen et al., 2007; Lambrecht et al., 2018; Schulz et al., 2008).

ADAM10 is essential for the commitment of marginal zone B cells via shedding of Notch 2 (Gibb et al., 2010). In germinal center B cells, ADAM10 is higher expressed than in naïve B cells, with ADAM10 loss leading to impaired formation of the GC, decreased follicular dendritic cells networks and reduced numbers of T follicular helper cells. This in turn results in weaker

antibody responses in mice (Chaimowitz et al., 2011; Lambrecht et al., 2018; Lownik et al., 2017). Moreover, ADAM10 regulates the differentiation of plasma cells by cleaving transcription factors, such as BLIMP1, XBP1 or IRF4.

In natural killer (NK) cells, ADAM10 sheds NKG2D ligands leading to lower surface expression levels on the cell itself along with downregulation on surrounding cells mediated by the shedded ectodomain. As NK cells are activated by NKG2D and other ligands, the shedding by ADAM10 represents a strategy for cancer cells to evade immunosurveillance with higher levels of the shedded ligands being associated with poorer survival in patients (Chitadze et al., 2013; Kohga et al., 2009; Lambrecht et al., 2018; Nückel et al., 2010).

In myeloid cells, the shedding of L-selectin on neutrophils which alters their rolling and recruitment, or the induction of pro-inflammatory signaling via the STAT1 and NF-κB pathways after cleavage of SIRPα are important processes with ADAM10 involvement (Lambrecht et al., 2018; Londino et al., 2015; Pruessmeyer et al., 2014).

In addition, ADAM10 activity was associated with disease progression in several tumor types, including T-ALL (Atapattu et al., 2016; Lambrecht et al., 2018; Mullooly et al., 2016; Smith et al., 2020). ADAM10 was for example shown to promote metastasis formation of colon cancers via L1-CAM cleavage and HER2 overexpressing breast cancer cells through shedding of the HER2 extracellular domain (Gavert et al., 2007; Liu et al., 2006).

In summary, ADAM10 is involved in diverse processes in healthy hematopoiesis and in disease. Main affected pathways are intracellular signaling, adhesion and transendothelial migration as well as cytokine processing.

1.5. Aim of the Project

Although enormous improvements have been made in the treatment of acute leukemia in recent decades, still many patients succumb to their disease. Today, probably the biggest hurdle is when a relapse occurs in patients who initially responded to treatment and achieved complete remission. Treatment options are often very limited and overall survival rates continue to stay at unacceptable low levels. A rare, dormant cell population of LSCs that resides in the bone marrow microenvironment and is thus protected from routine chemotherapy is causing these relapses. Disruption of their interaction with the protective niche sensitizes them again towards chemotherapeutic agents. This might help to eradicate as many LSCs as possible and therefore prevent the development of relapse.

In this study, we aimed to find a new candidate gene with the potential to serve as a therapeutic target in the future treatment of acute leukemia patients. For this we used our recently established pipeline for functional CRISPR/Cas9 knockout screens in the PDX model *in vivo*, which represents the currently most clinically relevant model system for functional assays. Utilizing this pipeline, we tested a customized surface molecule library targeting around 100 genes. Our aim was to identify vulnerabilities of acute leukemia, which might help to disrupt the interaction of LSCs and their safeguarding BM niche. We molecularly validated candidates from the screen using competitive *in vivo* assays.

With our top candidate, ADAM10, we performed *in vivo* reconstitution assays and investigated the effect of ADAM10 loss compared to control cells using transcriptome, proteome and secretome experiments. To further elucidate its characteristics as a vulnerability of acute leukemias we used early engraftment assays, limiting dilution transplantation assays; colony formations assays; and competitive chemotherapy trials *in vivo*.

2 Material

2.1 Animals

Table 1: Laboratory animals

Laboratory Animal	Provider
NOD.Cg-Prkdcscid Il2rgtm1Wjl/SzJ (NSG) mice	Jackson Laboratory (Bar Harbor, USA)

2.2 Cell lines

Table 2: Cell lines

Cell line	Provider
H293T	DSMZ (Braunschweig, Germany)
human CD34+ blood progenitor cells	Lonza (Basel, Switzerland)
NALM-6	DSMZ (Braunschweig, Germany)
SEM	DSMZ (Braunschweig, Germany)

2.3 Bacterial strains

Table 3: Bacterial Strains

Bacterial Strain	Provider
E.coli DH5α	Thermo Fisher Scientific (Waltham, USA)
E.coli XL10-Gold Ultracompetent Cells	Agilent Technologies (Santa Clara, USA)
Endura Competent cells	Lucigen (Middleton, USA)

2.4 Chemicals and reagents

Table 4 Chemicals and reagents

Name	Manufacturer
β-Mercaptoethanol	Sigma Aldrich (St. Louis, USA)
2-propanol	Merck Millipore (Darmstadt, Germany)
Acetic acid	Carl Roth (Karlsruhe, Germany)
Agar-Agar Kobe I	Carl Roth (Karlsruhe, Germany)
Agarose	Invitrogen (Carlsbad, USA)
Alt-R CRISPR-Cas9 tracrRNA ATTO550	IDT (Leuven, Belgium)
Ampicillin	Sigma Aldrich (St. Louis, USA)
BD Horizon™ BV711 Annexin V	BD Biosciences (Heidelberg, Germany)
Annexin V Binding Buffer	Biozol (Eching, Germany)
Bambanker	NIPPON Genetics EUROPE (Düren, Germany)
BSA	Carl Roth (Karlsruhe, Germany)
$CaCl_2$	Carl Roth (Karlsruhe, Germany)
Cell lysis buffer (10x)	Cell Signaling Technology (Boston, USA)

Cut Smart buffer	New England Biolabs (Frankfurt am Main, Germany)
DAPI	Sigma Aldrich (St. Louis, USA)
D-Luciferin	Biomol GmbH (Hamburg, Germany)
DMEM	Gibco (San Diego, USA)
DMSO	Sigma Aldrich (St. Louis, USA)
DNA ladder	Thermo Fisher Scientific (Waltham, USA)
DNA loading dye	Thermo Fisher Scientific (Waltham, USA)
DNAse I	Thermo Fisher Scientific (Waltham, USA)
dNTPs	Takara Bio Inc. (Kusatsu, Japan)
DTT (Diethiothreitol)	Thermo Fisher Scientific (Waltham, USA)
EDTA (0.5 M)	Lonza (Basel, Switzerland)
Endura recovery medium	Lucigen (Middleton, USA)
Ethanol	Carl Roth (Karlsruhe, Germany)
ExTaq buffer (10x)	Takara Bio Inc. (Kusatsu, Japan)
FACS Lysing Solution (10x)	BD Biosciences (Heidelberg, Germany)
FBS	Gibco (San Diego, USA)
FD buffer	Thermo Fisher Scientific (Waltham, USA)
Ficoll	GE Healthcare (Solingen, Germany)
Glutamine	Gibco (San Diego, USA)
Glycerin 98%	Carl Roth (Karlsruhe, Germany)
Hepes pH 7.4	Sigma Aldrich (St. Louis, USA)
IMDM	Pan-Biotech
Isoflurane	Sigma Aldrich (St. Louis, USA)
Isopropyl alcohol	Merck Millipore (Darmstadt, Germany)
Kanamycin Sulfate	Thermo Fisher Scientific (Waltham, USA)
KCl	Merck Millipore (Darmstadt, Germany)
L-Glutamine	Gibco (San Diego, USA)
Leupeptin	SERVA Electrophoresis GmbH (Heidelberg, Germany
LightCycler® 480 SYBR Green I Master	Roche (Mannheim, Germany)
Midori Green	NIPPON Genetics EUROPE (Düren, Germany)
$MnCl_2$	Sigma Aldrich (St. Louis, USA)
MOPS	Sigma Aldrich (St. Louis, USA)
Na_2HPO_4	Sigma Aldrich (St. Louis, USA)
Na_3VO_4	Thermo Fisher Scientific (Waltham, USA)
NaF	Thermo Fisher Scientific (Waltham, USA)
NaCl	Carl Roth (Karlsruhe, Germany)
NP-40 Surfact-Amps™ Detergent	Thermo Fisher Scientific (Waltham, USA)
Paraformaldehyde solution 4% in PBS	Santa Cruz Biotechnology (Dallas, USA
PBS	Gibco (San Diego, USA)
Penicillin/Streptavidin (P/S)	Gibco (San Diego, USA)
PMSF	Cell Signaling Technology (Boston, USA)
Polybrene	Sigma Aldrich (St. Louis, USA)
Polyethylenimine	Polysciences (Warrington, USA)
ProLong™ Gold Antifade Mountant	Fisher Scientific GmbH (Schwerte, Germany)
Protein Assay Dye Reagent Concentrate	Bio-Rad Laboratories GmbH (Feldkirchen, Germany)
Recombinant human granulocyte macrophage-colony stimulating factor (GM-CSF)	Sigma Aldrich (St. Louis, USA)

Recombinant human FMS-like tyrosine kinase 3 ligand (FLT3L)	R&D Systems (Minneapolis, USA)
Recombinant human interleukin 3 (IL3)	Peprotech (Rocky Hill, USA)
Recombinant human interleukin 6 (IL6)	Peprotech (Rocky Hill, USA)
Recombinant human interleukin 7 (IL7)	Peprotech (Rocky Hill, USA)
Recombinant human stem cell factor (SCF)	Peprotech (Rocky Hill, USA)
Recombinant human thrombopoietin (TPO)	Peprotech (Rocky Hill, USA)
RLT Plus Buffer	Qiagen (Hilde, Germany)
RPMI-1640	Gibco (San Diego, USA)
Selected peptone 140	Gibco (San Diego, USA)
Skim Milk Powder for blotting	SERVA Electrophoresis GmbH (Heidelberg, Germany)
Sodium pyruvate	Sigma Aldrich (St. Louis, USA)
StemPro-34 medium	Thermo Fisher Scientific (Waltham, USA)
StemPro-34 Nutrient Supplement	Thermo Fisher Scientific (Waltham, USA)
StemSpan™ SFEM II	Stemcell Technologies (Vancouver, Canada)
SYBR™ Green PCR Master Mix	Thermo Fisher Scientific (Waltham, USA)
T4 DNA Ligase Buffer	Thermo Fisher Scientific (Waltham, USA)
Tris	Carl Roth (Karlsruhe, Germany)
Tris-HCl	Carl Roth (Karlsruhe, Germany)
Trypan blue	Sigma Aldrich (St. Louis, USA)
Trypsine dissociation agent	Gibco (San Diego, USA)
Tween® 80	Carl Roth (Karlsruhe, Germany)
Yeast extract	Carl Roth (Karlsruhe, Germany)

2.5 Chemotherapeutic agents and chemical inhibitors

Table 5: Chemotherapeutic agents and chemical inhibitors

Chemotherapeutic agent / chemical inhibitor	**Manufacturer**
Cyclophosphamide	TEVA GmbH (Ulm, Germany)
Aderbasib (INCB007839)	MedChemExpress (Monmouth Junction, USA)
Cytarabine incl. Sodium- (S)-lactate solution (50%)	Cell Pharma GmbH (Vilbel, Germany)
Daunorubicin	Pfizer (Ney York City, USA)
Doxorubicin	Medac GmbH (Wedel, Germany)
GI254023X	Selleckchem (Houston, USA)
Vincristine	Cell Pharm GmbH (Hannover, Germany)

2.6 Buffers and media

Table 6: Buffers

Buffer	**Composition**
Annealing buffer	50 mM Hepes pH 7.4, 100 mM NaCl
PBS + 0.5% BSA	PBS, 0.5% BSA
TAE buffer	40 mM Tris-base, 1 mM EDTA, 20 mM acetic acid

Table 7: Media

Media	Composition
LB Medium	1% selected peptone, 0.5% Yeast extract, 1% NaCl
LB Agar	1% selected peptone, 0.5% Yeast extract, 1% NaCl, 1.5% Agar-Agar Kobe I
Cultivation medium of H293-T cells	DMEM, 10% FCS, 1% L-Glutamine
Cultivation medium of acute leukemia cell lines	RPMI-1640, 10% FCS, 1% L-Glutamine
Cultivation medium of PDX ALL cells	StemSpan™ SFEM II, 1% Pen/Strep
Cultivation medium of PDX AML cells	StemPro-34 Medium, StemPro-34 Nutrient Supplement, 2% FCS, 1% L-Glutamine, 1% Pen/Strep, 10 ng/ml FLT3L, 10 ng/ml SCF, 10 ng/ml IL3, 10 ng/ml TPO

2.7 Antibodies

Table 8: Flow Cytometry Antibodies

Antibody	Manufacturer
APC Mouse IgG1 kappa Isotype	Biolegend (San Diego, USA)
anti-human CD33-PE, clone IV M505, #555450	BD Bioscience (Heidelberg, Germany)
anti-human CD38 PE, clone HB7, #345806	BD Bioscience (Heidelberg, Germany)
anti-murine CD45-APC, clone 30-F11, #103112	Biolegend (San Diego, USA)
anti-human CD156c (ADAM10)-APC, clone SHM14, #352706	Biolegend (San Diego, USA)

Table 9: Western Blot and Simple WES Antibodies

Antibody	Manufacturer
anti-β-Actin, clone AC-15, #NB600-501SS	Novus Biologicals (Centennial, Germany)
anti-human β -actin, Mouse mAb, clone C4 HRP, #sc-47778	Santa Cruz Biotechnology (Heidelberg, Germany)
anti-human ADAM10, Rabbit pAb #14194	Cell Signaling Technology (Boston, USA)
anti-human GAPDH, Mouse mAb, clone H-12 HRP, #sc-166574	Santa Cruz Biotechnology (Heidelberg, Germany)
anti-human Syntaxin-4 (E6W7B) Rabbit mAb #67657	Cell Signaling Technology (Boston, USA)
Anti-mouse IgG, HRP-linked Antibody #7076	Cell Signaling Technology (Boston, USA)
Anti-rabbit IgG, HRP-linked Antibody #7074	Cell Signaling Technology (Boston, USA)
Anti-rat IgG Horseradish Peroxidase-conjugated Antibody, #HAF005	R&D Systems (Minneapolis, USA)

Table 10: Immunohistochemistry Antibodies

Antibody	Manufacturer
Anti-Human ADAM-10 Azide Free, clone 11G2	Diaclone (Besancon Cedex, France)
anti-human ADAM10, Rabbit pAb #14194	Cell Signaling Technology (Boston, USA)

IgG (H+L) Cross-Adsorbed Goat anti-Mouse, Alexa Fluor™ 647, Invitrogen™, #A21235	Fisher Scientific GmbH (Schwerte, Germany)
V5-Tag (D3H8Q) Rabbit mAb #13202	Cell Signaling Technology (Boston, USA)

Table 11: MACS beads

MACS beads	Manufacturer
Dead cell removal kit	Miltenyi (Bergisch Gladbach, Germany)
Mouse cell depletion kit	Miltenyi (Bergisch Gladbach, Germany)
MACSelect Kk MicroBeads	Miltenyi (Bergisch Gladbach, Germany)

2.8 Enzymes

Table 12: Enzymes

Enzyme	Manufacturer
AgeI-HF	New England Biolabs (Frankfurt am Main, Germany)
Alt-R S.p. Cas9 Nuclease V3	IDT (Leuven, Belgium)
BamHI-HF	New England Biolabs (Frankfurt am Main, Germany)
BpiI FD	Thermo Fisher Scientific (Waltham, USA)
EcoRI-HF	New England Biolabs (Frankfurt am Main, Germany)
ExTaq Polymerase	Takara Bio Inc. (Kusatsu, Japan)
NheI-HF	New England Biolabs (Frankfurt am Main, Germany)
NotI-HF	New England Biolabs (Frankfurt am Main, Germany)
NsiI-HF	New England Biolabs (Frankfurt am Main, Germany)
OneTaq® DNA Polymerase	New England Biolabs (Frankfurt am Main, Germany)
Phusion High-Fidelity PCR Master Mix with HF Buffer	Thermo Fisher Scientific (Waltham, USA)
Proteinase K	Thermo Fisher Scientific (Waltham, USA)
Q5® High-Fidelity DNA Polymerase	New England Biolabs (Frankfurt am Main, Germany)
SalI-HF	New England Biolabs (Frankfurt am Main, Germany)
T4 DNA Ligase	Thermo Fisher Scientific (Waltham, USA)
XhoI	New England Biolabs (Frankfurt am Main, Germany)

2.9 Plasmids

Table 13: Plasmids

Plasmid	Provider
pMD2.G	Addgene (Cambridge, USA)
pMDLg/pRRE	Addgene (Cambridge, USA)

pRSV-Rev	Addgene (Cambridge, USA)
pCDH-EF1a-ADAM10_variant1-Full-ADAM10(∆Pro-domain)-T2A-T-Sapphire	cloned by Jan Philipp Schmid for this project
pCDH-EF1a-ADAM10_variant2-delta-Dis-ADAM10(∆Pro-domain)-T2A-T-Sapphire	cloned by Jan Philipp Schmid for this project
pCDH-EF1α-eFFly-T2A-eGFP	cloned by Michela Carlet
pCDH-EF1α-eFFly-T2A-mCherry	cloned by Michela Carlet
pCDH-H1-scrambled sgRNA-scaffold-EF1α-iRFP-H2Kk	cloned by Jan Philipp Schmid for this project
pCDH-H1-scrambled sgRNA-scaffold-EF1α-mCherry-H2Kk	cloned by Jan Philipp Schmid for this project
pCDH-H1-sgRNA-scaffold-EF1α-mtagBFP-H2Kk	cloned by Ehsan Bahrami
pCDH-H1-sgRNA surface molecule library-scaffold-EF1α-mtagBFP-H2Kk	cloned by Ehsan Bahrami
pCDH-H1-ADAM10 sgRNA 1-scaffold-EF1α-mtagBFP-H2Kk	cloned by Jan Philipp Schmid for this project
pCDH-H1-ADAM10 sgRNA 2-scaffold-EF1α-mtagBFP-H2Kk	cloned by Jan Philipp Schmid for this project
pCDH-H1-ADAM10 sgRNA 3-scaffold-EF1α-mtagBFP-H2Kk	cloned by Jan Philipp Schmid for this project
pCDH-H1-ADAM10 sgRNA 4-scaffold-EF1α-mtagBFP-H2Kk	cloned by Jan Philipp Schmid for this project
pCDH-H1-ADAM10 sgRNA 5-scaffold-EF1α-mtagBFP-H2Kk	cloned by Jan Philipp Schmid for this project
pCDH-H1-CD79A sgRNA 1-scaffold-EF1α-mtagBFP-H2Kk	cloned by Jan Philipp Schmid for this project
pCDH-H1-CD79A sgRNA 2-scaffold-EF1α-mtagBFP-H2Kk	cloned by Jan Philipp Schmid for this project
pCDH-H1-CD79A sgRNA 3-scaffold-EF1α-mtagBFP-H2Kk	cloned by Jan Philipp Schmid for this project
pCDH-H1-CD79A sgRNA 4-scaffold-EF1α-mtagBFP-H2Kk	cloned by Jan Philipp Schmid for this project
pCDH-H1-CD79A sgRNA 5-scaffold-EF1α-mtagBFP-H2Kk	cloned by Jan Philipp Schmid for this project
pCDH-H1-CD81 sgRNA 1-scaffold-EF1α-mtagBFP-H2Kk	cloned by Jan Philipp Schmid for this project
pCDH-H1-CD81 sgRNA 2-scaffold-EF1α-mtagBFP-H2Kk	cloned by Jan Philipp Schmid for this project
pCDH-H1-CD81 sgRNA 3-scaffold-EF1α-mtagBFP-H2Kk	cloned by Jan Philipp Schmid for this project
pCDH-H1-CD81 sgRNA 4-scaffold-EF1α-mtagBFP-H2Kk	cloned by Jan Philipp Schmid for this project
pCDH-H1-CD81 sgRNA 5-scaffold-EF1α-mtagBFP-H2Kk	cloned by Jan Philipp Schmid for this project
pCDH-H1-CXCR4 sgRNA 1-scaffold-EF1α-mtagBFP-H2Kk	cloned by Jan Philipp Schmid for this project
pCDH-H1-CXCR4 sgRNA 2-scaffold-EF1α-mtagBFP-H2Kk	cloned by Jan Philipp Schmid for this project
pCDH-H1-CXCR4 sgRNA 3-scaffold-EF1α-mtagBFP-H2Kk	cloned by Jan Philipp Schmid for this project
pCDH-H1-CXCR4 sgRNA 4-scaffold-EF1α-mtagBFP-H2Kk	cloned by Jan Philipp Schmid for this project

pCDH-H1-CXCR4 sgRNA 5-scaffold-EF1α-mtagBFP-H2Kk	cloned by Jan Philipp Schmid for this project
pCDH-H1-F11R sgRNA 1-scaffold-EF1α-mtagBFP-H2Kk	cloned by Jan Philipp Schmid for this project
pCDH-H1-F11R sgRNA 2-scaffold-EF1α-mtagBFP-H2Kk	cloned by Jan Philipp Schmid for this project
pCDH-H1-F11R sgRNA 3-scaffold-EF1α-mtagBFP-H2Kk	cloned by Jan Philipp Schmid for this project
pCDH-H1-F11R sgRNA 4-scaffold-EF1α-mtagBFP-H2Kk	cloned by Jan Philipp Schmid for this project
pCDH-H1-F11R sgRNA 5-scaffold-EF1α-mtagBFP-H2Kk	cloned by Jan Philipp Schmid for this project
pCDH-H1-ITGB1 sgRNA 1-scaffold-EF1α-mtagBFP-H2Kk	cloned by Jan Philipp Schmid for this project
pCDH-H1-ITGB1 sgRNA 2-scaffold-EF1α-mtagBFP-H2Kk	cloned by Jan Philipp Schmid for this project
pCDH-H1-ITGB1 sgRNA 3-scaffold-EF1α-mtagBFP-H2Kk	cloned by Jan Philipp Schmid for this project
pCDH-H1-ITGB1 sgRNA 4-scaffold-EF1α-mtagBFP-H2Kk	cloned by Jan Philipp Schmid for this project
pCDH-H1-ITGB1 sgRNA 5-scaffold-EF1α-mtagBFP-H2Kk	cloned by Jan Philipp Schmid for this project
pCDH-H1-POTEI sgRNA 1-scaffold-EF1α-mtagBFP-H2Kk	cloned by Jan Philipp Schmid for this project
pCDH-H1-POTEI sgRNA 2-scaffold-EF1α-mtagBFP-H2Kk	cloned by Jan Philipp Schmid for this project
pCDH-H1-POTEI sgRNA 3-scaffold-EF1α-mtagBFP-H2Kk	cloned by Jan Philipp Schmid for this project
pCDH-H1-POTEI sgRNA 4-scaffold-EF1α-mtagBFP-H2Kk	cloned by Jan Philipp Schmid for this project
pCDH-H1-POTEI sgRNA 5-scaffold-EF1α-mtagBFP-H2Kk	cloned by Jan Philipp Schmid for this project
pCDH-H1-SLC3A2 sgRNA 1-scaffold-EF1α-mtagBFP-H2Kk	cloned by Jan Philipp Schmid for this project
pCDH-H1-SLC3A2 sgRNA 2-scaffold-EF1α-mtagBFP-H2Kk	cloned by Jan Philipp Schmid for this project
pCDH-H1-SLC3A2 sgRNA 3-scaffold-EF1α-mtagBFP-H2Kk	cloned by Jan Philipp Schmid for this project
pCDH-H1-SLC3A2 sgRNA 4-scaffold-EF1α-mtagBFP-H2Kk	cloned by Jan Philipp Schmid for this project
pCDH-H1-SLC3A2 sgRNA 5-scaffold-EF1α-mtagBFP-H2Kk	cloned by Jan Philipp Schmid for this project
pCDH-H1-SLC19A1 sgRNA 1-scaffold-EF1α-mtagBFP-H2Kk	cloned by Jan Philipp Schmid for this project
pCDH-H1-SLC19A1 sgRNA 2-scaffold-EF1α-mtagBFP-H2Kk	cloned by Jan Philipp Schmid for this project
pCDH-H1-SLC19A1 sgRNA 3-scaffold-EF1α-mtagBFP-H2Kk	cloned by Jan Philipp Schmid for this project
pCDH-H1-SLC19A1 sgRNA 4-scaffold-EF1α-mtagBFP-H2Kk	cloned by Jan Philipp Schmid for this project
pCDH-H1-SLC19A1 sgRNA 5-scaffold-EF1α-mtagBFP-H2Kk	cloned by Jan Philipp Schmid for this project
pCDH-H1-TFRC sgRNA 1-scaffold-EF1α-mtagBFP-H2Kk	cloned by Jan Philipp Schmid for this project

pCDH-H1-TFRC sgRNA 2-scaffold-EF1α-mtagBFP-H2Kk	cloned by Jan Philipp Schmid for this project
pCDH-H1-TFRC sgRNA 3-scaffold-EF1α-mtagBFP-H2Kk	cloned by Jan Philipp Schmid for this project
pCDH-H1-TFRC sgRNA 4-scaffold-EF1α-mtagBFP-H2Kk	cloned by Jan Philipp Schmid for this project
pCDH-H1-TFRC sgRNA 5-scaffold-EF1α-mtagBFP-H2Kk	cloned by Jan Philipp Schmid for this project
pCDH-H1-scrambled sgRNA-scaffold-EF1α-T-Sapphire-H2Kk	cloned by Jan Philipp Schmid for this project
pCDH-SFFV-C-intein-C-Cas9-P2A-CC	cloned by Martin Becker
pCDH-SFFV-hspCas9wt-T2A-eGFP	cloned by Ehsan Bahrami
pCDH-SFFV-YN-N-Cas9-N-Intein	cloned by Martin Becker

2.10 Oligonucleotides and Primers

Table 14: Oligonucleotides for sgRNAs

Oligonucleotide	**Sequence 5' to 3'**
ADAM10-1F	tcccGCCCATAAATACGGTCCTCAG
ADAM10-2F	tcccGTTTCAACCTACGAATGAAGA
ADAM10-3F	tcccGTTCCATCAATAACAGACCCA
ADAM10-4F	tcccGCCGTTTCCCAAATATTGGTG
ADAM10-5F	tcccGGTAATGTGAGAGACTTTGGG
ADAM10-1R	aaacCTGAGGACCGTATTTATGGGC
ADAM10-2R	aaacTCTTCATTCGTAGGTTGAAAC
ADAM10-3R	aaacTGGGTCTGTTATTGATGGAAC
ADAM10-4R	aaacCACCAATATTTGGGAAACGGC
ADAM10-5R	aaacCCCAAAGTCTCTCACATTACC
CD79A-1F	tcccGGGATGATCAGCGTACCATTG
CD79A-2F	tcccGACCGAATCATCACAGCCGAG
CD79A-3F	tcccGTCCTCCATGGCAACTACACG
CD79A-4F	tcccGGAGTCATACCAGCAGTCCTG
CD79A-5F	tcccGAATGTGAACAAGAGCCATGG
CD79A-1R	aaacCAATGGTACGCTGATCATCCC
CD79A-2R	aaacCTCGGCTGTGATGATTCGGTC
CD79A-3R	aaacCGTGTAGTTGCCATGGAGGAC
CD79A-4R	aaacCAGGACTGCTGGTATGACTCC
CD79A-5R	aaacCCATGGCTCTTGTTCACATTC
CD81-1F	tcccGATGAGGATGTAGATGCCTTG
CD81-2F	tcccGCGGGTCATGGCGGAGCCACA
CD81-3F	tcccGTGATGACGCCAACAACGCCA
CD81-4F	tcccGGGCAAACAGGATGACCAGGC
CD81-5F	tcccGGTTGACAAAGCCCCAGATGC
CD81-1R	aaacCAAGGCATCTACATCCTCATC
CD81-2R	aaacTGTGGCTCCGCCATGACCCGC
CD81-3R	aaacTGGCGTTGTTGGCGTCATCAC
CD81-4R	aaacGCCTGGTCATCCTGTTTGCCC
CD81-5R	aaacGCATCTGGGGCTTTGTCAACC
CXCR4-1F	tcccGCAACCACCCACAAGTCATTG
CXCR4-2F	tcccGTGACATGGACTGCCTTGCAT
CXCR4-3F	tcccGCAGGACAGGATGACAATACC

CXCR4-4F	tcccGTCTTCTGGTAACCCATGACC
CXCR4-5F	tcccGAGGGAAGCGTGATGACAAAG
CXCR4-1R	aaacCAATGACTTGTGGGTGGTTGC
CXCR4-2R	aaacATGCAAGGCAGTCCATGTCAC
CXCR4-3R	aaacGGTATTGTCATCCTGTCCTGC
CXCR4-4R	aaacGGTCATGGGTTACCAGAAGAC
CXCR4-5R	aaacCTTTGTCATCACGCTTCCCTC
ITGB1-1F	tcccGTAGGCCTCTGGGCTTTACGG
ITGB1-2F	tcccGGAACGGGGTGAATGGAACAG
ITGB1-3F	tcccGTTGGCTGGAGGAATGTTACA
ITGB1-4F	tcccGAATGTAACCAACCGTAGCAA
ITGB1-5F	tcccGTACAAGCAGGGCCAAATTGT
ITGB1-1R	aaacCCGTAAAGCCCAGAGGCCTAC
ITGB1-2R	aaacCTGTTCCATTCACCCCGTTCC
ITGB1-3R	aaacTGTAACATTCCTCCAGCCAAC
ITGB1-4R	aaacTTGCTACGGTTGGTTACATTC
ITGB1-5R	aaacACAATTTGGCCCTGCTTGTAC
F11R-1F	tcccGTCAAACTTCCACTCCACACG
F11R-2F	tcccGTCACCTTCAAGTCCGTGACA
F11R-3F	tcccGTGTAACACTGCCCAATGCCA
F11R-4F	tcccGGAGGAGGGGATGTTAACTGT
F11R-5F	tcccGGGAAGGCGGCAACAGCTATG
F11R-1R	aaacCGTGTGGAGTGGAAGTTTGAC
F11R-2R	aaacTGTCACGGACTTGAAGGTGAC
F11R-3R	aaacTGGCATTGGGCAGTGTTACAC
F11R-4R	aaacACAGTTAACATCCCCTCCTCC
F11R-5R	aaacCATAGCTGTTGCCGCCTTCCC
POTEI-1F	tcccGAAGCACGGAAGTACTCACGT
POTEI-2F	tcccGATGCGCTGGATAGATATGGA
POTEI-3F	tcccGGTGGTATCTCGGCTCCACGA
POTEI-4F	tcccGGTAGATAGCGTAGTGTAGAG
POTEI-5F	tcccGACTCCACTATGAAGACACTC
POTEI-1R	aaacACGTGAGTACTTCCGTGCTTC
POTEI-2R	aaacTCCATATCTATCCAGCGCATC
POTEI-3R	aaacTCGTGGAGCCGAGATACCACC
POTEI-4R	aaacCTCTACACTACGCTATCTACC
POTEI-5R	aaacGAGTGTCTTCATAGTGGAGTC
SLC3A2-1F	tcccGCAGGCCCGTGAACTTAGCCG
SLC3A2-2F	tcccGTGAGTGGCAAAATATCACCA
SLC3A2-3F	tcccGGCGCAGAAGTGGTGGCACAC
SLC3A2-4F	tcccGAGAACCACGAGTTCTCACCC
SLC3A2-5F	tcccGGTCTGATTCTGGTTCTACTG
SLC3A2-1R	aaacCGGCTAAGTTCACGGGCCTGC
SLC3A2-2R	aaacTGGTGATATTTTGCCACTCAC
SLC3A2-3R	aaacGTGTGCCACCACTTCTGCGCC
SLC3A2-4R	aaacGGGTGAGAACTCGTGGTTCTC
SLC3A2-5R	aaacCAGTAGAACCAGAATCAGACC
SLC19A1-1F	tcccGCGACTACCTGCGCTACACGC
SLC19A1-2F	tcccGGGCCCGACAAGAACTTCACG
SLC19A1-3F	tcccGTCTTCAACCGCGACGACCGG
SLC19A1-4F	tcccGGGAGGAATAGGCGATGCGCG
SLC19A1-5F	tcccGGGGCTTCGTGAAGATCCGCT
SLC19A1-1R	aaacGCGTGTAGCGCAGGTAGTCGC

SLC19A1-2R	aaacCGTGAAGTTCTTGTCGGGCCC
SLC19A1-3R	aaacCCGGTCGTCGCGGTTGAAGAC
SLC19A1-4R	aaacCGCGCATCGCCTATTCCTCCC
SLC19A1-5R	aaacAGCGGATCTTCACGAAGCCCC
TFRC-1F	tcccGGAATACCTCTAGCCATTCAG
TFRC-2F	tcccGCTATACGCCACATAACCCCC
TFRC-3F	tcccGGGAGCTGCAAAATCCGGTGT
TFRC-4F	tcccGAAATTCATATGTCCCTCGTG
TFRC-5F	tcccGAATTGGTGTGTTGATATACA
TFRC-1R	aaacCTGAATGGCTAGAGGTATTCC
TFRC-2R	aaacGGGGGTTATGTGGCGTATAGC
TFRC-3R	aaacACACCGGATTTTGCAGCTCCC
TFRC-4R	aaacCACGAGGGACATATGAATTTC
TFRC-5R	aaacTGTATATCAACACACCAATTC

All sgRNAs were ordered from Sigma Aldrich (St. Louis, USA).

Table 15: crRNAs for RNPs

crRNA	Sequence 5’ to 3’
Alt-R CRISPR-Cas9 crRNA ADAM10 sg1	CCCAUAAAUACGGUCCUCAGGUUUUAGAGCUAUGCU
Alt-R CRISPR-Cas9 crRNA ADAM10 sg3	UUCCAUCAAUAACAGACCCAGUUUUAGAGCUAUGCU
Alt-R CRISPR-Cas9 crRNA ADAM10 sg5	GUAAUGUGAGAGACUUUGGGGUUUUAGAGCUAUGCU
Alt-R CRISPR-Cas9 crRNA non-targeting	ACGGAGGCUAAGCGUCGCAAGUUUUAGAGCUAUGCU

All crRNAs were ordered from IDT (Leuven, Belgium).

Table 16: Primers

Application	Primer	Sequence 5’ to 3’
Cloning	ADAM10-cCDN-Age-F	CACACCGTCCACCATGGTGTTGCTGAGAGTGTTA
Cloning	ADAM10-cCDN-Xho-R	CCACTCGAGTTACAGCAGGTCCTCCTCGCTGATC
Cloning	iRFP-Bam-F	AAGTCGACTCACTTGTACAGCTCGTCCATGC
Cloning	iRFP-Sal-R	AAGGATCCATGGTGAGCAAGGGCGAGGA
Cloning	T-Saph-Bam-F	AAGGATCCATGGCTGAAGGCTCCGTAGC
Cloning	T-Saph-Sal-R	AAGTCGACTCACTCTTCCATCACGCCGAT
qPCR	ADAM10-CisR-q-F	TGTGCCAGTTCTGATGGCAA
qPCR	ADAM10-CisR-q-R	ATCCAGGTTGCAGGGTGATG
qPCR	ADAM10_qPCR_F	TTACGGAACACGAGAAGCTG (probe 61)
qPCR	ADAM10_qPCR_R	AAACGGAAAGGATTTGTAGGG (probe 61)
qPCR	GAPDH-fw	GAGAGAAACCCGGGAGGCTA
qPCR	GAPDH-rev	CCCATGGTGTCTGAGCGATG
qPCR	GAPDH_qPCR_F	CTCTGCTCCTCCTGTTCGAC (probe 60)
qPCR	GAPDH_qPCR_R	ACGACCAAATCCGTTGACTC (probe 60)
qPCR	HPRT-fw	TGCAGACTTTGCTTTCCTTGGT
qPCR	HPRT-rev	CGTGGGGTCCTTTTCACCAG
Sequencing	AD10_C-terminal_R	CTGACGCTGGGGTTGCTGAAT
Sequencing	AD10_cysteine_R	ATCCAGGTTGCAGGGTGATG
Sequencing	EF1_seq_new_F	TTCTGCGCCGTTACAGATCCAA

Sequencing	iRFP2-fwd	CGATTGATCTTAGCTTCGCCATCC
Sequencing	Seq_fwd_pCDH-EF1	TTTGCCTGACCCTGCTTG
Sequencing	T-Sapphire_seq_R	CAGCTTGGACTGGATGCTCA
Sequencing	WPRE-REV	CATAGCGTAAAAGGAGCAACA

All primers were ordered from Sigma Aldrich (St. Louis, USA).

Table 17: NGS Primers

Primer	Sequence 5' to 3'
cppt-NGS-F	GGGTACAGTGCAGGGGAAAGAATA
EF1a-NGS-R	GAGCCAGTACACGACATCACTTTCC
P5-H1-S0	AATGATACGGCGACCACCGAGATCTACACTCTTTCCCTACAC GACGCTCTTCCGATCTTGTATGAGACCACTCTTTCCCG
P5-H1-S1	AATGATACGGCGACCACCGAGATCTACACTCTTTCCCTACACG ACGCTCTTCCGATCTCTGTATGAGACCACTCTTTCCCG
P5-H1-S2	AATGATACGGCGACCACCGAGATCTACACTCTTTCCCTACACG ACGCTCTTCCGATCTGCTGTATGAGACCACTCTTTCCCG
P5-H1-S3	AATGATACGGCGACCACCGAGATCTACACTCTTTCCCTACACGA CGCTCTTCCGATCTAGCTGTATGAGACCACTCTTTCCCG
P5-H1-S4	AATGATACGGCGACCACCGAGATCTACACTCTTTCCCTACACGA CGCTCTTCCGATCTCAACTGTATGAGACCACTCTTTCCCG
P5-H1-S5	AATGATACGGCGACCACCGAGATCTACACTCTTTCCCTACACGA CGCTCTTCCGATCTTGCACCTGTATGAGACCACTCTTTCCCG
P5-H1-S6	AATGATACGGCGACCACCGAGATCTACACTCTTTCCCTACACGA CGCTCTTCCGATCTACGCAACTGTATGAGACCACTCTTTCCCG
P5-H1-S7	AATGATACGGCGACCACCGAGATCTACACTCTTTCCCTACACGA CGCTCTTCCGATCTGAAGACCCTGTATGAGACCACTCTTTCCCG
P7-Ef1-A01	CAAGCAGAAGACGGCATACGAGATCGGTTCAAGTGACTGGAGTTCA GACGTGTGCTCTTCCGATCTGAGCCAGTACACGACATCACTTTC
P7-Ef1-A11	CAAGCAGAAGACGGCATACGAGATATTGTCAAGTGACTGGAGTTCAGACG TGTGCTCTTCCGATCTGAGCCAGTACACGACATCACTTTC
P7-Ef1-A12	CAAGCAGAAGACGGCATACGAGATTATGTCTTGTGACTGGAGTTCAGACG TGTGCTCTTCCGATCTGAGCCAGTACACGACATCACTTTC
P7-Ef1-B01	CAAGCAGAAGACGGCATACGAGATATTGGATTGTGACTGGAGTTC AGACGTGTGCTCTTCCGATCTGAGCCAGTACACGACATCACTTTC
P7-Ef1-B02	CAAGCAGAAGACGGCATACGAGATATACTCGGGTGACTGGAGTTCA GACGTGTGCTCTTCCGATCTGAGCCAGTACACGACATCACTTTC
P7-Ef1-B03	CAAGCAGAAGACGGCATACGAGATTATGAGAAGTGACTGGAGTTCA GACGTGTGCTCTTCCGATCTGAGCCAGTACACGACATCACTTTC
P7-Ef1-B04	CAAGCAGAAGACGGCATACGAGATGCACAGTTGTGACTGGAGTTCA GACGTGTGCTCTTCCGATCTGAGCCAGTACACGACATCACTTTC
P7-Ef1-B05	CAAGCAGAAGACGGCATACGAGATCGTGGATTGTGACTGGAGTTCA GACGTGTGCTCTTCCGATCTGAGCCAGTACACGACATCACTTTC
P7-Ef1-B11	CAAGCAGAAGACGGCATACGAGATATCACTGGGTGACTGGAGTTC AGACGTGTGCTCTT CCGATCTGAGCCAGTACACGACATCACTTTC
P7-Ef1-B12	CAAGCAGAAGACGGCATACGAGATCGCATCAAGTGACTGGAGTTC AGACGTGTGCTCTT CCGATCTGAGCCAGTACACGACATCACTTTC
P7-Ef1-C01	CAAGCAGAAGACGGCATACGAGATGCACGACCGTGACTGGAGTT CAGACGTGTGCTCTTCCGATCTGAGCCAGTACACGACATCACTTTC
P7-Ef1-C02	CAAGCAGAAGACGGCATACGAGATTACACTCCGTGACTGGAGTTC AGACGTGTGCTCTTCCGATCTGAGCCAGTACACGACATCACTTTC

P7-Ef1-C03	CAAGCAGAAGACGGCATACGAGATCGGTCTAAGTGACTGGAGTT CAGACGTGTGCTCTTCCGATCTGAGCCAGTACACGACATCACTTTC
P7-Ef1-C04	CAAGCAGAAGACGGCATACGAGATATGTTCGGGTGACTGGAGTT CAGACGTGTGCTCTT CCGATCTGAGCCAGTACACGACATCACTTTC
P7-Ef1-C05	CAAGCAGAAGACGGCATACGAGATCGTGGACCGTGACTGGAGTT CAGACGTGTGCTCTTCCGATCTGAGCCAGTACACGACATCACTTTC
P7-Ef1-C06	CAAGCAGAAGACGGCATACGAGATATTGAGCCGTGACTGGAGTT CAGACGTGTGCTCTTCCGATCTGAGCCAGTACACGACATCACTTTC
P7-Ef1-C07	CAAGCAGAAGACGGCATACGAGATTAGTTCGGGTGACTGGAGTT CAGACGTGTGCTCTTCCGATCTGAGCCAGTACACGACATCACTTTC
P7-Ef1-C08	CAAGCAGAAGACGGCATACGAGATCGGTGAGGGTGACTGGAGTT CAGACGTGTGCTCTTCCGATCTGAGCCAGTACACGACATCACTTTC
P7-Ef1-C09	CAAGCAGAAGACGGCATACGAGATCGTGAGTTGTGACTGGAGTTC AGACGTGTGCTCTTCCGATCTGAGCCAGTACACGACATCACTTTC
P7-Ef1-C10	CAAGCAGAAGACGGCATACGAGATATCAGATTGTGACTGGAGTTC AGACGTGTGCTCTTCCGATCTGAGCCAGTACACGACATCACTTTC
P7-Ef1-C11	CAAGCAGAAGACGGCATACGAGATTAGTGATTGTGACTGGAGTTC AGACGTGTGCTCTTCCGATCTGAGCCAGTACACGACATCACTTTC
P7-Ef1-C12	CAAGCAGAAGACGGCATACGAGATCGGTTCGGGTGACTGGAGTTC AGACGTGTGCTCTTCCGATCTGAGCCAGTACACGACATCACTTTC
P7-Ef1-E05	CAAGCAGAAGACGGCATACGAGATGCGTTCAAGTGACTGGAGTTC AGACGTGTGCTCTTCCGATCTGAGCCAGTACACGACATCACTTTC
P7-Ef1-E06	CAAGCAGAAGACGGCATACGAGATCGCAAGAAGTGACTGGAGTTCAGAC GTGTGCTCTTCCGATCTGAGCCAGTACACGACATCACTTTC
P7-Ef1-E07	CAAGCAGAAGACGGCATACGAGATCGACAGCCGTGACTGGAGTTCAGAC GTGTGCTCTTCCGATCTGAGCCAGTACACGACATCACTTTC
P7-Ef1-E08	CAAGCAGAAGACGGCATACGAGATCGACTCGGGTGACTGGAGTTCAGAC GTGTGCTCTTCCGATCTGAGCCAGTACACGACATCACTTTC
P7-Ef1-E09	CAAGCAGAAGACGGCATACGAGATTACAAGAAGTGACTGGAGTTCA GACGTGTGCTCTTCCGATCTGAGCCAGTACACGACATCACTTTC
P7-Ef1-E10	CAAGCAGAAGACGGCATACGAGATCGCAGATTGTGACTGGAGTTC AGACGTGTGCTCTT CCGATCTGAGCCAGTACACGACATCACTTTC
P7-Ef1-E11	CAAGCAGAAGACGGCATACGAGATATTGCTCCGTGACTGGAGTTC AGACGTGTGCTCTT CCGATCTGAGCCAGTACACGACATCACTTTC
P7-Ef1-E12	CAAGCAGAAGACGGCATACGAGATGCACTCGGGTGACTGGAGTT CAGACGTGTGCTCTT CCGATCTGAGCCAGTACACGACATCACTTTC
P7-Ef1-F01	CAAGCAGAAGACGGCATACGAGATATGTTCTTGTGACTGGAGTTC AGACGTGTGCTCTT CCGATCTGAGCCAGTACACGACATCACTTTC
P7-Ef1-F02	CAAGCAGAAGACGGCATACGAGATATGTCTCCGTGACTGGAGTT CAGACGTGTGCTCTT CCGATCTGAGCCAGTACACGACATCACTTTC
P7-Ef1-F03	CAAGCAGAAGACGGCATACGAGATGCACTCAAGTGACTGGAGTT CAGACGTGTGCTCTT CCGATCTGAGCCAGTACACGACATCACTTTC
P7-Ef1-F04	CAAGCAGAAGACGGCATACGAGATTAGTAGCCGTGACTGGAGTT CAGACGTGTGCTCTT CCGATCTGAGCCAGTACACGACATCACTTTC
P7-Ef1-F05	CAAGCAGAAGACGGCATACGAGATTAGTAGCCGTGACTGGAGTT CAGACGTGTGCTCTT CCGATCTGAGCCAGTACACGACATCACTTTC
P7-Ef1-F06	CAAGCAGAAGACGGCATACGAGATGCGTTCTTGTGACTGGAGTT CAGACGTGTGCTCTT CCGATCTGAGCCAGTACACGACATCACTTTC
P7-Ef1-F07	CAAGCAGAAGACGGCATACGAGATGCCAAGCCGTGACTGGAGTT CAGACGTGTGCTCTTCCGATCTGAGCCAGTACACGACATCACTTTC

All primers were ordered from Sigma Aldrich (St. Louis, USA).

2.11 Consumables

Table 18: Consumables

Consumable	Manufacturer
12-230 kDa Wes Separation Module	Proteinsimple (San Jose, USA)
4–20% Mini-PROTEAN® TGX™ Precast Protein Gels, 15-well, 15 µl	Bio-Rad (München, Germany)
Amicon-Ultra 15ml centrifugal filter units	Merck Millipore (Darmstadt, Germany)
Bacterial tubes	Corning (Corning, USA)
BD microfine 1ml syringe	BD Bioscience (Heidelberg, Germany)
Blunt-End Needles, 16 Gauge	Stemcell Technologies (Vancouver, Canada)
Cell culture EasyFlask T75	Thermo Fisher Scientific (Waltham, USA)
Cell culture flasks (T25, T75)	Greiner bio-one (Kremsmünster, Germany)
Cell strainer (70µm)	Greiner bio-one (Kremsmünster, Germany)
Cell strainer (30µm, 70µm)	Miltenyi (Bergisch Gladbach, Germany)
Cryotubes	Thermo Fisher Scientific (Waltham, USA)
Disposable serological pipettes	Greiner bio-one (Kremsmünster, Germany)
Eppendorf reagent tubes	Greiner bio-one (Kremsmünster, Germany)
Erlenmeyer flasks	SCHOTT AG, Mainz, Germany
FACS tubes (with and without filter)	Corning (Corning, USA)
Filterunit Millex-HV 0.45 µm	Merck Millipore (Darmstadt, Germany)
LightCycler 480 Multiwell plate 96	Roche (Mannheim, Germany)
LS columns	Miltenyi (Bergisch Gladbach, Germany)
MethoCult™ H4034 Optimum	Stemcell Technologies (Vancouver, Canada)
Omnifix® Luer Solo (3, 5, 20 ml)	B. Braun SE (Melsungen, Germany)
Needles RN G32 PST3 51MM	Hamilton (Reno, USA)
Nitrile gloves	Starlab (Hamburg, Germany)
PCR tubes	Sigma Aldrich (St. Louis, USA)
Petri dishes	Greiner bio-one (Kremsmünster, Germany)
Pipette tips (with and without filter)	Starlab (Hamburg, Germany)
QiaShredder	Qiagen (Hilden, Germany)
Sealing Foil for LightCycler 480	Roche (Mannheim, Germany)
SmartDish™	Stemcell Technologies (Vancouver, Canada)
SuperSignal™ West Femto Maximum Sensitivity Substrate	Fisher Scientific GmbH (Schwerte, Germany)
Surgical disposable scalpel	Braun (Melsungen, Germany)
Well plates for tissue culture (6, 12, 24, 48, 96)	Corning (Corning, USA)

2.12 Devices and equipment

Table 19: Devices and eqipment

Device / equipment	Manufacturer
4D-Nucleofector	Lonza Group, Basel, Switzerland
B 6060 microbiological incubator	Heraeus (Hanau, Germany)
Bioanalyzer 2100	Agilent Technologies (Santa Clara, USA)
Biological safety cabinet Safe 2020	Thermo Fisher Scientific (Waltham, USA)

Calibration check pH meter HI 221	Hanna Instruments Deutschland GmbH (Vöhringen, Germany)
Cell sorter BD FACS AriaIII	BD Biosciences (San Jose, USA)
Centrifuge Rotanta 460R	Andreas Hettich GmbH & Co.KG (Tuttlingen, Germany)
Cryotube label printer BMP51	Brady (Egelsbach, Germany)
BD FACS AriaIII	BD Biosciences (Heidelberg, Germany)
BD LSRFortessa X20	BD Biosciences (Heidelberg, Germany)
Freezer (−20◦C)	Siemens (Berlin, Germany)
Freezer (−80◦C)	Thermo Fisher Scientific (Waltham, USA)
Fusion FX	Vilber Lourmat GmbH (Eberhardzell, Germany)
Gel documentation station E-box VX5	Peqlab (Erlangen, Germany)
Heating block MixerHC	Starlab (Hamburg, Germany)
Illumina HiSeq 2000	Illumina (San Diego, USA)
Illumina HiSeq 4000	Illumina (San Diego, USA)
Illumina NovaSeq 6000	Illumina (San Diego, USA)
Incubator Hera Cell 150i	Heraeus (Hanau, Germany)
IVIS Lumina II Imaging System	Caliper Life Sciences (Mainz, Germany)
Leica TCS SP5 confocal microscope	Leica Mikrosysteme Vertrieb GmbH (Wetzlar, Germany)
LightCycler-® 480 Instrument II	Roche (Mannheim, Germany)
Light microscope 550 1317	Zeiss (Jena, Germany)
Magnetic stirrer MR3001	Heidolph Instruments (Schwabach, Germany)
Micro Scales Artorius 2001 MP2	Sartorius AG (Göttingen, Germany)
Microwave MW 1226CB	Bomann (Kempen, Germany)
Mini-PROTEAN Tetra Vertical Electrophoresis Cell	Bio-Rad (München, Germany)
MACSmix Tube Rotator	Miltenyi (Bergisch Gladbach, Germany)
MiSeq Sequencer	Illumina (San Diego, USA)
MultiMACS™ Cell24 Separator Plus	Miltenyi (Bergisch Gladbach, Germany)
Nanodrop OneC	Thermo Fisher Scientific (Waltham, USA)
Pellet bath	Memmert (Schwabach, Germany)
PerfectBlue Gelsystem Mini S	Peqlab (Erlangen, Germany)
Power supply PowerPac	Bio-Rad (München, Germany)
Primovert	Zeiss (Jena, Germany)
ProFlex PCR system	Life Technologies (Carlsbad, USA)
QuadroMACS™ Separator	Miltenyi (Bergisch Gladbach, Germany)
Refrigerator	Liebherr (Bulle, Germany)
Roller mixer SRT6D	Stuart (Staffordshire, UK)
STEMgrid™-6	Stemcell Technologies (Vancouver, Canada)
Table Centrifuge mini Spin	Eppendorf (Hamburg, Germany)
Trans-Blot Turbo Cassette	Bio-Rad (München, Germany)
Trans-Blot® Turbo™ Transfer System	Bio-Rad (München, Germany)
Wes by Protein Simple	ProteinSimple (San Jose, USA)

2.13 Commercial Kits

Table 20: Commercial Kits

Kit	Manufacturer
BCA Protein Assay Kit	Cell Signaling Technology (Boston, USA)
CloneJET PCR cloning Kit	Thermo Fisher Scientific (Waltham, USA)
DNeasy Blood & Tissue Kit	Qiagen (Hilden, Germany)
FIX & PERM Cell Fixation & Cell Permeabilization Kit	Thermo Fisher Scientific (Waltham, USA)
MinElute PCR purification kit	Qiagen (Hilden, Germany)
NucleoBond Xtra Maxi Kit	Macherey-Nagel (Düren, Germany)
NucleoBond Xtra Midi Kit	Macherey-Nagel (Düren, Germany)
NucleoSpin Gel and PCR Clean-Up	Macherey-Nagel (Düren, Germany)
NuleoSpin Plasmid Easy Pure	Macherey-Nagel (Düren, Germany)
P3 Primary Cell 4D-Nucleofector® X Kit L	Lonza Group, Basel, Switzerland
QIAamp DNA Blood Mini Kit	Qiagen (Hilden, Germany)
QIAamp DNA mini kit	Qiagen (Hilden, Germany)
QIAquick PCR Purification Kit	Qiagen (Hilden, Germany)
QuantiTect Reverse Transcription kit	Qiagen (Hilden, Germany)
RNase-free DNase Set	Qiagen (Hilden, Germany)
RNeasy Micro Kit	Qiagen (Hilden, Germany)
RNeasy Mini Kit	Qiagen (Hilden, Germany)
Trans-Blot Turbo RTA Mini 0.2 µm PVDF Transfer Kit	Bio-Rad (München, Germany)

2.14 Software

Table 21: Software

Software	Provider
Compass for SW 4.0.0	ProteinSimple (San Jose, USA)
Cytoscape 3	open source
Endnote 20	Alfasoft GmbH, Frankfurt am Main, Germany
FlowJo 10	FlowJo LLC (Ashley, USA)
GraphPad Prism 9	Graphpad Prism (La Jolla, USA)
Living Image Software 4.4	PerkinElmer (Krakow, Poland)
LightCycler 480 software 1.5.1	Roche, Mannheim, Germany
Microsoft Office 2019	Microsoft Corporation (Tulsa, USA)
MyIMouse	Bioslava (Hagenbach, Germany)
R version 4	open source

3 Methods

3.1 Ethical Statements:

3.1.1 Patient material:

The written consent of all patients or the consent of their parents/carers in case of minors was obtained. The experiments for this project were conducted according to the ethical standards of the responsible committee on human experimentation (written approval by Ethikkommission des Klinikums der Ludwig-Maximilians-Universität München, Ethikkommission@med.unimuenchen.de, April 2008 and September 2012, number 068-08 and 222-10, respectively) and in concordance with the Helsinki Declaration of 1975, as revised in 2013.
ALL and AML patient's cells for this project were obtained from residual bone marrow aspirates or peripheral blood samples of routine diagnostics in the clinic between diagnosis of primary disease or relapse and treatment start.

3.1.2 Animal trials:

All experiments or trials involving animals were conducted according to the most recent ethical standards of the official committee on animal experimentation (written approval by Regierung von Oberbayern, ROB-55.2Vet-2532.Vet_02-15-193, ROB-55.2Vet-2532.Vet_03-16-56, and ROB-55.2Vet-2532.Vet_02-16-7, ROB-55.2-2532.Vet_02-20-159, ROB-55.2-2532.Vet_0321-9).

3.2 Patient-derived xenograft (PDX) models of acute leukemia:

3.2.1 Animal Model:

Female and male six to 16 weeks old NOD.Cg-Prkdc^{scid}Il2rg^{tm1Wjl}/SzJ (NSG) mice (The Jackson Laboratory, Bar Harbour, USA) were utilized for this study. Mice were maintained with a 12h light-dark cycle, 45–65% humidity, a temperature of 20–24 °C and under specified pathogen-free (SPF) conditions in accordance with Annex A of the European Convention 2007/526 EC. Animals were kept with unlimited water and food access. Structural enrichment was always available in the cages, while their maximum stocking density was in concordance with Annex III of the 2010/63 EU. All animals were maintained in held ventilated cages (IVCs). According to the most recent FELASA recommendation hygiene monitoring was conducted at least quarterly.

3.2.2 Establishment of PDX models:

ALL and AML PDX models were generated as previously described (Ebinger et al., 2016). Primary patient cells were injected into the tail vein of mice. After successful engraftment, tumor growth was monitored (see below) and PDX cells were isolated from murine BM and spleen of animals with an advanced stage of leukemia for serial re-transplantation or genetic engineering of the respective PDX model. Stable expression of transgenes like Luciferase, split-Cas9, different marker proteins, shRNA and sgRNA constructs enables addressing of various experimental questions within the PDX model, which is highly representative of the primary patient's tumor.

3.2.3 Monitoring of the leukemic burden in the peripheral blood of mice:

Engraftment and growth of leukemia cells in the animals is controlled by sampling of 50 µl peripheral blood from the tail vein every one to two weeks starting two weeks before the typical advanced leukemia stage of each individual sample is reached, in line with their growth kinetics. ALL blood samples were stained for human CD38 and murine CD45, while AML samples were stained using human CD45 and human CD33. Stained samples were measured using flow cytometry and PDX cell engraftment and growth was monitored by analyzing the flow cytometry data.

3.2.4 *In vivo* bioluminescence imaging:

PDX cells stably expressing a codon optimized form of the eFFly Luciferase were generated, enabling *in vivo* bioluminescence imaging (BLI) as previously described (Barrett et al., 2011; Bomken et al., 2013; Rabinovich et al., 2008; Terziyska et al., 2012). Mice were anesthetized using isoflurane and bioluminescence signal was quantified in living mice utilizing an IVIS Lumina II (Perkin Elmer) after i.v. injection. 150 mg/kg D-Luciferin (BIOMOL GmbH, Hamburg, Germany) was used and the signal was measured directly for 30 to 120 seconds using a 12.5 cm field of view, binning 8, f/stop 1 and open filter setting and the measurement was quantified using Living Image Software (Caliper Life Sciences, Mainz, Germany). The entire mouse was included in the region of interest and total flux calculated. Pictures and values were always depicted in a logarithmic scale.

3.2.5 Experimental endpoints:

If not stated otherwise, experimental and donor mice utilized for the amplification of PDX cells were sacrificed at an advanced stage of leukemia, which was monitored using peripheral blood

sampling and/or *in vivo* bioluminescent imaging (see above). Additionally, mice were sacrificed in case of apparent early symptoms of sickness (e.g., reduced motility, paralysis, hunchback or rough fur). 20 to 25 weeks after injection of the cells, animals were sacrificed if no clinical signs of leukemic disease or PDX engraftment (blood sampling, *in vivo* imaging) could be observed. This was again controlled by performing flow cytometry analysis on isolated BM cells. During treatment trials, animals were sacrificed upon therapy-related toxicity if they lost more than 15% of body weight. Exclusion of mice with leukemia-unrelated symptoms or anomalies was stated in the respective legend. Cervical dislocation was utilized as method of choice for sacrificing animals.

3.2.6 Isolating PDX cells from the bone marrow:

Murine spine, sternum, hip, femora, tibiae and fibulae were isolated from the sacrificed animals and smashed with mortar and pestle. Cells were filtered in order to remove residual pieces of bone and debris and washed once (5 min, 400 g @RT), before lysing the red blood cells. Following three additional washing steps, cells were resuspended depending on the downstream application either in PBS, a corresponding cell culture medium or a buffer of choice.

3.2.7 Isolating PDX cells from the spleen:

Enlargement of the spleen can be observed for many ALL and some AML samples at a well-advanced stage of leukemia. The spleen of these animals was isolated and smashed within a 70 µm cell strainer using the backside of a plunger of a syringe. The suspension was filled up to 10 ml using PBS and 4 ml Ficoll is sub-layered to efficiently separate the different cell types by centrifugation (30 min, 400 g @RT without brake). PDX cells were recovered from the interphase layer using aspiration. Following two additional washing steps, cells were resuspended as describe above.

3.2.8 *In vivo* competitive assay:

An sgRNA targeting either the gene of interest or a non-targeting control sgRNA was stably integrated into Cas9-expressing PDX cells using lentiviral transduction. GOI sgRNA expression was coupled to H-2K^{k}-BFP expression, while H-2K^{k}-T-Sapphire expression was coupled to control sgRNA expression. Maintaining the transduced PDX cells *in vitro* for 7-10 days allowed the establishment of the KO of the targeted gene. Cells of the control and KO population were checked by flow cytometry, mixed in a 1:1 ratio and injected into mice. At an advanced stage of leukemia, the mice were sacrificed and the isolation of PDX cells from BM

and spleen was conducted as described above. Using comparative flow cytometry analysis, the distribution of the control and the KO population was determined.

3.2.9 Early engraftment and homing assay:

Early engraftment capacity of different groups of PDX cells was investigated by injecting 10^7 cells per mouse, sacrificing the animals three days after injection, isolating cells from the BM and measuring the absolute number as well as the percentage of human cells within the BM utilizing flow cytometry. In order to elucidate the effect of chemical inhibition of ADAM10 on the early engraftment capacity of PDX cells, in the treatment group Cas9-positive cells were incubated *ex vivo* with a chemical inhibitor of ADAM10 (GI254023X (100 µM; Absource, Germany) or Aderbasib (100 µM; MedChemExpress, USA)) while the control group was treated with solvent (DMSO, Thermo Fisher Scientific, USA) for two to three days before injection.

3.2.10 Competitive *in vivo* treatment trials:

PDX cells from the *in vivo* competitive assays were sorted from the two populations and either injected to donor mice or directly used for the treatment trial. In order to start with a close to 1:1 ratio upon start of therapy (SOT), ADAM10 KO cells were injected in excess (3:1 to 4:1) to the control cells. Leukemia growth was followed by *in vivo* imaging. At a defined tumor load, treatment of the animals with a chemotherapeutic agent or the solvent control was started. After two weeks of treatment, animals of all groups were sacrificed and PDX cells were isolated from BM and spleen. The percentage of human cells and the distribution of the ADAM10 KO and the control population was determined using flow cytometry. A summary of the performed competitive treatment trials is depicted in the table below (Table 22).

Table 22: Overview of used drugs in competitive *in vivo* treatment trials

PDX sample	Drug dosage & route of admission	Treatment schedule
ALL-265	Cyclophosphamide 70 mg/kg, i.p.	1 per week, 2 weeks
ALL-265	Vincristine 0.3 mg/kg, i.v.	1 per week, 2 weeks
AML-661	Cytarabine 100 mg/kg, i.p.	4 per week, 2 weeks

3.2.11 Competitive limiting dilution transplantation assay (LDTA):

PDX cells were isolated from sacrificed donor animals and counted three times independently using the Neubauer counting chamber. In this competitive setting of the LDTA, control and ADAM10 KO cells were mixed in a 1:1 ratio, which was checked using flow cytometry. This

mix was then serially diluted to the desired cell numbers of each group and injected into mice. Successful engraftment and leukemia growth were observed by *in vivo* bioluminescence imaging. When an advanced stage of leukemia was reached for the high cell number groups monitored by *in vivo* imaging, all animals were sacrificed and the cells re-isolated from the BM. Using flow cytometry, the distribution of the ADAM10 KO and the control population was measured and analyzed utilizing the FlowJo software (FlowJo™ Software, version 10.7, Ashland, USA). Positive engraftment was defined as 1% of the respective population within the BM, while the associated LIC frequencies were calculated with the help of the ELDA software (http://bioinf.wehi.edu.au/software/elda/index.html).

3.2.12 Labeling PDX cells using a proliferation dye:

For this project a far-red proliferation dye (CellTraceTM Far Red – Cell proliferation kit, Thermo Fisher Scientific, USA) was used for the labelling of PDX cells similarly as previously described for the usage of CFSE (Ebinger et al., 2016), as CFSE is not compatible with the Cas9-GFP expressing cells used here. PDX cells were retrieved from sacrificed donor animals and labeled according to the manufacturer's protocol. Cells were washed using PBS to remove excessive dye before injection into recipient animals. Per mouse the maximal number of 10^7 was injected, in order to enable the retrieval of the highest number of label-retaining cells (LRCs) feasible.

3.2.13 Enrichment of LRC PDX cells from the murine BM using flow cytometry:

Similarly as previously described (Ebinger et al., 2016), PDX cells were retrieved from the murine BM, washed and filtered. Magnetic beads (Mouse Cell Depletion Kit, Miltenyi Biotech, Bergisch Gladbach, Germany) were utilized to diminish the number of murine cells with slight adaptations to the manufacturer's protocol using a reduced volume of 200 µl MicroBeads and two LS columns per mouse. The LRC and non-LRC cell population was enriched via flow cytometry. Events were gated for lymphocytes and singlets by FSC/SSC, for human cells using mCherry (EFFly Luciferase) and GFP (Cas9). Purity settings were utilized to enrich LRC and non-LRC cell populations with the FACSAriaIII device based on the intensity of the proliferation dye. In order to quantify LRCs and non-LRCs, a portion of labeled cells was kept *ex vivo* for 48 hours. Intensity of the far-red proliferation dye was measured and the mean fluorescence intensity (MFI) defined as zero divisions. This MFI value was then step-wise divided by two to simulate cell divisions. Slow-cycling LRCs were defined as cells with less than three divisions, while fast-cycling non-LRCs must have undergone at least seven divisions.

3.2.14 CRISPR/Cas9 KO screens in PDX models:

PDX cells expressing Cas9 were isolated from sacrificed donor animals and lentivirally transduced with a customized surface molecule library at a multiplicity of infection (MOI) lower than 0.3, producing mainly single integrations. The sgRNA constructs comprised in the library carried a H-2K^k-mTagBFP fusion protein, which enabled measuring the transduction efficiency via flow cytometry as well as enrichment of library-positive PDX cells via magnetic beads three days post transduction. An additional *in vitro* culturing period allowed an established KO of the targeted gene before injection of the cells to the animals. This approach was chosen to also detect genes important for the early engraftment and homing of the leukemic cells into the BM. Tumor growth after injection was monitored by blood measurement. Animals were sacrificed at an advanced stage of leukemia and cells were re-isolated from spleen and BM as described above.

3.2.15 Calculation of the size of customized sgRNA libraries:

Aiming on being able to recover the whole library from a single animal, the maximum number of genes within the library was calculated based on sample-specific LIC frequencies (~1% for the used ALL-199 and ALL-265), the maximum number of cells, which can be injected into one mouse (10^7), the usage of five sgRNAs targeting each gene and a sgRNA fold coverage of 200 cells per sgRNA using the following general formula:

$$\frac{\text{injected cell number} \times \text{sample-specific engraftment efficiency}}{\text{number of cells harboring each sgRNA} \times \text{number of sgRNAs targeting each gene}}$$

Entering the pre-defined values for the surface molecule library used in this study leads to the following calculation:

$$\frac{10^7 \times 0.01}{200 \times 5} = 100$$

The number of donor mice required for generating sufficient Cas9-positive PDX cells for each biological replicate was determined based on the number of technical replicates, transduction efficiency favoring single integration per cell, cell viability after 10-14 days of *in vitro* culture and cells retrievable from each mouse. The following formula was used to determine the number of donor mice required for every independent biological experiment:

$$\frac{\text{number of replicates} \times \text{injected cell number}}{\text{MOI} \times \text{cell viability } \textit{in vitro}} \times \frac{1}{\text{number of isolated cells per donor animal}}$$

$$\frac{4\times10^{7}}{0.2\times0.5} \times \frac{1}{1.5*10^{8}} = \frac{4*10^{7}}{0.1} \times \frac{1}{1.5*10^{8}} = 4*10^{8} \times \frac{1}{1.5*10^{8}} = \frac{4}{1.5} = 2{,}67$$

Using this formula for our exemplary PDX sample and considering the desired number of replicate mice, we determined that three donor mice were needed.

3.3 Molecular biology methods

3.3.1 Agarose gel electrophoresis:

Agarose gels were used to both separate DNA fragments of different sizes and as quality controls for PCR reactions. Depending on the fragment size 1-2% (w/v) agarose was dissolved in TAE buffer by heating. 8 µl Midori Green (Nippon Genetics Europe, Düren, Germany) per 100 ml agarose gel was added for DNA visualization before polymerization in the gel chamber. Electrophoresis was conducted in TAE buffer for 30 – 60 min at 100 V. A gel documentation station was used for the visualization of DNA fragments. If DNA fragments were used for restriction enzymatic cloning, they were cut out from the gel and purified according to the manufacturer's protocol.

3.3.2 Restriction digest:

In general plasmids were incubated for 1 hour at 37 °C for restriction enzymatic cleavage with one or more enzymes.

Table 23: Reaction mix restriction enzymatic cleavage

1-2 µg	Donor plasmid
0.5-1 µl (5-20 U)	Enzymes (FD or HF)
2 µl	10x digest buffer
ad 20 µl	H_2O

DNA fragments were separated using gel electrophoresis and purified as described above.

3.3.3 Ligation:

DNA fragments produced by restriction enzymatic cleavage were ligated into backbone plasmids with complementary overhangs using ligase. 50 ng of the backbone vector were used with the respective insert in a molar ratio of 1:3 to 1:5 calculated using the NEBiocalculator (https://nebiocalculator.neb.com/#!/ligation).

Table 24: Reaction mix ligation

50 ng	Backbone vector
	Insert
2 µl	10x ligase buffer
1 µl	T4 ligase
ad 20 µl	H_2O

Ligation was performed preferably over night at 16 °C or for 2 hours at RT.

3.3.4 H-2K^k-mTagBFP, -iRFP and -T-Sapphire cloning:

The H-2K^k-mTagBFP fusion cassette was received from IDT as gBlock and transferred to a pCDH lentiviral backbone using the EcoRI and SalI restriction sites. Expression of the fusion protein was tested both in the NALM-6 and the H293T cell lines by stable integration via lentiviral transduction or transient expression after transfection. In order to generate a H-2K^k-T-Sapphire and H-2k^k-iRFP fusion construct, iRFP and T-Sapphire were amplified via PCR from a pre-existing plasmid, containing both fluorochromes (pCDH-SFFV-FLIP cassette-iRFP-T-Sapphire-miR30_Renilla). For the PCR following settings were used:

Table 25: Reaction mix amplification of fluorochrome inserts for cloning

PCR reaction	
25 ng	plasmid
1.5 µl	fwd primer
1.5 µl	rev primer
1 µl	dNTPs
5 µl	Betaine
2.5 µl	Pfu 5x buffer
0.3 µl	Pfu polymerase
Ad 25 µl	H_2O

Cycler program		
Cycles	Temperature	Time
1	95 °C	5 min
25	94 °C	30 s
	58 °C	30 s
	72 °C	2 min
1	72 °C	5 min

With both the H-2K^k-mTagBFP plasmid and the amplified PCR products, a restriction digest according to the following setting was performed for 1 hour at 37 °C:

Table 26: Reaction mix restriction enzymatic cleavage of inserts and plasmid backbones for cloning

20 µl	PCR product (insert)
0.5 µl	BamHI
0.5 µl	SalI
2.5 µl	CutSmart buffer
1.5 µl	H_2O

1 µg	plasmid
1 µl	BamHI
1 µl	SalI
2.5 µl	CutSmart buffer
ad 25 µl	H_2O

Ligation of the respective fluorochromes with the H-2K^k pCDH backbone was performed using the following set-up for 2 hours at RT:

Table 27: Reaction mix ligation of inserts and plasmid backbones for cloning

50 ng	Backbone
150 ng	insert
2 µl	10x T4 DNA ligase buffer
1 µl	T4 ligase
ad 20 µl	H_2O

Plasmids were amplified by transformation of *E. coli* using the heat shock method, lentiviruses were produced and the expression of the respective fluorochrome as well as the functioning of the H-2K^k tag was measured using flow cytometry and MACS enrichment with anti-H-2K^k microbeads according to the manufacturer's protocol, respectively.

3.3.5 Design of the customized sgRNA library:

sgRNA targets were chosen based on previous multi-omics results together with potential targets found by literature research. For sgRNA design the GPP sgRNA Designer tool (https://portals.broadinstitute.org/gpp/public/) from the Broad Institute was used, which was the predecessor of the current CRISPick tool (https://portals.broadinstitute.org/gppx/crispick/public). Per gene the top five ranking sgRNAs were chosen from the tool, while adding extra nucleotides to enable the downstream cloning strategy, leading to the following oligo structure:

Forward oligo: 5'-TCCCGN_{20}(Gene of interest)-3'

Reverse oligo: 5' AAACN_{20}(Gene of interest)-3'

Additionally, 20 non-targeting sgRNAs were added to the library as negative controls.

3.3.6 Annealing of the sgRNAs and golden gate cloning:

For annealing the sgRNAs the following reaction and cycler settings were used:

Table 28: Reaction mix and cycler conditions for sgRNA annealing

Annealing reaction	
2 µl	forward oligo (100 µM)
2 µl	reverse oligo (100 µM)
2 µl	T4 DNA ligase
14 µl	H_2O

Cycler program	
Temperature	Time
95 °C	5 min
Ramp to 25 °C	0.1 °C per s

The annealed sgRNAs were pooled and diluted 1:500. The pCDH-H-2K^k-mTagBFP lentiviral plasmid was pre-digested (500 ng with 0.5 µl BpiI for 10 min @ 37°C). For golden gate cloning the following reaction and cycler settings were used:

Table 29: Reaction mix and cycler conditions for golden gate reaction

Golden gate reaction	
2 µl	diluted sgRNA pool
2 µl	T4 ligase buffer
1 µl	FastDigest BpiI
1 µl	T4 ligase
100 ng	Pre-digested plasmid
Ad 20 µl	H_2O

Cycler program		
Cycles	Temperature	Time
20	37 °C	3 min
	16 °C	10 min
1	55 °C	5 min
1	85 °C	5 in

2.5 µl of the product of this reaction was amplified using electrocompetent Endura bacteria as described in the manufacturer's protocol (Lucigen, Middleton, USA). Half of the bacteria were plated on square 245 mm bacterial plates, while additional dilutions were plated to 10cm petri dishes (e.g., 1:1.000, 1:10.000), enabling calculation of the transformation efficiency and therefore the coverage of the library. After overnight incubation at 32°C, transformation efficiency was evaluated with 50 colonies representing each sgRNA as minimum number to continue with the next steps. If this quality control was passed, bacteria were harvested and

the plasmid DNA was isolated according to the manufacturer's protocol (NucleoBond Xtra Midi kit, Macherey-Nagel, Düren, Germany).

3.3.7 Next generation sequencing (NGS) and MAGeCK analysis:

Amplifying the sgRNA library was performed using a nested PCR approach. The following reactions and cycler conditions were used for the two PCR reactions:

Table 30: Reaction mix and cycler conditions for NGS

1st PCR	
1.7 µg	gDNA
0.7 µl	ExTaq Polymerase
5 µl	ExTaq buffer
4 µl	dNTPs
1.5 µl	cPPT-forward primer (5 µM)
1.5 µl	EF1α-reverse primer (5 µM)
Ad 50 µl	H_2O

Cycler program		
Cycle	Temperature	Time
1	95 °C	5 min
16	94 °C	30 s
	57 °C	30 s
	72 °C	30 s
1	72 °C	5 min

2nd PCR	
5 µl	1st PCR product
1.5 µl	ExTaq Polymerase
10 µl	ExTaq buffer
8 µl	dNTPs
0.5 µl	P5-H1 primer mix (100 µM)
10 µl	P7- EF1α index primer
Ad 100 µl	H_2O

Cycler program		
Cycle	Temperature	Time
1	95 °C	3 min
25	94 °C	30 s
	53 °C	30 s
	72 °C	20 s
1	72 °C	10 min

As a quality control, 10 µl of the products of the second PCR reactions were run and imaged on an agarose gel (2%, 100V for 45 min), while the remaining PCR product was purified according to the manufacturer's protocol (QIAquick PCR Purification Kit, Qiagen, Germany). Sequencing of the samples was performed using a HiSeq2000 (Illumina, San Diego, USA). The Illumina Demultiplex software was utilized on Galaxy to demultiplex the reads and to map them to the sgRNA's sequence according to the reference list. The MAGeCK-count algorithm (Li et al., 2014) was utilized to obtain sgRNA normalized read count tables, while identification of the dropouts was performed via the MAGeCK-test algorithm (Li et al., 2014), which yields the *p* value, the false discovery rate (FDR) and the RRA depletion score for each tested gene.

3.3.8 Production of lentiviruses and lentiviral transduction:

As previously described (Ebinger et al., 2016), the third-generation lentiviral packaging plasmids pRSV-Rev, pMDLg/pRRE, and pMD_2.G pseudotyping was used for the generation of lentiviruses. The following transfection mix was prepared to produce viral particles:

Table 31: Reaction mix for production of lentiviruses

1 ml	DMEM
5 µg	pRSV-Rev
10 µg	pMDLg/pRRE
1.25 µg	pMD_2.G
5 µg	pCDH plasmid of interest
53.125 µl	PEI

The transfection mix was incubated for 20 min at RT before being added dropwise to the H293T cells. 72 hours post transfection, viral particles were filtered and enriched using Amicon centrifugal filter units (Merck Millipore, Darmstadt, Germany) for 30 min at 2.000 g and RT. The viral titer was evaluated by transducing cell lines (e.g., NALM-6, SEM) with serially diluted virus and analyzing the transduction efficiencies 72 hours post transduction using flow cytometry. Viruses were stored at -80 °C until usage.

In general, cells were lentivirally transduced using volumes according to the previous titration with the addition of 8 µg/ml polybrene. For more difficult to transduce PDX cells, the volume was increased by a factor of two. 24 hours post transduction the viruses were removed from the cells by repeated washing using PBS, before cells were resuspended in their respective medium.

Transduction of the PDX cells with the surface molecule library was performed as described in (Bahrami et al., 2023). In brief, PDX cells were seeded to wells of 6 well plates, seeding each 10^7 cells per well in 1 ml of StemSpan II medium (Stemcell Technologies, Vancouver, Canada) with added polybrene. 24 hours post transduction the viral particles were removed by washing and seven to ten days post transduction the library-positive cells were enriched by MACS and injected to mice.

3.3.9 ADAM10 variant cloning:

Designing of the ADAM10 variants was conducted *in silico*. gBlocks (Integrated DNA Technologies, USA) were ordered and introduced to the pCDH lentiviral backbone utilizing restriction enzymatic cleavage by XhoI and AgeI. Expression of the ADAM10 variants was

coupled via a T2A peptide to T-Sapphire expression, enabling both measurement and enrichment via flow cytometry.

3.3.10 Sanger sequencing and analysis of genome editing:

Extraction of gDNA of $1x10^6$ NALM-6 or PDX cells was performed according to the manufacturer's protocol (QIAampDNA Mini kit, Qiagen, Hilden, Germany). Specific primers amplifying the locus targeted by the respective sgRNA were utilized with an input of 100 ng gDNA. PCR products were run on an 1% agarose gel as quality control before being cut out of the gel and cleaned up according to the manufacturer's protocol (NucleoSpin Gel and PCR Clean-Up, Macherey-Nagel, Düren, Germany). The cleaned PCR amplicons were Sanger sequenced and efficiency of gene editing was calculated by the Inference of CRISPR edits (ICE) algorithm (Brinkman et al., 2014).

3.3.11 RT-qPCR Analysis:

Flow cytometrically enriched PDX cells were washed and the RNA was isolated according to the manufacturer's protocol (RNeasy Micro, Qiagen, Hilden, Germany). RNA quantity was measured with a spectrophotometer before transcription of 400 ng RNA into cDNA according to the manufacturer's protocol (QuantiTect Reverse Transcription Kit, Qiagen, Hilden, Germany). For the evaluation of the relative ADAM10 variant expression levels, both HPRT and GAPDH were used as housekeeping genes. Analysis of the samples was performed on a LightCycler® 480 Instrument II (Roche, Mannheim, Germany) using the corresponding SYBR green master mix (LightCycler® 480 SYBR Green I Master, Roche, Mannheim, Germany) and cycler program. Pre-analysis of the data was conducted using the on-device software, while quantification of the relative ADAM10 expression was performed using the $\Delta\Delta$CT method.

3.3.12 Analysis of transcriptomic data:

Analysis of transcriptomic data was performed as described in (Bahrami et al., 2023). In brief, analysis of whole transcriptome data of PDX ALL samples was performed according to the TruSeq Stranded mRNA library preparation protocol from Illumina. 100 bp paired-end sequencing with a HiSeq 4000 instrument (Illumina, San Diego, USA) was conducted. 700-1000 ng total RNA with an RNA integrity number (RIN) not lower than seven was used for the analysis. Gene and transcript analysis was performed using Salmon (v0.9.1) (Patro et al., 2017), while statistical analyses were calculated with R version 3.6.1. Gene expression data were uploaded to the Gene Expression Omnibus Website (https://www.ncbi.nlm.nih.gov/geo/) with the following accession number: GSE139553.

3.3.13 Analysis of differential gene expression and protein expression:

Analysis of differential gene expression and protein expression was performed as described in (Bahrami et al., 2023). In brief, the R package *edgeR* (version 3.30.3) was used for pre-processing of the raw read counts, while protein expression and differential gene expression was analyzed using the R package *limma* (version 3.44.3). Genes with *p* values ≤0.05 and |logFC|>1 were defined as statistically significant differentially expressed. Statistical significance of proteins was reached with adjusted *p* values of ≤0.05.

3.3.14 Confocal microscopy of ADAM10 variants:

H293T cells were transfected with the respective ADAM10 variants using PEI. 24 hours post transfection cells were fixed using 4% PFA for 15 min. After three washing cycles using PBS, the primary antibody (anti-Human ADAM-10 (11G2), Diaclone SAS, Besancon Cedex, France) was added to the cells in PBS + 0.1% BSA for 1 hour at RT enabling extracellular staining of the ADAM10 variant. The cells were washed three times using PBS before incubation with the secondary antibody ((IgG (H+L) Cross-Adsorbed Goat anti-Mouse, Alexa Fluor™ 647, Invitrogen™, Fisher Scientific GmbH, Schwerte, Germany), which was performed in the same buffer for 1 hour. 3 min DAPI counter-staining was conducted in the same buffer at RT. The cells were washed with PBS three times, before mounting (ProLong™ Gold Antifade Mountant, Fisher Scientific GmbH, Schwerte, Germany) and sealing with transparent nail polish. Confocal microscopy images were acquired with a Leica TCS SP5 confocal microscope (Leica Mikrosysteme Vertrieb GmbH, Wetzlar, Germany) capturing the DAPI signal with the 405 nm UV diode and the Alexa Fluor™ 647 with the 633 nm helium/neon laser line utilizing the 63x, 1.4 NA oil objective in z-stacks. Images were analyzed with FIJI (Schindelin et al., 2012).

3.4 Detection of proteins

3.4.1 Simple Western (WES):

Cell lysis buffer with PMSF added 1:200 was used to lyse NALM-6 cells for 30 min on ice, before cellular debris was removed by centrifugation for 20 min at >20.000 g. The protein containing supernatant was transferred to new pre-chilled tubes and the protein concentration was measured performing a BCA assay according to the manufacturer's protocol (BCA Protein Assay Kit, Cell Signaling Technologies, USA). Using a WES simple western device, protein quantification and analysis were conducted according to the manufacturer's protocol and using the corresponding Compass software.

3.4.2 Whole cell lysis and SDS-PAGE:

Cell lysis buffer with PMSF added 1:200 was used to lyse PDX cells or cell lines for 30 min on ice. Samples were centrifuged at >20.000 g for 30 min at 4°C, before the protein containing supernatant was transferred to new pre-chilled tubes. Bradford assay was used to determine the relative protein concentrations. Separation of proteins was conducted using pre-cast SDS-PAGE gels and proteins were transferred to PVDF membranes using semi-dry blotting according to the manufacturer's protocol (Trans-Blot® Turbo™ Transfer System, Bio-Rad, München, Germany). 5% skim-milk in TBS/T (0.025% Tween) was used for blocking the membranes for 1 hour at 4°C. The primary and secondary antibodies were incubated using the same buffer overnight at 4 °C and for 1 hour at RT, respectively. For the housekeeping gene, GAPDH, a directly HRP conjugated antibody was used with an incubation time of 30 min at RT. ECL was used for the detection of proteins according to the manufacturer's protocol on a western blot documentation station (Fusion FX, Vilber Lourmat GmbH, Germany).

3.4.3 Purification of transmembrane proteins:

H293T cells were harvested using trypsin and washed two times using pre-chilled PBS. Transmembrane proteins were purified by resuspension in buffer A, homogenization via pipetting and shearing of the samples through a 25G needle for four times using a syringe. After 10 min of centrifugation at 1.000 g at 4°C, the supernatant was removed, while the pellet was reconstituted in buffer B before incubation for 15 min on ice. For better purification the samples were mixed every 5 min. After a second 10 min centrifugation step, the pellets were resuspended in buffer C. After an incubation period of 60 min on ice with mixing of the samples every 20 min, the samples were centrifuged for 30 min at 16.000 g and 4 °C. The protein-containing supernatant was transferred to fresh pre-chilled tubes and stored at -80 °C until usage.

Table 32: Buffer composition for transmembrane protein purification

Reagent	**Buffer A**	**Buffer B**	**Buffer C**
Tris pH 8.0	50 mM	50 mM	50 mM
DTT	0.5 mM	0.5 mM	0.5 mM
PMSF	1 mM	1 mM	1 mM
Leupeptin	5 µg/ml	5 µg/ml	5 µg/ml
NaF	10 mM	10 mM	10 mM
Na_3VO_4	1 mM	1 mM	1 mM
NP-40	0.1% (v/v)	-	1% (v/v)

3.5 Flow cytometry

In general, flow cytometry was conducted utilizing a BD LSRFortessa X-20 device. Flow cytometric data were gated for viable cells by FSC/SCC, and fluorochromes either expressed or coupled to antibodies were analyzed utilizing the indicated laser and filter settings.

Table 33: BD LSRFortessa X-20 laser and filter configuration

Laser	Excitation [nm]	Long pass filter	Bandpass filter	Parameter
Violet	405	685	710/50	BV711
		505	525/50	T-Sapphire
			450/50	mtagBFP
Blue	488	505	530/30	GFP
			488/10	SSC
YellowGreen	561	600	610/20	mCherry
		505	586/15	PE
Red	640	690	730/45	iRFP
			670/30	APC

For routine stainings of surface molecules, cells were harvested and the medium was removed by washing with PBS. Either the amount recommended by the manufacturer or a previously titrated volume of directly conjugated antibody was added to 100 µl PBS per sample in a master mix, where applicable. If not otherwise stated, cells were incubated with the antibodies for 15 min at RT. Excess antibody was removed using a PBS washing step. Cells were afterwards resuspended in 100 µl PBS and the samples measured by flow cytometry.

Staining of intracellular proteins was conducted by fixing and permeabilizing the cells following the manufacturer's protocol (FIX & PERM Cell Fixation & Cell Permeabilization Kit, Thermo Fischer Scientific, USA) without the use of sodium azide.

Enrichment of cells using fluorescence-activated cell sorting was performed using the BD FACS AriaIII (BD Biosciences, Heidelberg, Germany) based on expressed or antibody-conjugated fluorochromes using the following laser and filter settings.

Table 34: BD FACS AriaIII laser and filter configuration

Laser	Excitation [nm]	Long pass filter	Bandpass filter	Parameter
Violet	405	502	530/30	T-Sapphire
			450/40	mtagBFP
Blue	488	502	530/30	GFP
			488/10	SSC
YellowGreen	561	600	610/20	mCherry
Red	633	735	780/60	iRFP
			660/20	APC

3.6 Cell culture and *in vitro* assays

3.6.1 Cell culture:

All cells were cultured in the appropriate medium as indicated in the tables below at 37 °C and 5 % CO_2. Cells were split according to their preferred density. Suspension cell lines were split roughly twice per week in order to maintain them at densities between 1-2x 10^6. AML PDX were seeded at 1x 10^6 per million cells and split according to their proliferation rate maintaining them at this density. The non-proliferating ALL PDX cells were maintained in culture by adding fresh medium without splitting. H293T cells were split by removing medium, washing once using PBS, detaching cells for 3 min using 1.5 ml trypsin, splitting them according to their density 1:5 to 1:20 and resuspending them in fresh medium.

Table 35: Cell culture media composition for cell lines and PDX cells

B-ALL cell lines	
	RPMI medium
10 %	FBS
1 %	L-Glutamine
1 %	HEPES
1 mM	Sodium pyruvate

H293T cells	
	DMEM medium
10 %	FBS
1 %	L-Glutamine

ALL PDX	
	StemSpan™ SFEM II
1 %	Pen / Strep

AML PDX	
	StemPro-34 medium
1.3 ml	Nutrient supplement
2 %	FBS
1 %	Pen / Strep
1 %	L-Glutamine
10 ng/ml	rhFLT3
10 ng/ml	rhIL3
10 ng/ml	rhSCF
10 ng/ml	rhTPO

For cryopreservation, cells were washed once using PBS before they were resuspended in Bambanker freezing medium (NIPPON Genetics EUROPE, Düren, Germany) and transferred to -80 °C. Cells were thawed quickly at 37 °C to yield high cell viabilities. Thawed cells were directly washed using PBS and resuspended in their respective culturing medium.

3.6.2 *In vitro* competitive assay:

Cells were transduced, enriched and mixed along with the cells of the *in vivo* competitive assay (see 3.2.8). The *in vitro* experiments were conducted for the same time period as the *in vivo* passage of the respective sample. For ALL-199, the experimental endpoint for the *in vitro* experiment was set to 14 days as a result of the limited feasibility of ALL PDX cultivation *in vitro*. Using flow cytometry, the distribution of the control and the ADAM10 KO population was compared between the initial mix and the mix at the experimental endpoints.

3.6.3 Analysis of the cell cycle:

For cell cycle analysis, ADAM10 surface staining was performed as described above (see 3.5), before cells were fixed for 15 min on ice using 0.5% PFA in PBS. PFA was removed by washing two times with PBS. Cells were permeabilized using 0.1% Triton X-100 in PBS combined with 1µg/ml DAPI to stain the cell's DNA content. Samples were measured using flow cytometry and analyzed via the FlowJo software, employing the cell cycle tool utilizing the Dean-Jett-Fox model.

3.6.4 CFU assay:

CFU assays were performed as described in (Bahrami et al., 2023). In brief, CFU assays were conducted using MethoCult™ H4034 Optimum according to manufacturer's protocol. Cells were resuspending in their corresponding medium and mixed with methylcellulose (1:10) by vortexing. 16G blunt-end needles and corresponding syringes were used to plate this mix to wells of meniscus-free 6-well plates. Colonies were scored after ten days using an inverted microscope with the help of a plate grid. A colony was defined by >20 cells forming a round cluster with a GM-CFU morphology.

For CFU assays including chemical inhibition of ADAM10, spleen derived PDX cells were pre-treated for 72 hours with GI254023X or its solvent DMSO. Reduction of ADAM10 expression was determined by flow cytometry of 3x 10^5 cells per condition stained for ADAM10 or the corresponding isotype control. The remaining cells were utilized for the CFU assay.

The CFU assays with healthy human CD34+ cells were performed as described above by our collaboration partner Sophie Kreissig from AG Wichmann. The cells were amplified in the medium described below, before being treated with a chemical ADAM10 inhibitor (GI254023X or Aderbasib) or DMSO for 72 hours. As for the PDX samples, ADAM10 expression was measured by flow cytometry and cells were plated and scored after ten days.

Table 36: Composition of cell culture medium for human CD34+ progenitor cells

human CD34+ cells	
	IMDM
20 %	FCS
100 U/ml	Penicillin
100 µg/ml	Streptomycin
2 mM	L-Glutamine
10 ng/ml	IL3
20 ng/ml	IL6
20 ng/ml	SCF
20 ng/ml	TPO
20 ng/ml	FLT3L
20 ng/ml	GM-CSF

3.6.5 Apoptosis assay:

PDX cells were seeded to wells of 6 well plates and either a chemical ADAM10 inhibitor (GI254023X) or its solvent DMSO was added. After 72 hours, cells were harvested and

resuspended in Annexin V binding buffer. A combined ADAM10 and Annexin V surface staining was performed with an incubation time of 10 min at RT. For the final 5 min of incubation, DAPI was added. The percentage of Annexin V-positive cells was measured by flow cytometry.
Electroporation of PDX cells with RNP complexes was performed to compare apoptosis rates of ADAM10 KO and control cells. The utilized RNPs either comprised a control sgRNA or a mix of three individual sgRNAs targeting ADAM10. For electroporation, a primary cell kit (P3 Primary Cell 4D-Nucleofector® X Kit L, Lonza Group, Basel, Switzerland) was used with a 4D-Nucleofector utilizing program #CA137. 72 hours post electroporation, the apoptosis assay was performed as described above.

3.6.6 *In vitro* chemotherapy assay:

PDX cells stably expressing different fluorochrome versions of the E-Firefly Luciferase (GFP or mCherry) were amplified via donor mice. After sacrificing the animals, PDX cells were electroporated with RNP complexes as described above (see 3.6.5). 72 hours post electroporation, control and ADAM10 KO cells were mixed in a 1:1 ratio and seeded to wells of 48-well plates using 60.000 cells in three technical replicates for each of the chemotherapeutic agents (Cytarabine, Daunorubicin & Doxorubicin), used concentration as well as tested sample. Using flow cytometry, the composition of the two cell populations was measured at the start of the experiment and 96 hours after adding the chemotherapeutic agents, comparing the composition of the two subpopulations of cells.

3.7 Software

Flow cytometric measurements were analyzed with the FlowJo Software.

Generation of graphs and statistical analyses were conducted with GraphPad Prism.

Analysis of GO networks was performed utilizing Cytoscape (Bindea et al., 2009; Shannon et al., 2003).

Writing of the thesis and implementation of the citations was conducted using Microsoft Word and Endnote 20, respectively.

3.8 Online resources

Graphics and schemes were generated using BioRender.com (https://biorender.com).

GSEA of transcriptomic data was conducted utilizing the web-resource (http://www.gsea-msigdb.org/gsea/index.jsp, (Mootha et al., 2003; Subramanian et al., 2005)) including both GO terms as well as KEGG pathways.

The expression of ADAM10 in different AML and ALL subtypes was investigated using the Leukemia MILE study dataset (202603_at, GSE13159) of the Bloodspot online database (https://servers.binf.ku.dk/bloodspot/, (Bagger et al., 2019)), while the TCGA AML dataset (202603_at) was used for investigating overall survival. Retrieved raw data were analyzed and adapted with GraphPad Prism.

ADAM10's effect on different tumor entities was investigated using the pathology section of the web-resource of the human protein atlas (https://www.proteinatlas.org, version 21.1, (Uhlén et al., 2015)).

4. Results

Therapeutic strategies for patients with acute leukemias have been improving during recent years, but options are still limited for patients with relapsed disease, elderly patients and patients within adverse risk groups. Thus, new targets for the treatment of acute leukemia patients are urgently needed. Especially disruption of the interaction of leukemic cells with the surrounding bone marrow microenvironment promises to eradicate LSCs, which often escape routine chemotherapy and can initiate relapses.

Therefore, the aim of the presented work was to identify new therapeutic acute leukemia targets by using customized surface molecule CRISPR/Cas9 dropout screens *in vivo* in PDX models and to subsequently functionally characterize such a potential vulnerability by using a broad array of approaches including multi-omics analyses, establishing KO and rescue models and investigating the effect of genetic KO or chemical inhibition of the candidate on essential leukemia cells' characteristics.

4.1 Customized CRISPR/Cas9 dropout screen on surface proteins in PDX leukemia models *in vivo* reveals ADAM10 as candidate with essential function

We searched for genes with essential function during PDX leukemia growth in mice *in vivo* and started by using an unbiased functional screening approach. We performed a CRISPR-Cas9 dropout screen using a customized library. In dropout screens, sgRNAs which were present at cell injection into mice, but depleted during tumor growth and absent at the time of analysis, have disabled a gene with essential function for *in vivo* leukemia growth. As we aimed for interrupting the leukemia-niche interaction, we focused on surface molecules.

Screening in PDX models presents various hurdles like low transduction and engraftment efficiency and immensely higher costs compared to cell line screens, while better resembling the primary disease. Therefore, whole genome CRISPR-Cas9 dropout screens are hardly feasible. Utilizing two ALL PDX models with known high LIC frequencies of around 1 in 100 permitted us to screen a customized library with a size of approximately 500 sgRNAs targeting around 100 candidate genes with a sufficiently high sgRNA representation of 200 cells per sgRNA in each individual animal (**Figure 6** and see 3.2.15). The candidates for the library were chosen from previously generated proteomics and transcriptomics data (Ebinger et al., 2016) combined with genes from the literature. Suitability of the chosen library size was confirmed by transduction of the library into Cas9 negative ALL-199 and ALL-265 samples and comparing the sgRNA distribution of the plasmid pool with the ones retrieved from the individual animals (Bahrami et al., 2023).

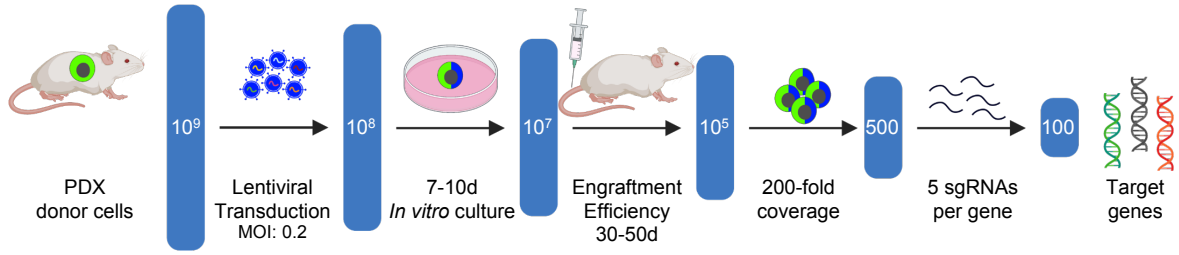

Figure 6: The challenges of CRISPR screens in the PDX model. High numbers of donor cells are needed for lentiviral transduction of the library at low MOIs. ALL PDX cells are difficult to culture *in vitro*. Per mouse a maximum of 10^7 PDX cells can be injected. With an early engraftment efficiency of 1%, a 200-fold coverage of the number of homed cells per sgRNA can be maintained using 5 sgRNAs per gene and targeting 100 genes. Adapted from (Bahrami, Schmid et al., 2023).

We generated PDX models stably expressing a split version of Cas9 together with a GFP fluorochrome (Bahrami et al., 2023). After amplification of these cells using donor mice, in a next step the sgRNA targeting the respective genes together with non-cutting negative and known essential positive control sgRNAs were stably integrated into the PDX cells via lentiviral transduction at low multiplicities of infection (MOIs), aiming for predominantly single integrations. sgRNAs were designed via the Broad Institute sgRNA design tool (Doench et al., 2016). sgRNA expression was coupled to a mTagBFP-H-2K^k fusion protein, enabling cell enrichment via both flow cytometry and magnetic-activated cell sorting. PDX cells were cultured *in vitro* for 7-10 days to allow a complete knockout of the respective targeted gene before they were enriched via MACS; then the input sample was taken and the cells were transplanted into mice. At an advanced stage of leukemia, animals were sacrificed and cells were re-isolated from the BM. The sgRNA locus was amplified using the two-step PCR approach (see 3.3.7) (Bahrami et al., 2023). PCR amplicons were sequenced via NGS and the reads were analyzed via the MAGeCK algorithm (**Figure 7A**) (Li et al., 2014).

Utilizing this workflow, we identified several sgRNAs which dropped out significantly during *in vivo* leukemia growth and had hit potential gene candidates with essential function, 11 in ALL-199 and seven in ALL-265, respectively. Among those, the positive controls *CXCR4* and *ITGB1* were depleted in both investigated PDX models. Importantly, at the same time the abundance of the non-targeting control sgRNAs was not altered in both samples. In addition to the quality controls, *SLC3A2*, *SLC19A1* and *ADAM10* were depleted in both tested models, while *TFRC* was depleted in ALL-265 and *NCSTN*, *CD81*, *CD79A*, *TRPM7* and *POTEI* in ALL-199, indicating the potential of our screening pipeline to identify both commonly depleted as well as sample specific essentialities (**Figure 7B-D**).

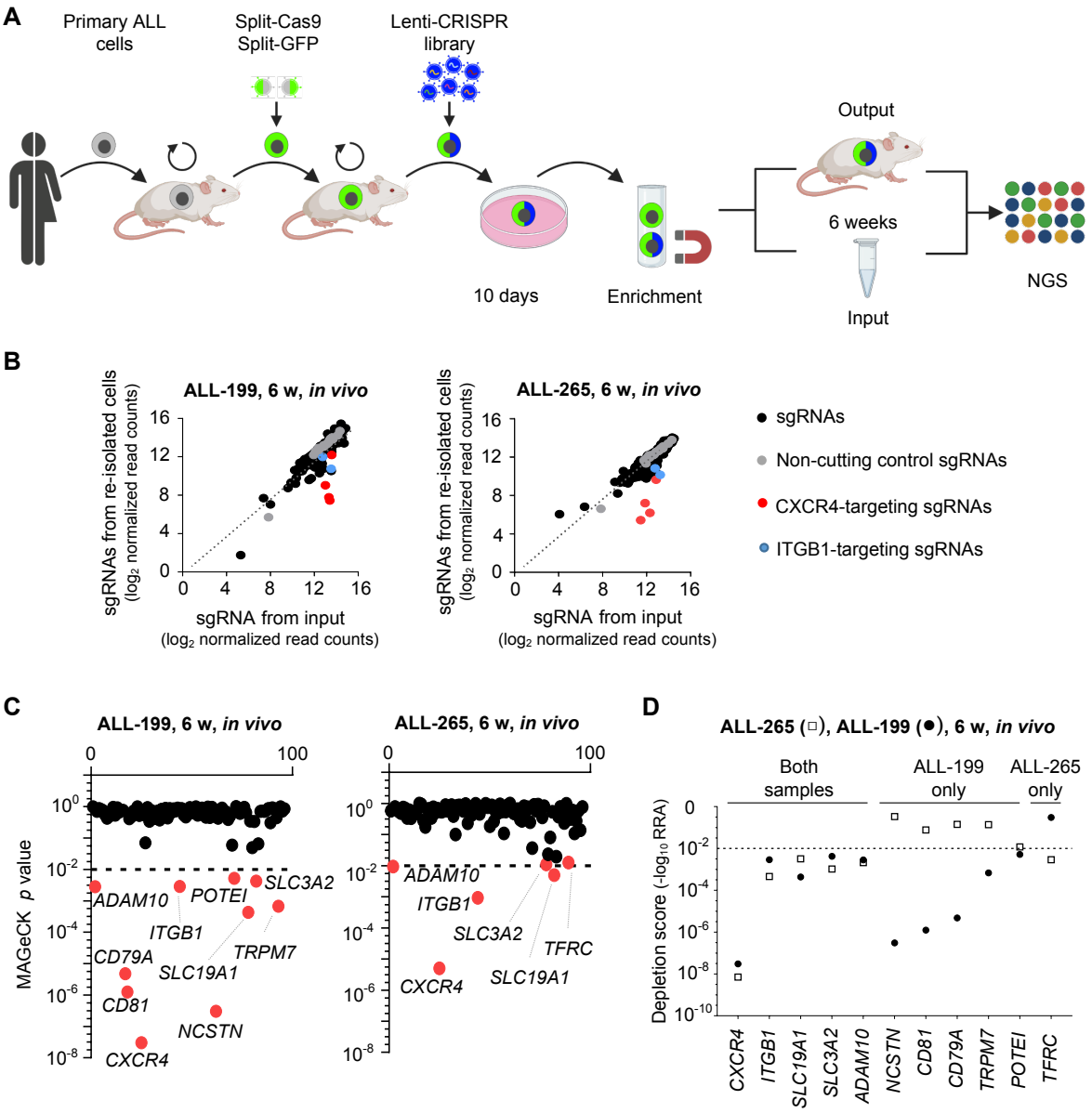

Figure 7: Surface molecule CRISPR-Cas9 dropout screen in two ALL PDX models. A Scheme of the CRISPR-Cas9 dropout screen pipeline. Patients' primary leukemic cells were serially transplanted into immunocompromised NSG mice. Via lentiviral transduction in the first step a split-version of Cas9 was stably integrated, while in a second step the PDX cells were transduced with a customized surface molecule library and cultured *in vitro*. Seven to ten days post transduction, library positive cells were MACS-enriched and injected to animals (ALL-199: n=5, ALL-265: n=8) after collecting an input sample. At an advanced leukemic stage, cells were re-isolated from the murine BM and the distribution of the sgRNAs was determined by NGS sequencing comparing the output samples with the input. **B** Abundance of sgRNAs in input and output (grey dots: non-targeting sgRNAs, red dots: CXCR4 sgRNA, blue dots: ITGB1 sgRNA). **C** Plot depicting the gene summary data of the MAGeCK analysis based on *p*-values. Red dots represent significantly depleted candidate genes. Threshold of $p<0.01$ is depicted by the dotted lines. **D** Comparison of shared and sample specific dropouts in both ALL PDX samples. The depletion scores were calculated via MAGeCK's robust ranking algorithm (RRA). Threshold of RRA<0.01 is depicted by the dotted line. Adapted from (Bahrami, Schmid et al., 2023).

4.2 ADAM10 expression is increased in primary acute leukemia cells and associated with worse overall survival in leukemia patients

Among the sample specific and commonly depleted candidates from the surface molecule CRISPR/Cas9 dropout screen, ADAM10 was particularly interesting for us, as we observed it to be upregulated in the LSC-resembling LRC fraction in the proteome experiment preceding the library compilation. Additionally, ADAM10's role in both healthy hematopoiesis and tumor progression of several cancer entities including T-ALL is well described in the literature (Atapattu et al., 2016; Duffy et al., 2009; Feldinger et al., 2014; Hartmann et al., 2002; Lambrecht et al., 2018; Minond, 2020; Mueller et al., 2021; Mullooly et al., 2016; Smith et al., 2020; Sulis et al., 2011; Venkatesh et al., 2017; Wu et al., 1997; Yoda et al., 2011).

We performed intensive data mining in order to better understand ADAM10's role in hematologic malignancies. According to the publicly available dataset 202603_at (Leukemia MILE study, GSE13159) accessed through the Bloodspot databank, ADAM10 expression is significantly increased in T-ALL, in all included BCP-ALL entities as well as in all AML patient subgroups except those with a complex karyotype compared to healty BM samples (**Figure 8A**). In line with theses data, ADAM10 protein levels were elevated in our ALL and AML PDX cohort, comprising 24 individual models, compared to healthy BM samples of hip replacement patients (**Figure 8B**).

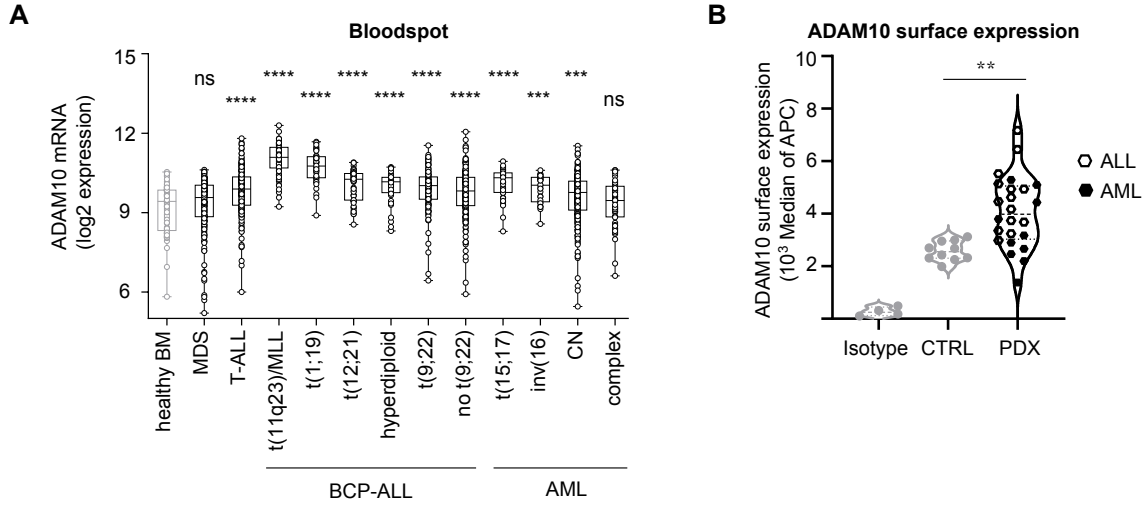

Figure 8: ADAM10 expression levels are elevated in most of the acute leukemia sub-types. A ADAM10 expression levels of different acute leukemia subtypes were analyzed using a publicly available dataset (202603_at; Leukemia MILE study; GSE13159) of the Bloodspot databank comparing subtypes of leukemic diseases with healthy controls. Median, 25th and 75th percentile are represented by the box, min/max by the whiskers. **** p<0.0001, *** p<0.001 by multiple t-test. ns: not significant, CN: cytogenetically normal. **B** Surface expression levels of ADAM10 in PDX models (ALL: n=14, AML: n=10) compared to BM cells of healthy donors measured using flow cytometry. Adapted from (Bahrami, Schmid et al., 2023).

Further data mining revealed that high ADAM10 expression had a tendency towards correlating with poorer overall survival of AML patients as shown in the dataset 202603_at (Human AML cells, GSE13159), underlining ADAM10's clinical importance (**Figure 9A**). In other tumor entities such as lung and pancreatic cancer, higher ADAM10 expression was significantly correlated with worse overall survival (**Figure 9BC**).

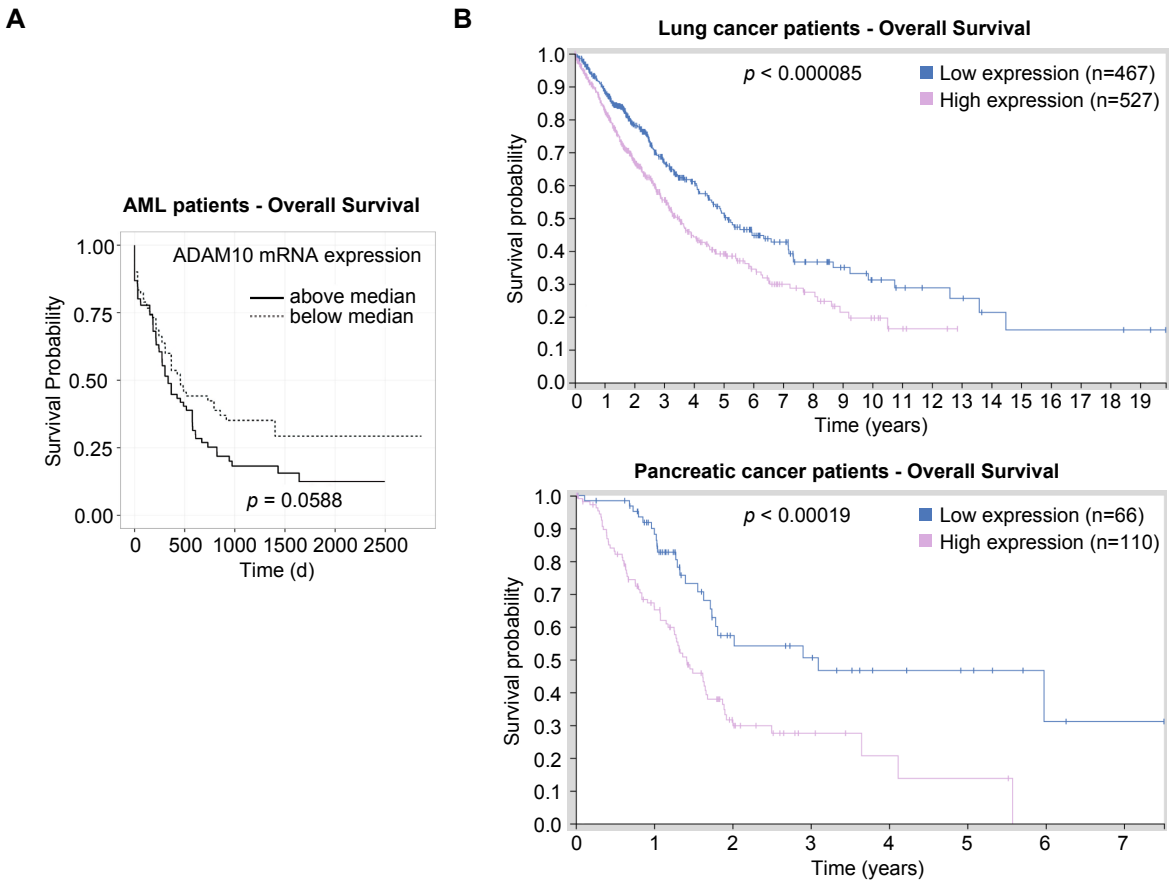

Figure 9: Higher ADAM10 expression is associated with worse overall survival. A Above median ADAM10 expression was correlated with overall survival in AML patients in a publicly available dataset (202603_at; Human AML cells; GSE13159). **B** Kaplan-Meier curves depicting correlation between ADAM10 expression and overall survival in lung and pancreatic cancer patients. Publicly available data from the Human Protein Atlas (v21.1.proteinatlas.org, https://www.proteinatlas.org/ENSG00000137845-ADAM10/pathology). Adapted from (Bahrami, Schmid et al., 2023).

ADAM10's elevated expression levels together with its association with poorer overall survival in several tumor entities prompted us to further elucidate ADAM10 as a vulnerability of acute leukemias.

4.3 Molecular validation of ADAM10 in PDX models *in vivo* and *in vitro*

Functional *in vivo* competitive assays were performed to molecularly validate the findings from the CRISPR/Cas9 KO screen and thereby confirm ADAM10's essentiality in PDX models of acute leukemia. Utilizing the three ADAM10-targeting sgRNAs with the strongest log fold changes in the CRISPR screens, complete KOs of ADAM10 could be achieved both in ALL and AML PDX samples (**Figure 10**).

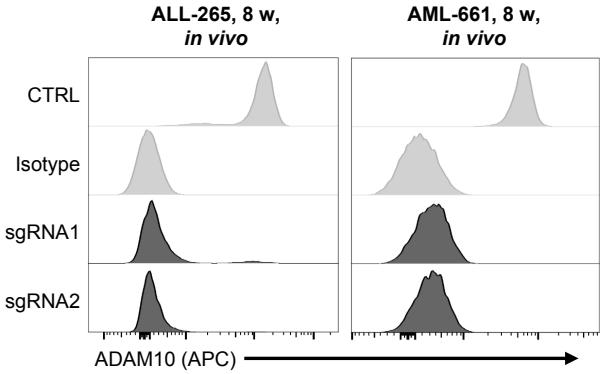

Figure 10: Efficient knockout of ADAM10 via CRISPR-Cas9. ALL and AML PDX models were lentivirally transduced using sgRNAs targeting ADAM10, enriched via flow cytometry and transplanted into mice. At an advanced stage of leukemia, animals were sacrificed, PDX cells re-isolated and ADAM10 surface protein levels were measured via flow cytometry. Histograms of the ADAM10 KO PDX cells compared to both the wild-type and the isotype control are depicted. Adapted from (Bahrami, Schmid et al., 2023).

Although ADAM10 was identified as vulnerability in two ALL PDX models, not only ALL, but also AML PDX models were used for validation, as ADAM10 expression levels were also increased in both, ALL and AML samples as well as primary samples (**Figure 8**), indicating a potentially broader ADAM10 essentiality.

A competitive approach was used in which cells with KO of ADAM10 or a control were injected into the same mouse and their ratio was monitored over time. The ADAM10 sgRNA was coupled to one of two different fluorochromes, while the control sgRNA was coupled to a second fluorochrome, allowing to compare the percentage of each cell population at injection and after sacrificing the mice via flow cytometry analysis. PDX cells were lentivirally transduced with either an sgRNA targeting ADAM10 labelled with mTagBFP or with a T-Sapphire-marked non-targeting control sgRNA. Cells were kept *in vitro* mimicking the approach used for screening, mixed in a 1:1 ratio by fluorescence activated cell sorting, injected into animals and an aliquot of each respective mix was measured as input sample using flow cytometry. Per sample, three animals, each harboring an individual sgRNA targeting ADAM10, were used (**Figure 11AB**). At advanced leukemia stages, the animals were sacrificed, PDX cell re-

isolated from BM and spleen and the distribution of the ADAM10 KO and control population in these output samples was determined by flow cytometry. The representative flow cytometry plots show, that the ADAM10 KO population was diminished at the output compared to the input, while the control population increased (**Figure 11C**).

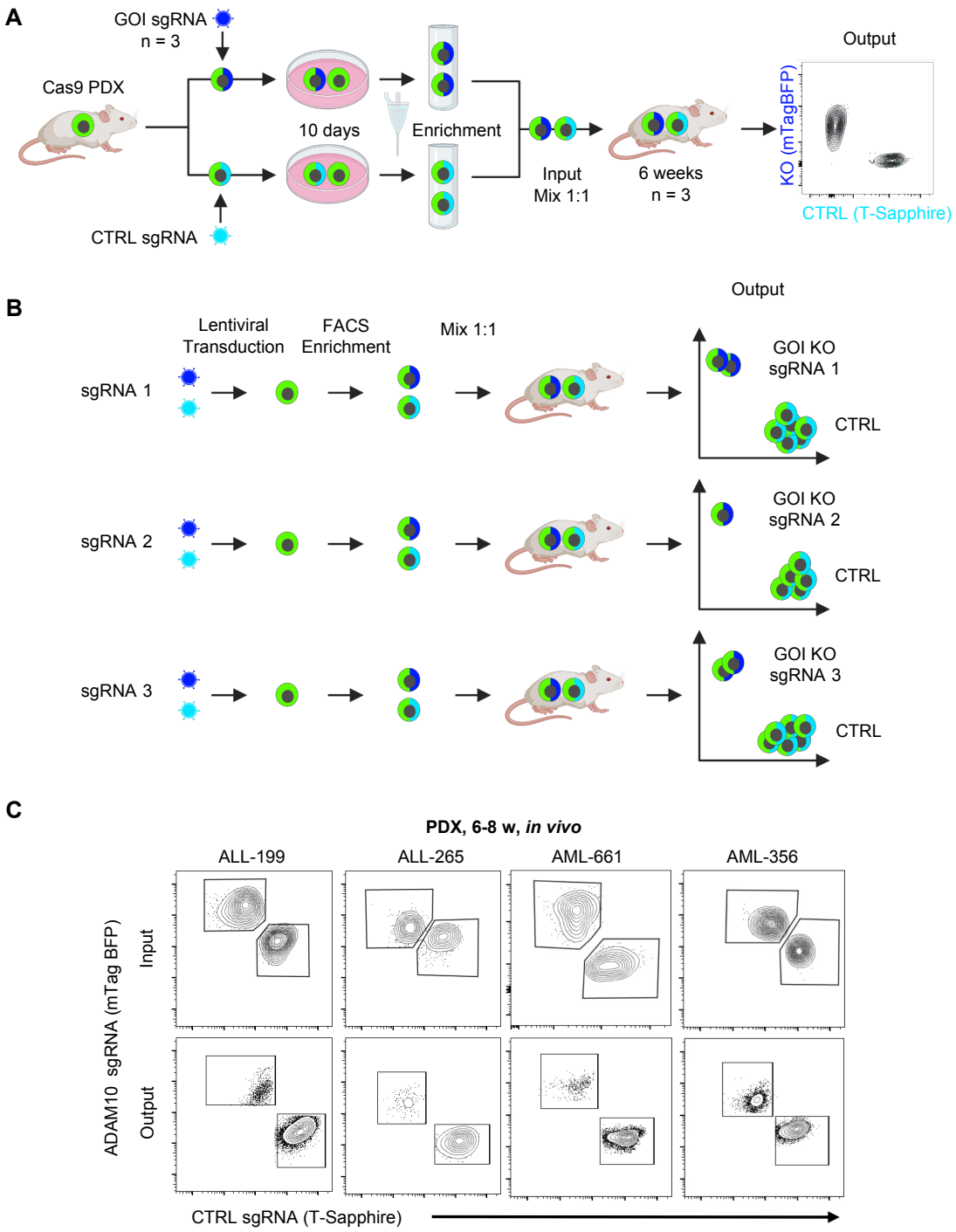

Figure 11: Validation of the CRISPR-Cas9 screen candidate ADAM10 by molecular *in vivo* competitive assays. AB Workflow of competitive *in vivo* assays. Cas9-transgenic PDX models were lentivirally transduced with either an ADAM10-targeting or a non-targeting control sgRNA and cultured *in vitro* for ten days. Construct-expressing cells were enriched via flow cytometry, mixed in a 1:1 ratio and injected into animals. Per PDX model, three individual sgRNAs targeting ADAM10 were tested in

one mouse each. At an advanced stage of leukemia, animals were sacrificed, PDX cells re-isolated from BM and spleen and the distribution of the ADAM10 KO and control population was measured using flow cytometry. **C** Representative flow cytometry plots from *in vivo* competitive assays in the PDX models ALL-199, ALL-265, AML-661 and AML-356 depicting the distribution of the ADAM10 KO and control population at the timepoint of injection (Input) and after re-isolation from the sacrificed animals (Output). Adapted from (Bahrami, Schmid et al., 2023).

ADAM10 loss diminished PDX growth and proliferation in two out of three ALL and in all of the five tested AML samples *in vivo* (**Figure 12A**). The unaltered distribution of the ADAM10 KO population and the controls in the ALL sample 502 proves the specific effect of the ADAM10 loss in the other samples, in contrast to a potential growth disadvantage due to the Cas9 activity and associated DNA damage repair taking place in these cells, thereby validating the appropriateness of our approach (**Figure 12B**). In contrast, in the *in vitro* setting only ALL-199 displayed a mild dependency on ADAM10, while its loss had no effect on the AML PDX samples *in vitro.* For these experiments, PDX cells were cultured for time frames comparable to the *in vivo* experiments (**Figure 12C**). In general, the effect of the ADAM10 KO is more pronounced in the spleen compared to the BM (**Figure 12D**). Sacrificing groups of animals at earlier timepoints elucidated that ADAM10 loss is detrimental already shortly after transplantation and that this growth disadvantage persists during the *in vivo* passage (**Figure 12E**). Therefore, ADAM10 loss might be crucial for both early engraftment as well as proliferation of PDX cells. In summary, essentiality of ADAM10 could be shown in seven out of eight ALL and AML PDX models, independent from their genetic alterations and molecular subgroup (**Figure 12F**). This indicates a broad susceptibility of acute leukemias towards loss of ADAM10.

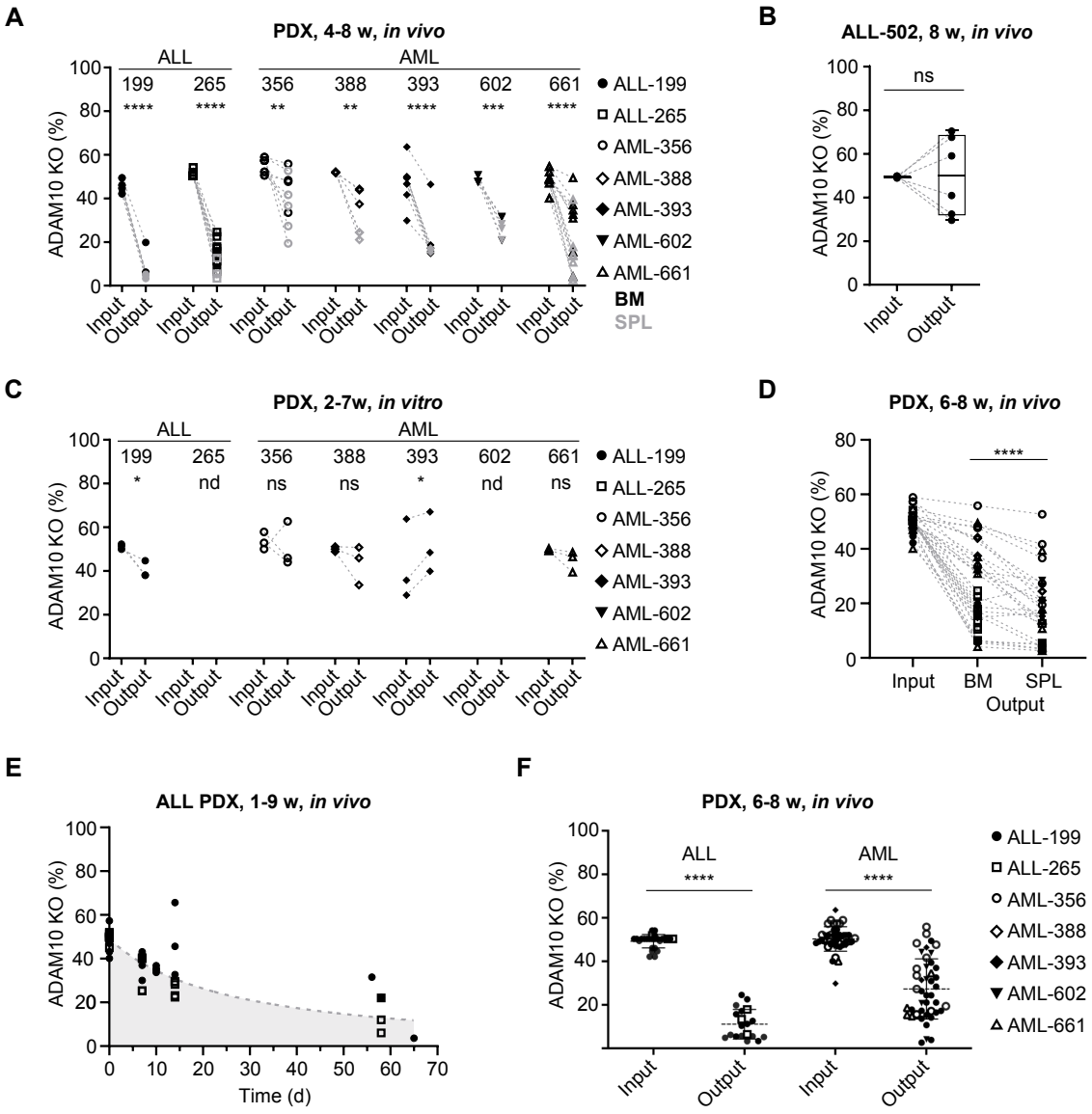

Figure 12: ADAM10 essentiality was validated by molecular in vivo competitive assays. A *In vivo* competitive assays for ADAM10 validation in ALL and AML PDX samples. ADAM10 KO percentage is depicted at the injection (Input) and after re-isolation (Output) from the BM (black symbols) and spleen (grey symbols) for the PDX samples ALL-199 (4 BM and 3 spleen measurements from 4 animals; n=7), ALL-265 (9 BM and 3 spleen measurements from 9 animals; n=12), AML-356 (5 BM and 4 spleen measurements from 5 animals; n=9), AML-388 (3 BM and 3 spleen measurements from 3 animals; n=6), AML-393 (6 BM and 3 spleen measurements from 6 animals; n=9), AML-602 (3 BM and 3 spleen measurements from 3 animals; n=6), and AML-661 (7 BM and 7 spleen measurements from 7 animals; n=14). **** p<0.0001, *** p<0.001, ** p<0.01 by paired t-test. **B** *In vivo* competitive assay for ADAM10 validation in PDX sample ALL-502 (3 BM and 3 spleen measurements from 3 animals; n=6). ns (not significant) by paired t-test. **C** *In vitro* competitive assays in ALL and AML PDX samples. ADAM10 KO percentage is depicted at the mixing timepoint (Input) and after *in vitro* cultivation (n=3 for all PDX samples). *p<0.05 by paired t-test, nd (not determined), ns (not significant). **D** Depletion of the ADAM10 KO population is more pronounced in the spleen than in the BM in many samples. p<0.0001 by paired t-test. **E** BM measurement of the *in vivo* competitive assays of the PDX samples ALL-199 and ALL-265 after the indicated *in vivo* proliferation times. Pade (1,1) approximant, robust fit was used for interpolation indicated by dotted grey line. **F** Same data as in **A** analyzed for ALL and AML lineage. **** p<0.0001 by paired t-test. Adapted from (Bahrami, Schmid et al., 2023).

4.4 Reconstitution of catalytically active ADAM10 in ADAM10 KO PDX cells rescues the phenotype *in vivo*

ADAM10 loss significantly diminished the proliferation and growth of both ALL and AML PDX models as shown in the *in vivo* competitive assays (**Figure 12**). Reconstitution assays were performed in order to confirm that this phenotype can be indisputably attributed to ADAM10's function. During ADAM10's translocation from the ER to the cell surface, its pro-domain is gradually cleaved by convertase proteins like PC7 and furin (Lambrecht et al., 2018). This processing is crucial for ADAM10 to become proteolytically active. Therefore, an ADAM10 variant lacking the pro-domain was utilized for reconstitution experiments in order to obtain a catalytically active protein (ACT) (**Figure 13**). A second ADAM10 variant additionally lacking the metalloproteinase domain (∆MP) enabled the evaluation of the importance of ADAM10's catalytic activity for the observed phenotype.

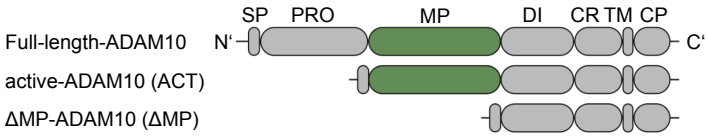

Figure 13: ADAM10 variants used for re-expression. Full-length-ADAM10 protein, catalytically active-ADAM10 variant (ACT) and catalytically inactive ∆MP-ADAM10 variant without the metalloproteinase domain (MP). Each variant comprised the C-terminal end with the cytoplasmic domain (CP), the transmembrane domain (TM), the cysteine-rich domain (CR) and the disintegrin domain (DI) as well as the signal peptide (SP). The pro-domain (PRO) was removed for both the catalytically active and inactive ADAM10 variant. Adapted from (Bahrami, Schmid et al., 2023).

Successful expression and correct localization of the ADAM10-ACT was quality controlled using both confocal microscopy and conventional western blots probing both whole cell lysates and the membrane fractions (**Figure 14**). For confocal microscopy, ADAM10 was knocked-out in H293T cells via lentiviral transduction. ADAM10 variants were re-expressed via transient transfection and wild-type ADAM10, ADAM10 KO and catalytically active ADAM10 (ACT) re-expressing cells were compared after extracellular immunohistochemical staining (see 3.3.14). This approach revealed that ADAM10 KO H293T cells did not show any remaining ADAM10, while re-expression of ACT did result in ADAM10 signals resembling the wild-type situation both with regards to expression levels and localization (**Figure 14A**). As a second proof-of-concept experiment, conventional western blots were conducted (see 3.4.2 and 3.4.3). Firstly, this confirmed the KO of ADAM10 and subsequently the successful re-expression. Additionally, comparing the whole lysate (cytosol) with the membrane-enriched fraction (membr.) displays an increased protein level in the membrane fraction, thus indicating a

stronger localization to the plasma membrane, which is in line with the confocal microscopy data (**Figure 14B**).

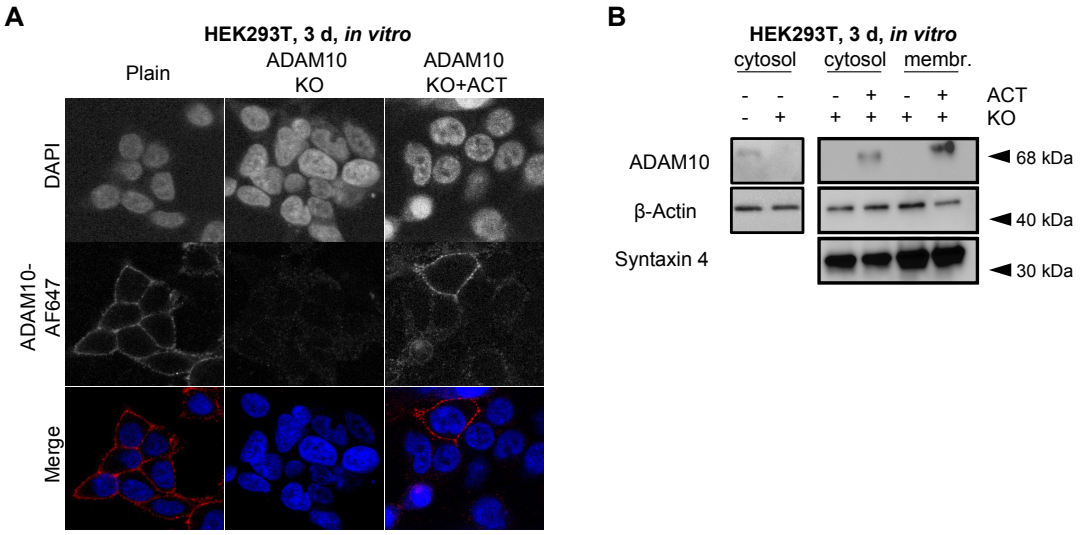

Figure 14: Quality controls of ADAM10 variant re-expression and localization. A Recombinant ADAM10 expression and localization depicted by confocal microscopy images. H293T control, ADAM10 KO and ADAM10 KO cells transfected with the catalytically active ADAM10 variant (ACT) were fixed and stained without permeabilization for ADAM10 using the primary anti-ADAM10 antibody and a secondary anti-mouse Alexa Fluor 647 (AF647) antibody. DAPI was utilized for staining of the nucleus. Representative images from three independently performed experiments are shown. **B** Western Blot of ADAM10 protein levels in whole cell lysates (cytosol) and membrane fraction lysates (membr.) of H293T wild-type and ADAM10 KO cells with and without re-expression of the catalytically active ADAM10 variant (ACT). β-Actin was used as loading control and Syntaxin 4 as membrane fraction marker protein. Adapted from (Bahrami, Schmid et al., 2023).

Passing the described quality controls, next the effect of ADAM10 reconstitution was evaluated using an *in vivo* competitive reconstitution assay in the ALL-199 PDX model. ADAM10 KO PDX cells were lentivirally transduced with either a T-Sapphire-labelled ADAM10 variant or a control vector conferring iRFP expression. PDX cells were mixed in a 1:1 ratio and injected into mice. Upon signs of advanced leukemia, animals were sacrificed, cells isolated from the BM and the distribution of the two populations was evaluated by flow cytometry (**Figure 15A**). Successful re-expression of either of the two ADAM10 variants was confirmed both by expression of T-Sapphire by flow cytometry and on mRNA level using RT-qPCR (**Figure 15BC** and see 3.3.11). This indicated a similar expression level of the two variants compared to the endogenous ADAM10 levels in the wild-type situation. Evaluation of the distribution of the ADAM10 KO control population and the ADAM10 KO population with a re-expressed ADAM10 variant *in vivo* showed a clear difference between the ACT and the ΔMP ADAM10 variant. While re-expression of ADAM10-ACT significantly enhanced PDX growth and proliferation, thereby rescuing the observed growth disadvantage phenotype, the ΔMP variant was not able to improve the growth kinetics of the leukemic cells (**Figure 15D**).

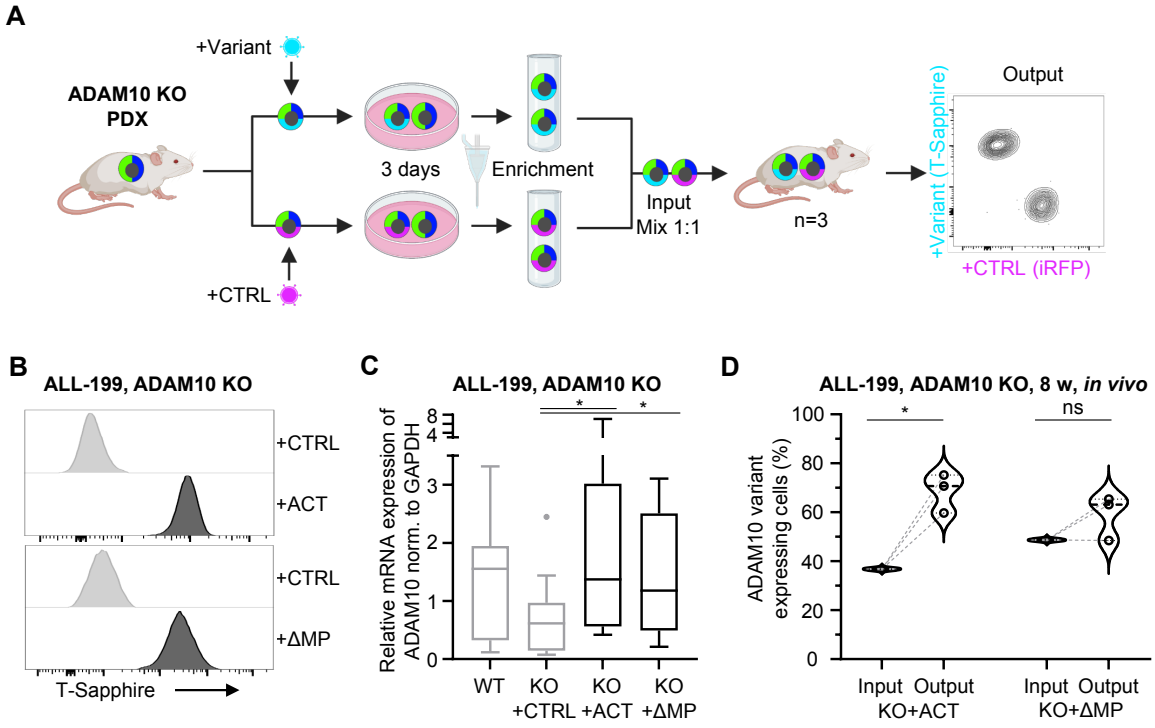

Figure 15: *In vivo* competitive ADAM10 reconstitution assay. A Scheme depicting the workflow of the *in vivo* competitive ADAM10 reconstitution assay. The assay was performed similar to the validation assays described in **Figure 10**. In contrast, ADAM10 KO PDX cells were lentivirally transduced with either an ADAM10 variant or an iRFP expressing control plasmid. Mixing, *in vivo* growth and analysis was performed as for the validation assays. **B** T-Sapphire expression of the control and the ADAM10 variant-transduced population is compared via flow cytometry. Per group, representative histograms of the two populations of one animal are depicted. **C** ADAM10 mRNA levels in Cas9- transgenic wild-type ALL-199 PDX cells (WT) and ADAM10 KO cells reconstituted with either the iRFP control (KO+CTRL), the catalytically active variant (KO+ACT) or the catalytically inactive variant (KO+ΔMP) was measured using RT-qPCR and normalized to GAPDH. Median, 25th and 75th percentile indicated by box; 25th percentile - 1.5 IQR and 75th percentile + 1.5 IQR indicated by whiskers. * p<0.05 by unpaired t-test. **D** Violin plot of the *in vivo* competitive ADAM10 reconstitution assay in ALL-199 (both ADAM10 variants n=3). The percentage of the ADAM10 KO population reconstituted with either of the two ADAM10 variants in the injection mix (Input) and after re-isolation from the sacrificed animals at an advanced stage of leukemia (Output) is depicted. Dashed lines indicate median, dotted lines the 25th and 75th percentile. ns not significant, * p<0.05 by paired t-test. Adapted from (Bahrami, Schmid et al., 2023).

In summary, these data affirm ADAM10's essentiality for leukemic cell growth *in vivo*, while ruling out potential off-target effects. Furthermore, ADAM10's enzymatic activity conferred by its metalloproteinase domain appears to be the key factor for ADAM10's importance.

4.5 Multi-omics data reveal alterations in cellular pathways upon ADAM10 loss

Next, our aim was to elucidate the downstream effects of ADAM10 or its loss in leukemic cells. Therefore, we chose a multi-omics approach including both transcriptomic and proteomic analysis of ADAM10 KO cells compared to their respective controls. In a first step, we performed proteome as well as secretome analyses of the B-ALL cell lines SEM and NALM-6 with and without the KO of ADAM10 after serum starvation for three days (**Figure 16**) in close collaboration with Ashok Kumar Jayavelu. ADAM10's sheddase activity is mediating the cleavage of a plethora of transmembrane proteins, therefore secretome analysis was performed as described in (Bahrami et al., 2023). Secretome analysis enabled investigation of the differentially secreted proteins upon ADAM10 loss.

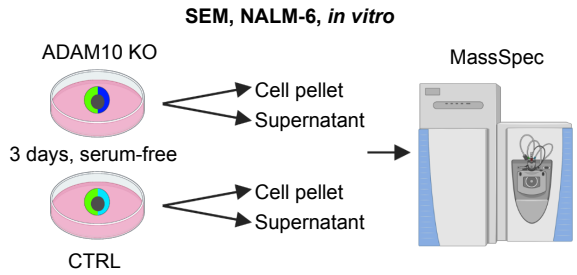

Figure 16: Workflow of the proteomic and secretomic profiling of B-ALL cell lines. SEM and NALM-6 KO and control cells were cultivated for three days under serum-free conditions. By centrifugation, cells and supernatant were separated and collected for proteome and secretome analysis, respectively. Adapted from (Bahrami, Schmid et al., 2023).

Proteomic profiling found 1120 proteins to be up- and 854 proteins to be downregulated in ADAM10 KO SEM cells compared to controls (**Figure 17A**). Pathways associated with cell death and apoptosis were upregulated the most strikingly (**Figure 17B**), while additionally metabolism, cell cycle and interestingly adhesion and membrane associated processes were altered (**Figure 17C**).

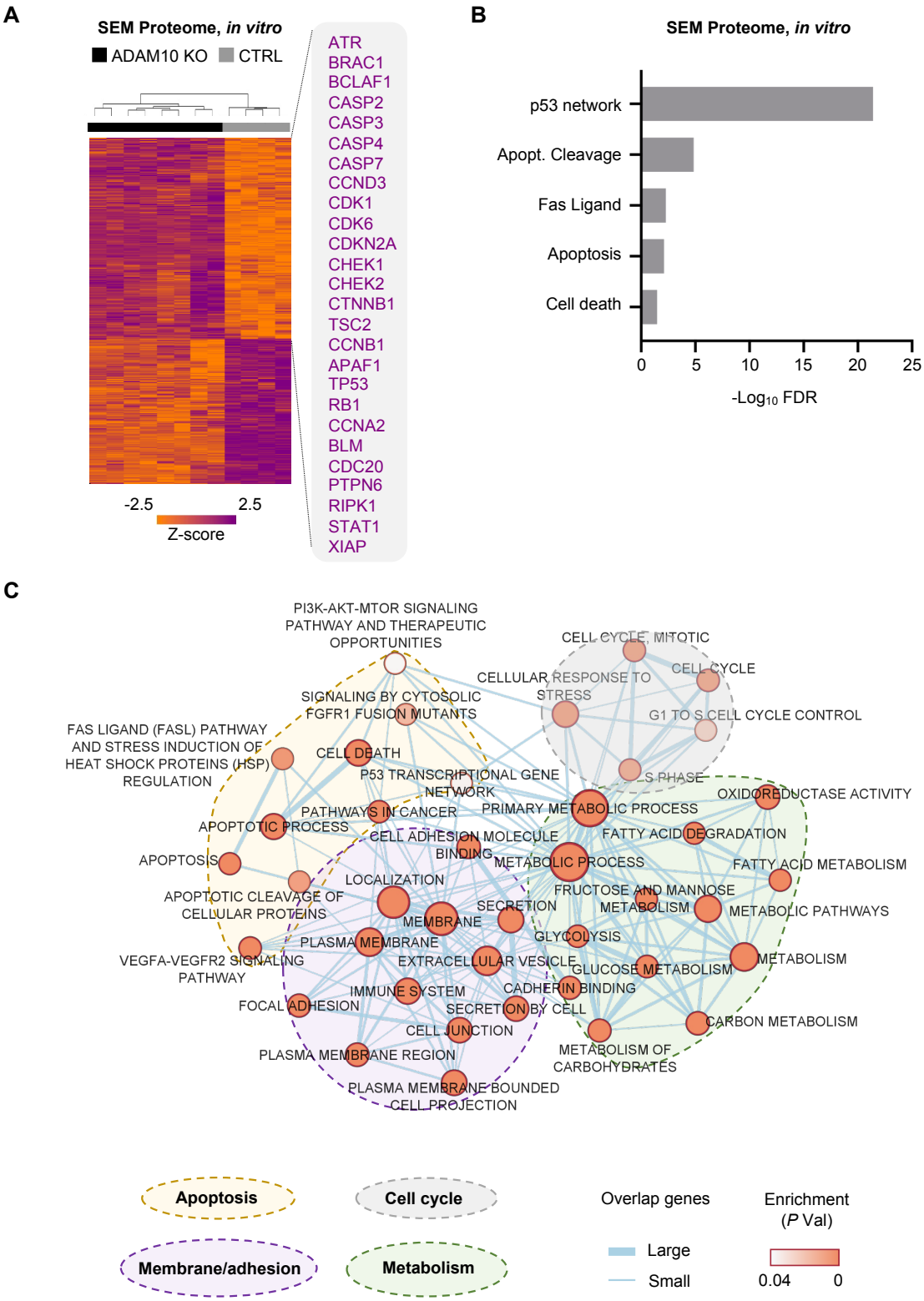

Figure 17: SEM proteome. A Heat map of SEM cells by unsupervised hierarchical clustering of significantly regulated proteins; ADAM10 KO (n=8) compared to control (n=4) (two-sample test, permutation-based FDR <0.05). Proteins enriched in the ADAM10 KOs are specified in purple. **B** Bar diagram indicating the five most significantly enriched pathways of the proteome results shown in **A**. **C** Comprehensive pathway enrichment analysis. The four most relevant, enriched functional processes are depicted. Each gene set is represented by a node, whose size is defined by the number of genes. The significance of its enrichment is indicated by its color. Lines represent overlap between the gene

sets, while line width is in proportion to the number of shared genes. Data were analyzed using GSEA 4.1.0 and depicted via Cytoscape 3.9.0. Adapted from (Bahrami, Schmid et al., 2023).

Analyzing the cleaved and secreted proteins in ADAM10 KO and control SEM and NALM-6 samples, 220 and 1000 proteins could be measured in the supernatants, respectively. From these, 44 and 62 proteins were secreted differently, respectively (**Figure 18AB**). As a proof-of-concept, strong reduction of the ADAM10 protein itself in the secretome upon KO was detected in SEM cells (**Figure 18C**). Additionally, five proteins were significantly altered in both tested cell lines, namely APP, GGH, H2AFX, HIST1H4A and HSP90AA1. APP (amyloid-beta precursor protein) is a well described direct target of ADAM10 and HSP90AA1 (heat shock protein 90 α) exerts known cancer related functions (**Figure 18D**). Furthermore, FLT3 (fms-like tyrosine kinase 3) secretion was altered in SEM cells. These results suggest that proteins cleaved by ADAM10 before secretion might convey ADAM10's pro-leukemic role.

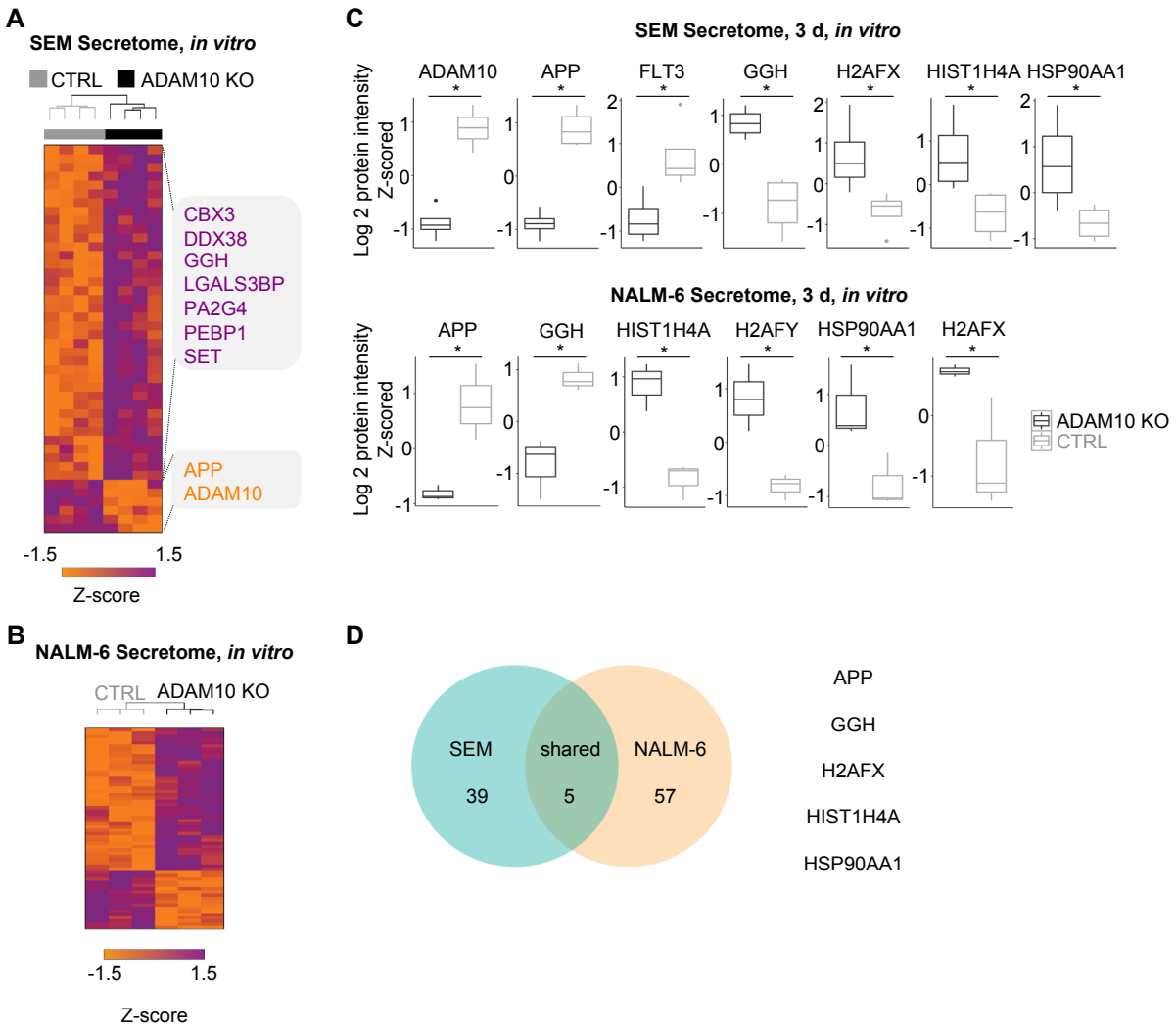

Figure 18: B-ALL cell line secretome. A Heatmap of SEM cells by unsupervised hierarchical clustering of proteins significantly differentially secreted in ADAM10 KO (n=4) compared to control (n=4) samples (two-sample test, permutation-based FDR <0.05). Secreted proteins enriched in the ADAM10 Kos are

specified in purple, depleted proteins in orange, respectively. **B** Heatmap of NALM-6 cells by unsupervised hierarchical clustering of proteins significantly differentially secreted in ADAM10 KO (n=3) compared to control (n=3) samples (two-sample test, p value <0.05). **C** Box plots of significantly differentially secreted proteins in SEM and NALM-6 cells with ADAM10 KO compared to controls depicted by z-scored log 2 protein intensity. **D** Differentially secreted proteins in SEM and NALM-6 cell lines are compared using a Venn diagram with indication of the commonly altered secreted proteins. Adapted from (Bahrami, Schmid et al., 2023).

As a next step, both transcriptome and proteome analysis were performed using PDX ALL-199 and ALL-265 cells. Transcriptomic profiling, which was conducted by Vindi Jurinovic, discovered 641 differentially expressed genes of ADAM10 KO vs. control PDX cells with 327 down- and 314 upregulated genes, respectively (**Figure 19A**). Significantly altered processes were clustered using enrichment map analysis (**Figure 19B**). Performing gene set enrichment analysis (GSEA), the Kyoto Encyclopedia of Genes and Genomes (KEGG) terms cell adhesion, oxidative phosphorylation and cell cycle were found to be significantly altered (**Figure 19C**).

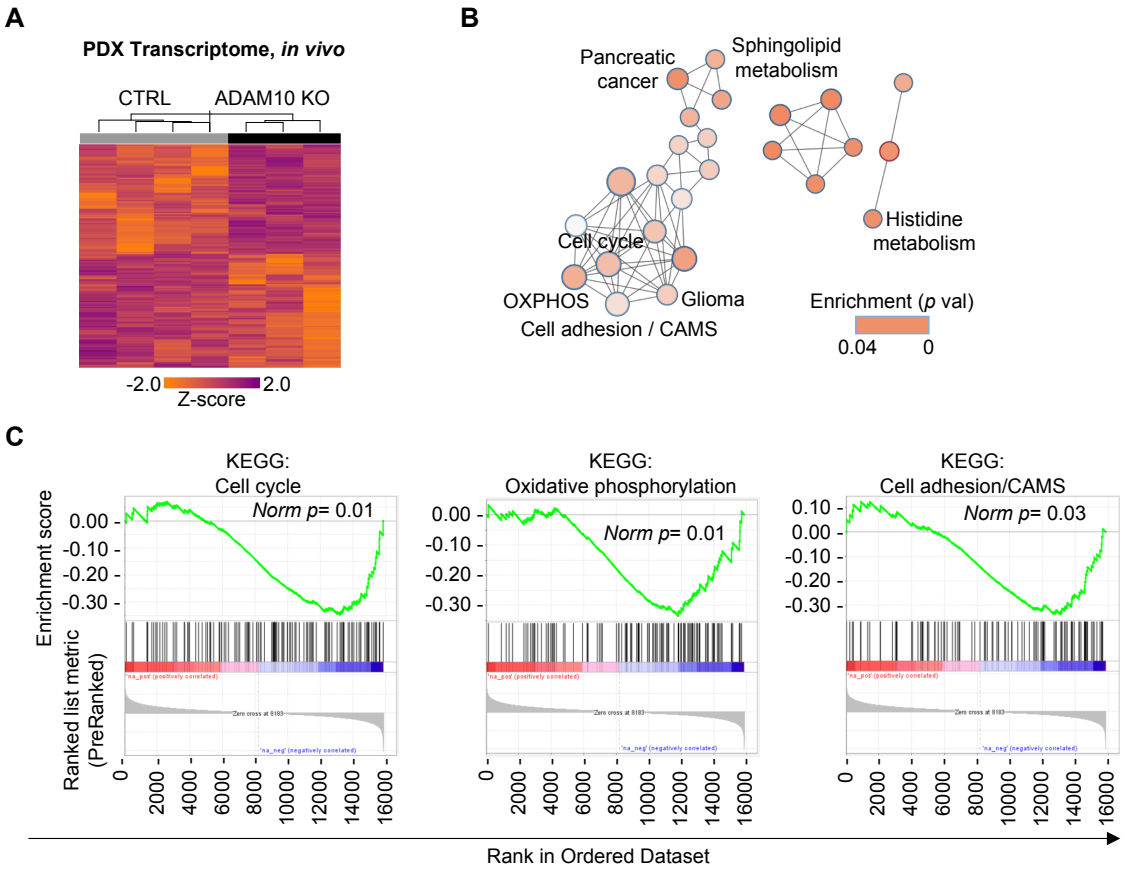

Figure 19: Transcriptome analysis of PDX ALL-199 and ALL-265. A Heatmap depicting the differentially expressed genes compared between ADAM10 KO (n=3) and control (n=4) ALL-199 and ALL-265 PDX samples by unadjusted *p* value of ≤0.05 and fold change <0.5 or >2. **B** Enriched pathways of differentially expressed genes shown in **A**. Most relevant, enriched functional processes are labelled. Each gene set is represented by a node, whose size is defined by the number of genes. The significance

of its enrichment is indicated by its color. Lines represent overlap between the gene sets, while line width is in proportion to the number of shared genes. Data were analyzed using GSEA 4.1.0 and depicted via Cytoscape 3.9.0. **C** Gene set enrichment analysis (GSEA) of the transcriptome data in **A** (p<0.005 and FDR q value<0.33, Norm p=0.01). Most relevant, significantly altered KEGG terms are depicted. Adapted from (Bahrami, Schmid et al., 2023).

To further decipher the cellular processes and pathways affected by the loss of ADAM10, we performed proteome analysis of ADAM10 KO and control ALL PDX samples with the help of Ashok Kumar Jayavelu. This approach identified numerous differentially regulated proteins in several biological pathways with oxidative phosphorylation- (OXPHOS), mitochondrion-, cell death- and cell cycle-associated pathways being the most affected as seen by enrichment analysis (**Figure 20**).

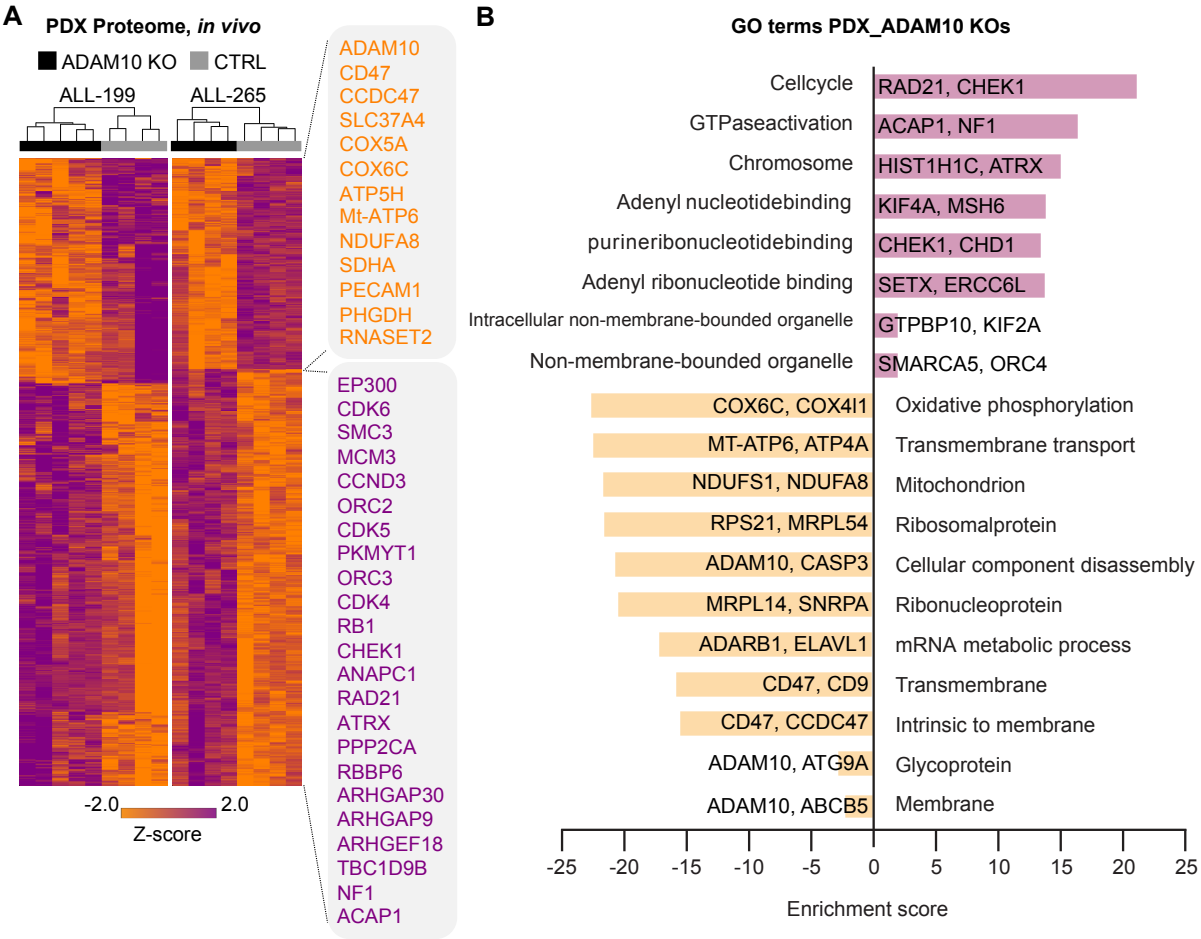

Figure 20: Proteome analysis of PDX ALL-199 and ALL-265. A Heatmap depicting the differentially regulated proteins compared between ADAM10 KO (ALL-199: n=4; ALL-265 n=4) and control (ALL-199: n=5; ALL-265 n=4) PDX samples by unsupervised hierarchical clustering (two-sample test, permutation-based FDR <0.05). Proteins enriched in the ADAM10 KOs are specified in purple, de-enriched proteins in orange, respectively. **B** Depiction of differentially regulated GO terms of the data in **A** by Fisher's exact test. Representative proteins of each displayed GO term are listed. Adapted from (Bahrami, Schmid et al., 2023).

Combining both transcriptomic and proteomic analysis data, we found especially metabolism, apoptosis / cell death and cell cycle to be commonly de-regulated in both -omics approaches and in both cell lines and PDX models *in vivo* as well as *in vitro*. These findings suggest a cell intrinsic component of ADAM10's essentiality in leukemic cells, which is independent from its importance for the interaction with the BM microenvironment.

As functional proof-of-concept experiments, we tested the effect of ADAM10 loss on cell cycle and cell death. Targeting members of the ADAM family including ADAM10 was the aim of several previous studies in different tumor entities (Minond, 2020; Mullooly et al., 2016; Pavlaki & Zucker, 2003; Rad et al., 2022; Smith et al., 2020; Venkatesh et al., 2017); therefore, we could use the commercially available small molecule inhibitor GI254023X for targeting ADAM10 in a more translatable approach. The effect of ADAM10 inhibition *in vitro* was analyzed using flow cytometry (**Figure 21AB** and see 3.6.3). Treatment of ALL-199 PDX cells with 490 µM GI254023X lead to a marked arrest of the cell cycle with a decreased fraction of cells in the S phase and a higher percentage of cells in the G1 phase (**Figure 21CD**). These effects increased with treatment time shown by comparing the flow cytometry measurements 24, 48 and 72 hours post treatment start. (**Figure 21D**).

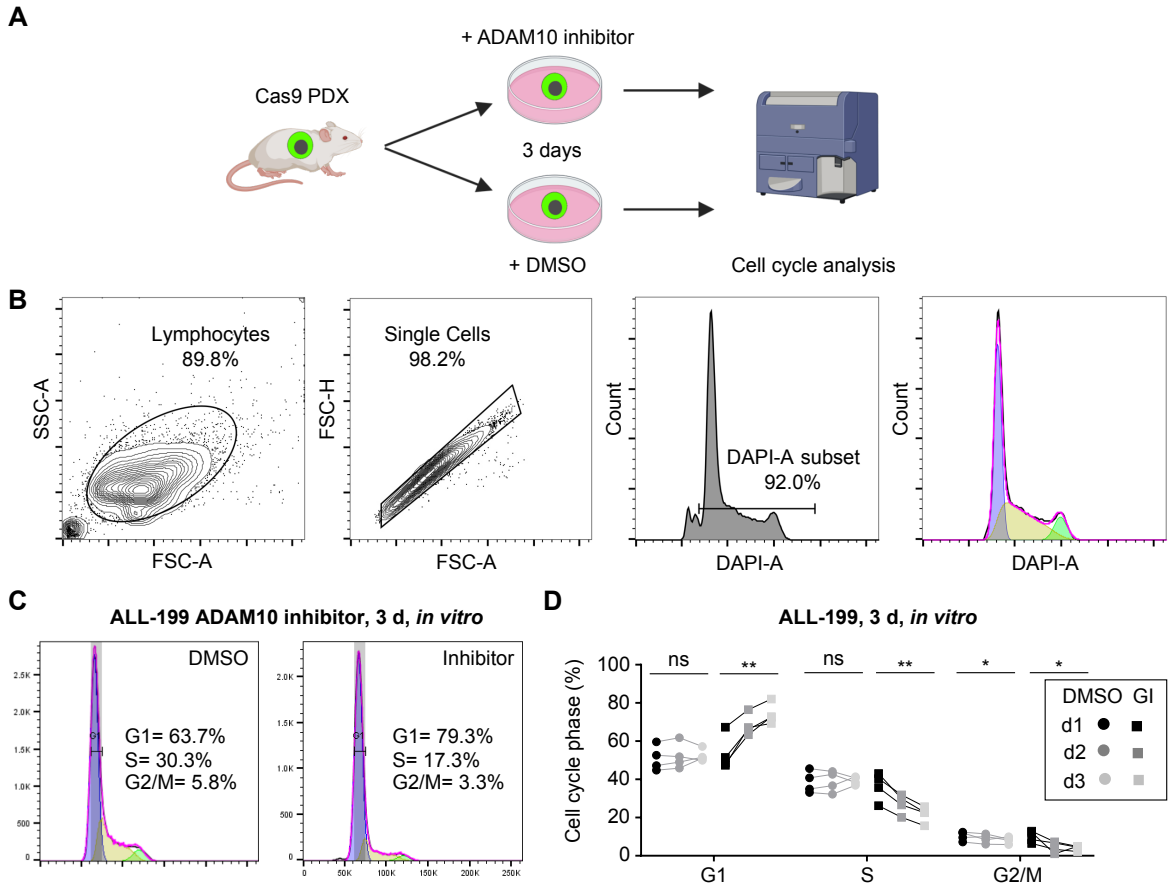

Figure 21: Cell cycle assay with PDX ALL-199 after chemical inhibition of ADAM10. A Workflow of the cell cycle assay. PDX cells were treated for three days with the chemical ADAM10 inhibitor GI254023X (490µM) or its solvent (DMSO) *in vitro* before cells were fixed, stained using DAPI and analyzed via flow cytometry. **B** Gating strategy used for cell cycle analysis. Lymphocytes and single cells were determined using SSC and FSC. Phases of cell cycle were discriminated by DAPI recording in the linear setting and using the Dean-Jett-Fox model of the FlowJo software. **C** Representative histograms of ADAM10 Inhibitor- and solvent-treated ALL-199 PDX cells. G1 = Gap phase 1, S = Synthesis phase, G2/M = Gap phase 2 / mitosis. **D** Quantification of four independent replicates either treated with the ADAM10 inhibitor or its solvent after one, two and three days of treatment, respectively. Each dot represents one independent measurement after the indicated time and treatment. ** p<0.01, * p<0.05 by paired t-test. Adapted from (Bahrami, Schmid et al., 2023).

We next validated the effect of ADAM10 loss on the rate of apoptosis and cell death. Here, we used the electroporation of RNPs to generate ADAM10 KO PDX cells, which we compared to control cells electroporated with non-targeting sgRNA containing RNPs (**Figure 22A** and see 3.6.5). Three days post electroporation, the apoptosis rate was determined via DAPI and Annexin V double staining. Excluding only small debris, the percentage of Annexin V-positive cells was measured via flow cytometry (**Figure 22B**). Both ALL and AML PDX models showed an increased percentage of Annexin V-positive cells resembling early apoptotic cells, although to a greater extent in ALL-199 compared to the AML models (**Figure 22CD**). Using the same strategy as for the cell cycle assay, we again inhibited ADAM10 chemically using GI254023X

(see 3.6.5) and detected a similar effect on the proportion of Annexin V-positive cells as in the KOs, further validating the effect of ADAM10 loss on cellular apoptosis rates (**Figure 22CD**).

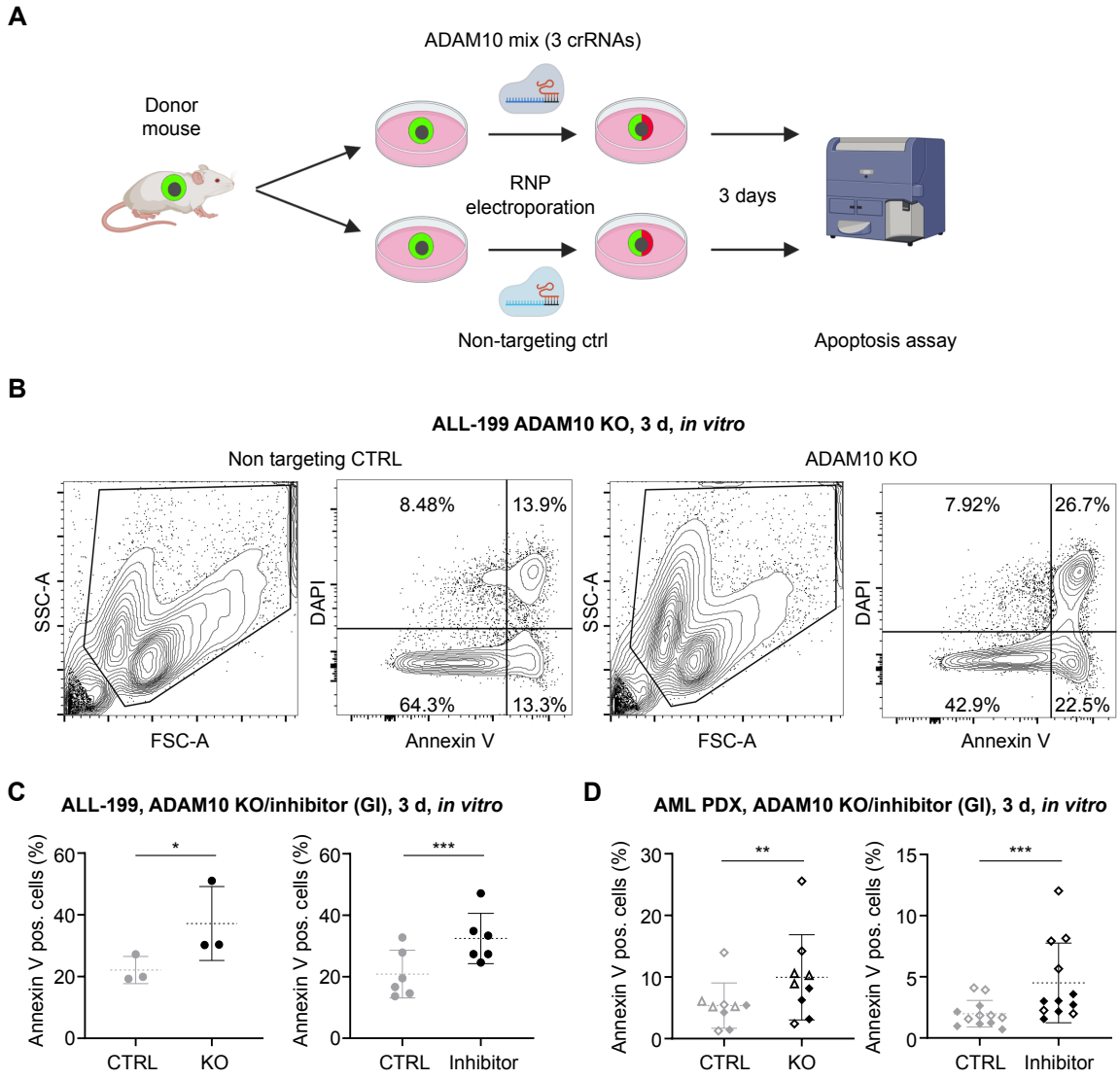

Figure 22: Apoptosis assay of PDX ALL-199 after RNP-mediated KO or chemical inhibition of ADAM10. A Workflow of RNP KO apoptosis assay. PDX cells were electroporated with RNPs containing either a mix of three crRNAs targeting ADAM10 or a non-targeting crRNA. Three days post electroporation, PDX cells were stained using Annexin V and DAPI and measured by flow cytometry. **B** Representative flow cytometry plots depict the gating strategy for the apoptosis assays. Debris removal was conducted by SSC and FSC. Using quadrant gates, Annexin V- and DAPI-positive and -negative populations were defined. **C** Quantification of the percentage of Annexin V-positive PDX ALL-199 cells after RNP KO or chemical inhibition of ADAM10 (RNP KO: n=3; GI254023X treatment (490µM): n=6). *** p<0.001, * p<0.05 by paired t-test. **D** Quantification of the percentage of Annexin V-positive PDX AML-388, AML-393 and AML-661 cells after RNP KO or chemical inhibition of ADAM10 (RNP KO: AML-388 (◇): n=3, AML-393 (◆): n=3, AML-661 (△): n=3; GI254023X treatment (490µM): AML-388: n=6, AML-393: n=6). *** p<0.001, ** p<0.01 by paired t-test. Adapted from (Bahrami, Schmid et al., 2023).

In conclusion, transcriptomic and proteomic data highlighted the downstream effects of ADAM10 loss with pathways, such as metabolism, apoptosis / cell death and cell cycle, being

most severely affected. We could functionally validate these findings using proof-of concept experiments. Chemical inhibition or genetic loss of ADAM10 resulted in both a block of cell cycle progression as well as an increase of apoptotic cells in ALL and AML PDX models *in vitro*, validating cell cycle and apoptosis as important processes which are altered upon KO of ADAM10.

4.6 ADAM10 reduction leads to decreased early engraftment capacity, stem cell frequency and CFU potential of PDX models *in vivo*

After observing cell-intrinsic effects of ADAM10 loss, namely on cell cycle and cell death via apoptosis, we aimed to further functionally characterize ADAM10's role in leukemia biology and to elucidate a potential clinical benefit of ADAM10 targeting for leukemia patients.
In order to investigate ADAM10's importance for the interaction of leukemic cells with the BM microenvironment, early engraftment and homing assays were performed (see 3.2.9). In these assays, we tested the effect of ADAM10 reduction via chemical inhibitors on the potential of freshly injected PDX cells to find their orthotopic niche and to engraft in the murine bone marrow. For this, ALL PDX cells were pre-treated *ex vivo* for two to three days with one of the two commercially available ADAM10 inhibitors GI254023X or Aderbasib. As ADAM10 was shown to be shuttled from the cell surface to the cytosol upon catalytic inactivation (Seifert et al., 2021), ADAM10 surface stainings could be used to determine effective inhibitor concentrations, which markedly reduce ADAM10 surface levels. The optimal concentration of each of the two inhibitors was determined in titration experiments displayed in **Figure 23**.

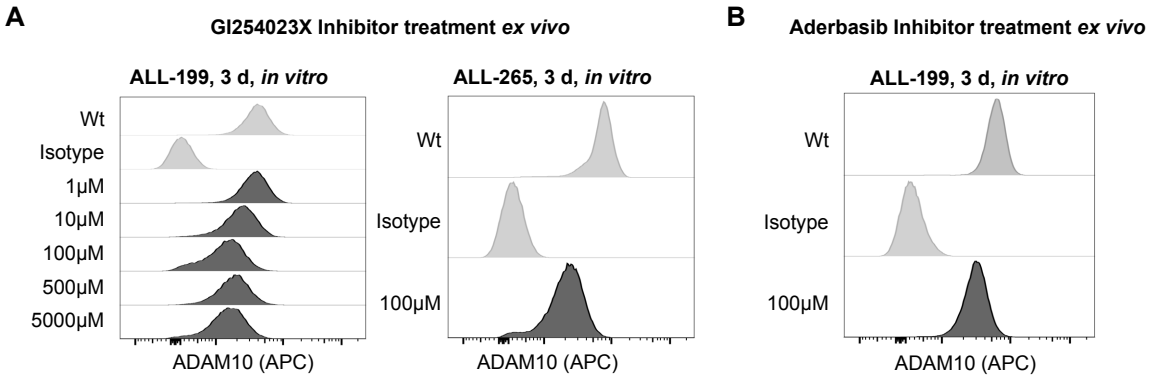

Figure 23: ADAM10 inhibitor treatment reduces ADAM10 surface levels. Representative flow cytometry histograms of proof-of-concept titration experiments determining the optimal concentration of the inhibitors GI254023X (**A**) and Aderbasib (**B**) on ALL-199 and ALL-265 are depicted. The inhibitor concentrations were evaluated based on the reduction of ADAM10 surface levels. Adapted from (Bahrami, Schmid et al., 2023).

The 48-72 hours pre-treatment with the chemical inhibitors had no effect on cell viability as shown in **Figure 24A-C**. Considering that the early engraftment process *in vivo* is very inefficient, 10^7 PDX cells – the maximal possible number – were transplanted per mouse to enable retrieval of cells after 72 hours *in vivo*, (Ebinger et al., 2016; Ebinger et al., 2020). For the treatment with Aderbasib, an additional control was included by keeping a small portion of cells *in vitro* in parallel to the in *vivo* passage. This allowed us to separate potentially delayed effects of the inhibitor treatment on cell viability from the effect of ADAM10 loss on early

engraftment of PDX cells. Since no increase in the percentage of dead cells was observed *in vitro* (**Figure 24D**), the differences in the engraftment levels between inhibitor-treated and control cells can most likely be attributed to the role of ADAM10.

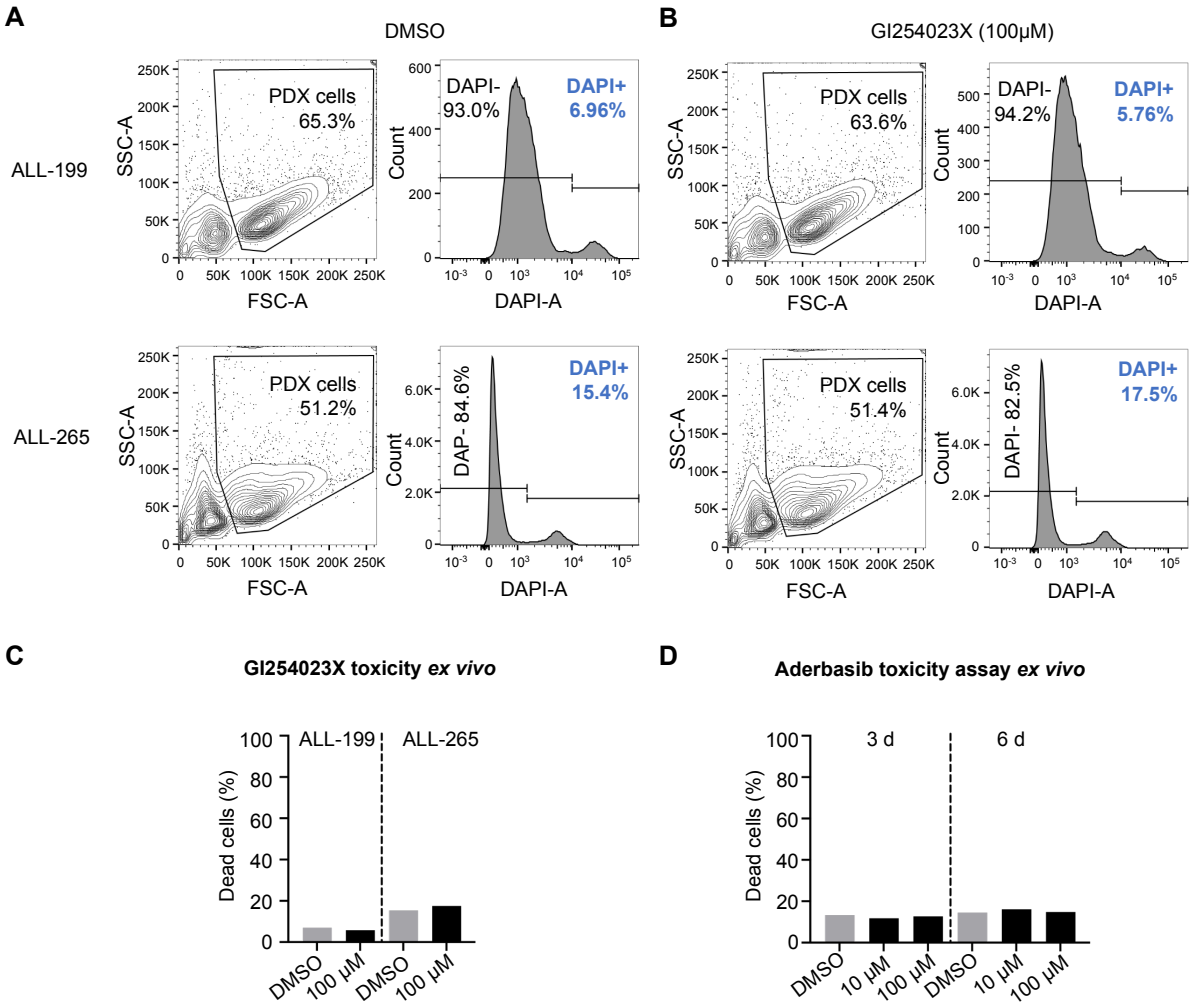

Figure 24: ADAM10 inhibition at the indicated concentrations is not toxic for PDX cell *in vitro*. **AB** Representative flow cytometry plots of a proof-of-concept experiment. Treatment of ALL-199 and ALL-265 with GI254023X at a concentration of 100 µM did not decrease the viability the cells compared to the solvent control as determined using a fixable live/dead cell staining. **C** Quantification of the data depicted in **A** and **B**. **D** Quantification of a proof-of-concept experiment treating ALL-199 PDX cells with the ADAM10 inhibitor Aderbasib at the indicated concentrations. Neither after three nor after additional three days in culture, Aderbasib decreased cell viability compared to the solvent control as determined using a fixable live/dead cell staining. Mean of three technical replicates per group is depicted. Adapted from (Bahrami, Schmid et al., 2023).

The *in vivo* experiment was conducted as depicted in **Figure 25A** and described in 3.2.9. PDX ALL cells were pre-treated with a chemical ADAM10 inhibitor or its solvent for two to three days and injected into groups of animals. Three days post transplantation, mice were sacrificed, cells isolated from the BM and the percentage as well as the absolute number of PDX cells within the bone marrow was measured by flow cytometry. Both tested inhibitors

significantly reduced the early engraftment capacity of PDX cells, underlining a crucial function of ADAM10 for leukemic cells during early engraftment and successful homing to the BM microenvironment (**Figure 25B**).

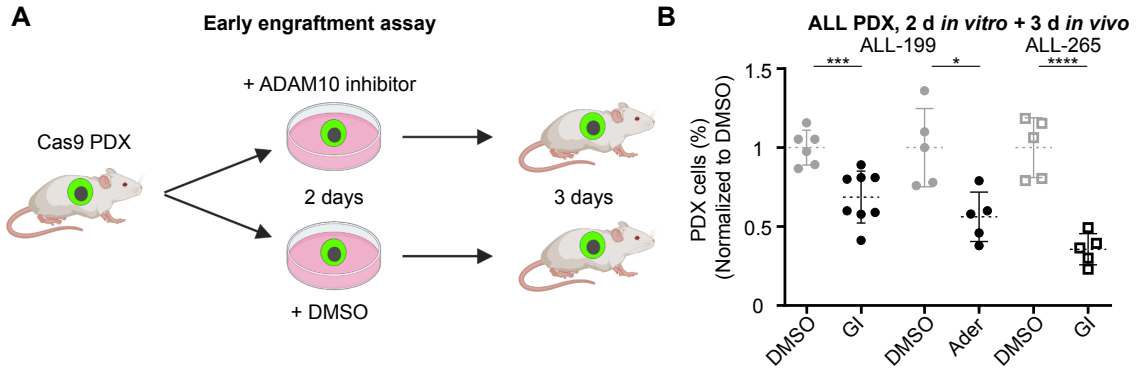

Figure 25: Chemical inhibition of ADAM10 significantly reduced early engraftment capacity of PDX cells. A Scheme depicting the procedure of the early engraftment assay. Cas9-transgenic PDX cells were treated with either an ADAM10 inhibitor or its solvent for 2-3 days before transplantation into groups of mice. Animals were sacrificed after 3 days, PDX cells re-isolated from the BM and analyzed via flow cytometry. **B** Quantification of the percentage of PDX cells engrafted in the BM normalized to the mean of the corresponding control group (ALL-199: GI 100 µM n=8 with n=6 DMSO controls, Ader 10 µM n=5 with n=5 DMSO controls; ALL-265: GI 100 µM n=5 with n=5 DMSO controls). **** $p<0.0001$, *** $p<0.001$, *$p<0.05$ by paired t-test. Adapted from (Bahrami, Schmid et al., 2023).

In a next step, the effect of ADAM10 loss on LSCs was investigated. LSCs reside in the bone marrow niche close to the endosteum in a dormant state. While fast proliferating blast cells are efficiently eradicated by standard chemotherapy, these LSCs are often unaffected, leading in many cases to a disease relapse. Therefore, targeting of the LSCs represents a critical approach for a successful treatment of acute leukemia. The gold standard to determine the LSC frequency are limiting dilution transplantation assays (LDTA) (Eaves, 2015; Maetzig et al., 2017), which were used in a competitive setting (**Figure 26**). We employed these LDT assays in a competitive setting (see 3.2.11).

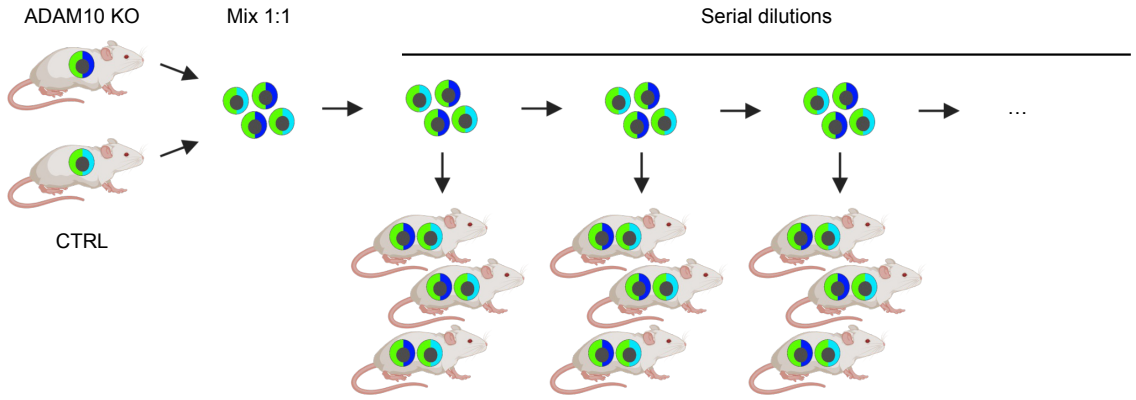

Figure 26: Competitive in vivo ADAM10 KO LDTA assay to determine LIC frequency. Scheme depicting the procedure of the competitive ADAM10 KO LDTA assay. Cas9-transgenic PDX cells were lentivirally transduced with a sgRNA targeting ADAM10 or a non-targeting control sgRNA, respectively. sgRNA-positive cells were amplified via donor animals, mixed in a 1:1 ratio and serially diluted until theoretically less than one leukemia-initiating cell (LIC) is present in the mixture according to the corresponding PDX model's LIC frequency. Serially diluted mixes were transplanted into mice and leukemic growth monitored via *in vivo* bioluminescence imaging. At a defined tumor burden, all animals were sacrificed, the PDX cells re-isolated from the BM and the distribution of the ADAM10 KO and control subpopulation analyzed using flow cytometry. A threshold of 1% of PDX cells within the cells in the BM was defined as positive engraftment. Adapted from (Bahrami, Schmid et al., 2023).

Using two ALL PDX models, ALL-199 and ALL-265, ADAM10 KO cells marked with mTagBFP and control cells labelled with T-Sapphire were mixed in a 1:1 ratio, step-wise diluted and transplanted into groups of mice. Leukemia growth was monitored using *in vivo* bioluminescence imaging (**Figure 27**) before animals were sacrificed and the composition of the ADAM10 KO and control population was measured using flow cytometry. Successful engraftment of the respective population was calculated based on the previously defined threshold of 1% within all BM cells (**Table 37**).

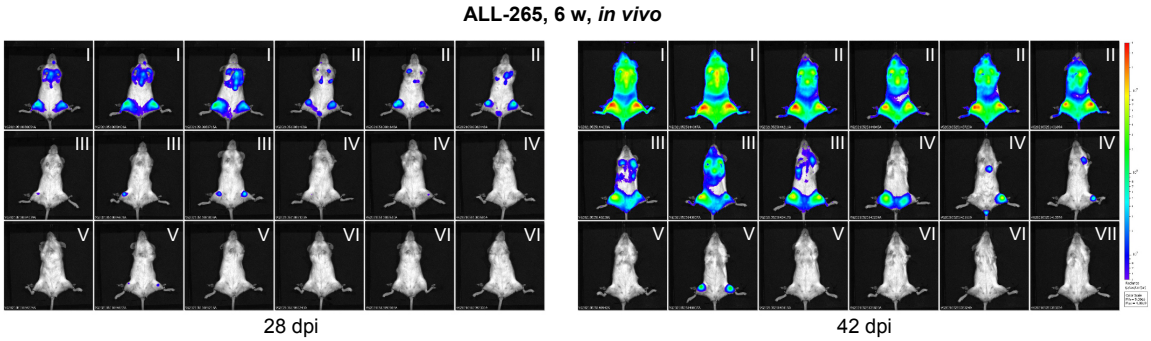

Figure 27: Monitoring of leukemic growth in the competitive *in vivo* ADAM10 KO LDTA assay. Representative pictures of the *in vivo* bioluminescence imaging of the competitive *in vivo* ADAM10 KO LDTA assay in the PDX sample ALL-265 four and six weeks post transplantation. The respective cell number injected per population for each group of animals is indicated using roman numerals (I = 20.000, II = 6.000, III = 2.000, IV = 600, V = 200, VI = 60, VII = 20). Adapted from (Bahrami, Schmid et al., 2023).

Table 37: Calculation of successful engraftment of ALL-199 cells in the competitive LDTA

Mouse sample	ALL-199 cell number	human	BFP+ = KO	T-Sapphire+ = Ctrl
20210408 - ALL199 take down_74072-81 10 50K P6_015.fcs	10	3,03%	0%	99,90%
20210408 - ALL199 take down_74073-82 10 100K P1_016.fcs		0%	0%	0%
20210408 - ALL199 take down_74074-83 10 100K P1_017.fcs		0%	0%	0%
20210408 - ALL199 take down_74075-84 20 100K P1_018.fcs	20	0%	0%	0%
20210408 - ALL199 take down_74076-85 20 100K P1_019.fcs		9,42E-06	0%	0%
20210408 - ALL199 take down_74077-86 20 100K P1_020.fcs		0%	0%	0%
20210408 - ALL199 take down_74078-87 20 50K P6_021.fcs		11,10%	0%	99,80%
20210408 - ALL199 take down_74032-41 40 100K P1_010.fcs	40	0%	0%	0%
20210408 - ALL199 take down_74079-88 40 50K P6_022.fcs		7,62%	99,80%	0,06%
20210408 - ALL199 take down_74080-89 40 50K P6_023.fcs		0,55%	98,70%	0,12%
20210408 - ALL199 take down_74081-90 40 50K P6_024.fcs		80,80%	0%	100,00%
20210408 - ALL199 take down_74033-42 60 200K P1_011.fcs	60	0,36%	0%	100%
20210408 - ALL199 take down_74034-43 60 200K P1_012.fcs		0,75%	0,33%	99,60%
20210408 - ALL199 take down_74035-44 60 100K P1_013.fcs		0%	0%	0%
20210408 - ALL199 take down_74036-45 60 50K P6_014.fcs		34,70%	99,90%	3,07E-05
20210408 - ALL199 take down_74027-36 120 200K P1_005.fcs	120	0,04%	0%	95,70%
20210408 - ALL199 take down_74028-37 120 50K P6_006.fcs		15,90%	0%	100,00%
20210408 - ALL199 take down_74029-38 120 100K P1_007.fcs		0%	0%	0%
20210408 - ALL199 take down_74030-39 120 50K P6_008.fcs		25,30%	5,39%	94,50%
20210408 - ALL199 take down_74022-31 360 50K P6_002.fcs	360	44,20%	0%	100,00%
20210408 - ALL199 take down_74023-32 360 50K P6_003.fcs		66,60%	1,21%	98,80%
20210408 - ALL199 take down_74031-40 360 50K P6_009.fcs		25,20%	0,63%	99,30%
20210323 - ALL199 high 1080_74024-33 1080 50K P6_002.fcs	1080	5,55%	0,38%	99,60%
20210408 - ALL199 take down_74025-34 1080 50K P6_004.fcs		43,50%	0%	99,90%
20210312 - ALL199 pos ctrl_74026-35 20K_001.fcs	20000	52,10%	14,00%	85,60%

engraftment
no engraftment

In both tested models, ADAM10 loss reduced the frequency of LSCs. While this reduction was significant and corresponds to a factor ten reduction in ALL-199, in ALL-265 the same trend with a three-fold reduction was observed (**Figure 28**). These results indicate that ADAM10 is important for LSCs and their targeting therefore might have the potential to improve the treatment outcome of leukemia patients.

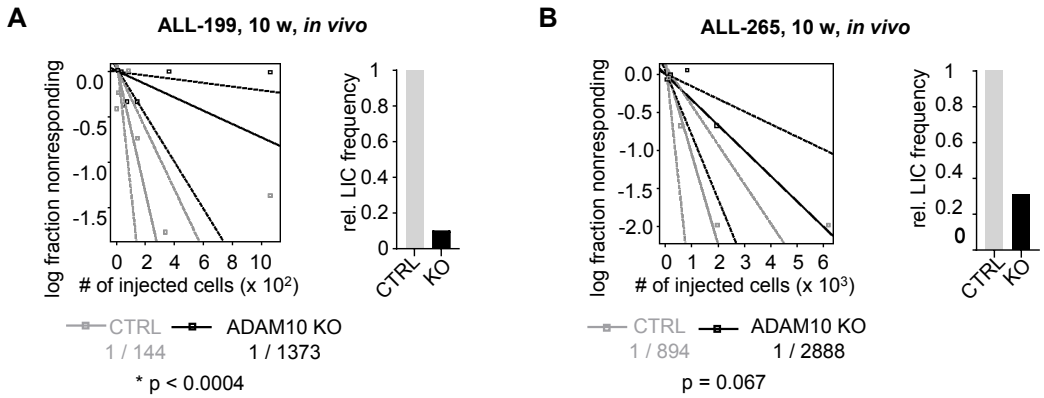

Figure 28: Loss of ADAM10 diminished the LIC frequency of PDX ALL-199 and ALL-265 cells in competitive *in vivo* LDTA assays. AB LIC frequency of the ADAM10 KO and control population is calculated using the ELDA software webtool based on the ratio of positively engrafted populations at the given cell number within each group. The mean of the LIC frequencies (solid) together with the 95% confidence interval (dashed) for the ADAM10 KO (black) and control (grey) populations are shown (**A** ALL-199: n=25; **B** ALL-265: n=25). The relative LIC frequency normalized to the respective control group is shown in the bar graphs. Adapted from (Bahrami, Schmid et al., 2023).

As a next step, with the help of former Master student Tania Duque, the CFU potential of PDX cells lacking ADAM10 compared to control cells was evaluated (see 3.6.4). In two independent approaches, ADAM10 was either knocked-out via lentiviral transduction or ADAM10 levels were reduced using chemical inhibition (**Figure 29** & **Figure 30**). In both experimental set ups, the shape of the individual colonies was not affected (**Figure 29B**, **C**). Nevertheless, in both settings, ADAM10 loss could be measured by flow cytometry and this reduction led to decreased CFU potentials in each setting and PDX model (**Figure 29D**, **Figure 30C** & **Figure 31AB**). Our collaboration partner Sophie Kreissig performed a similar experiment using healthy human CD34+ progenitor cells in combination with chemical inhibition of ADAM10 using either GI254023X or Aderbasib. This approach did not reduce their CFU potential (**Figure 30B, D** & **Figure 31C**), emphasizing the higher sensitivity of leukemic cells towards ADAM10 targeting, thus suggesting a possible therapeutic window for the treatment of leukemia patients.

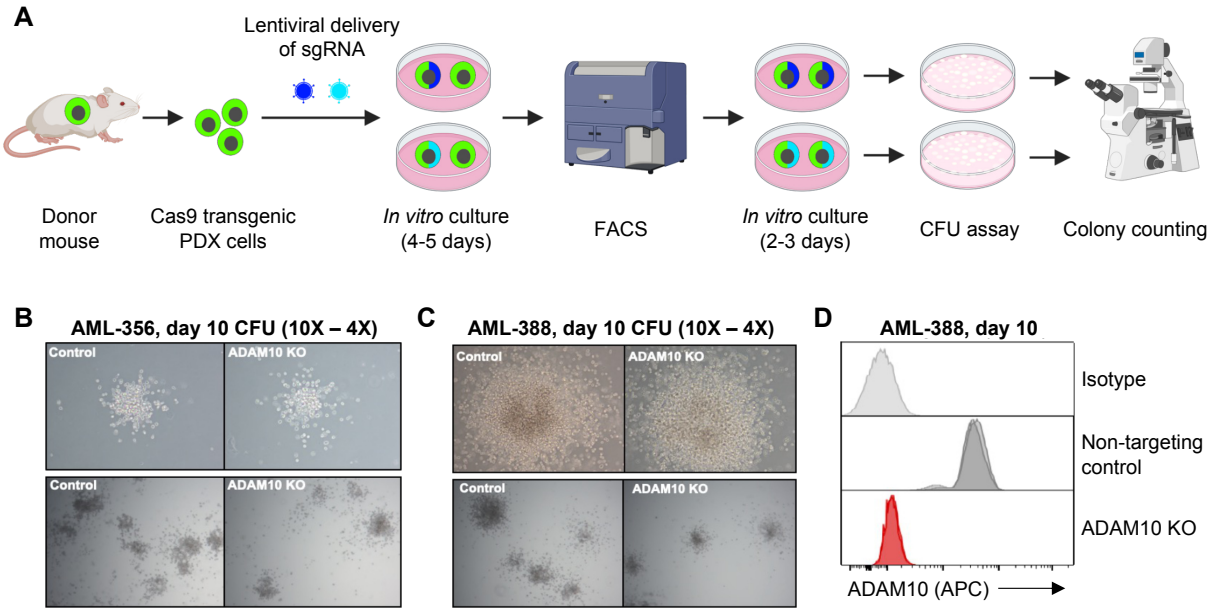

Figure 29: Scheme and quality controls of the influence of ADAM10 loss on CFU potential of AML PDX models. A Depiction of the procedure of the PDX ADAM10 KO CFU assays. Cas9-transgenic PDX cells were lentivirally transduced with an sgRNA targeting ADAM10 or a non-targeting control sgRNA, cultured *in vitro* for four to five days, enriched via flow cytometry, cultured for another two to three days before 1x 10^3 cells were seeded in methylcellulose for the CFU assay. After ten days, colonies were manually counted using an inverted fluorescence microscope. **BC** Representative bright light images of three (AML-356, **B**) and four (AML-388, **C**) independent ADAM10 KO and control cell CFU assays at a magnification of 10x (upper row) and 4x (lower row), respectively, are depicted. **D** Representative flow cytometry histograms of four independent experiments depicting ADAM10 surface levels at the end of the CFU assays. PDX cells transduced with an sgRNA targeting ADAM10 or transduced with a non-targeting control sgRNA were compared. Adapted from (Bahrami, Schmid et al., 2023).

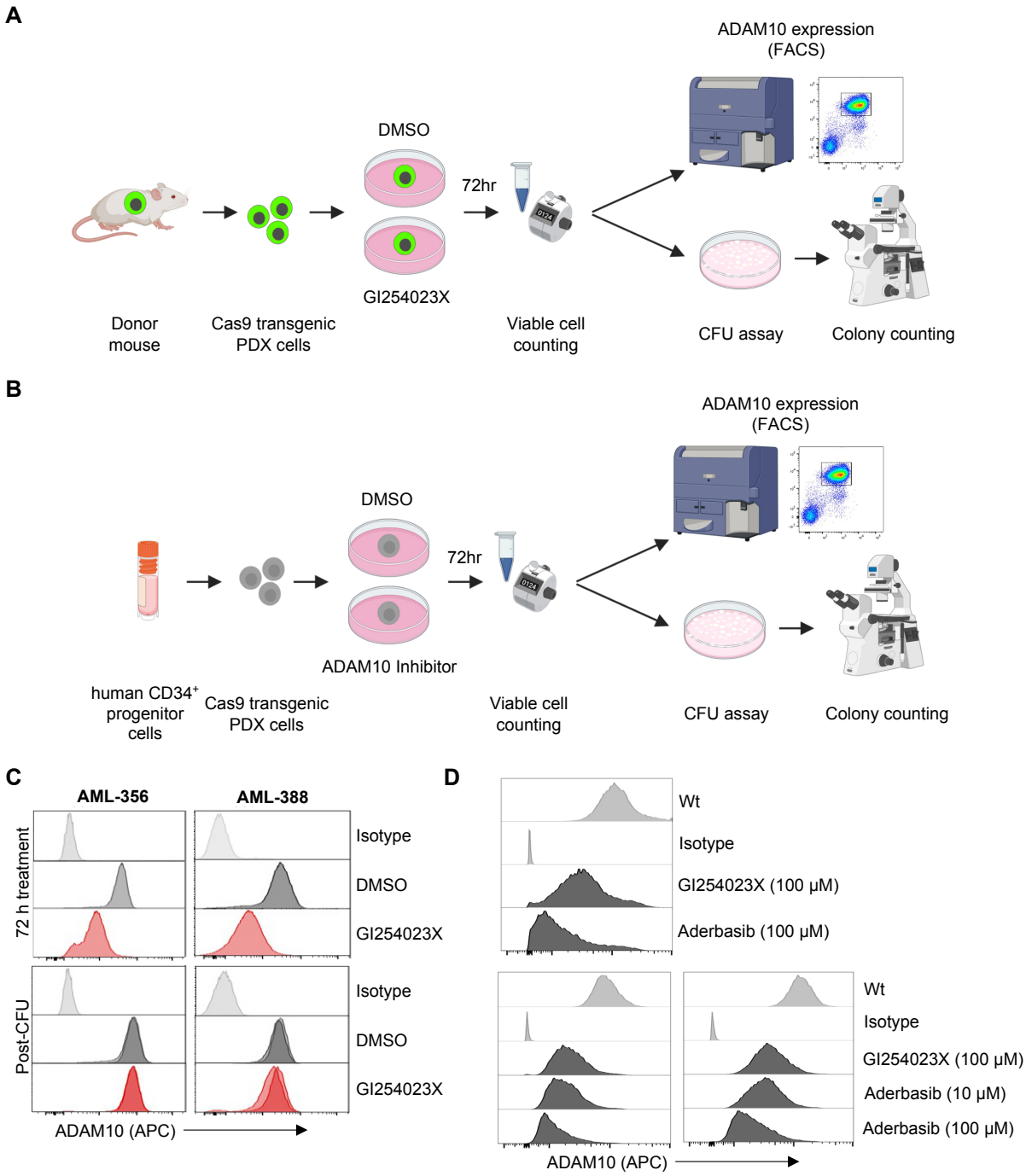

Figure 30: Schemes and quality controls of the influence of ADAM10 inhibition on CFU potential of AML PDX models and healthy human CD34+ blood progenitor cells. A Depiction of the procedure of the PDX ADAM10 inhibition CFU assays using GI254023X. Cas9-transgenic PDX cells were treated with 100 µM GI254023X or its solvent for three days *in vitro*. Viable cells were counted, the ADAM10 surface level reduction was confirmed using flow cytometry and 1x 10^3 cells were seeded for the CFU assay in methylcellulose. After ten days, colonies were manually counted using an inverted fluorescence microscope and ADAM10 surface levels were re-measured by flow cytometry. **B** Depiction of the procedure for the ADAM10 inhibition CFU assays with healthy human CD34$^+$ blood progenitor cell using GI254023X and Aderbasib. Experiment was performed as in **A**, except seeding 2x 10^3 cells for the CFU assay and treating the cells with 100 µM GI254023X or 10 µM Aderbasib. **CD** Representative flow cytometry histograms of three independent experiments depicting ADAM10 surface levels at the timepoint of CFU seeding (upper row) and at the end of the CFU assays (lower row). PDX AML-356 and AML-388 cells (**C**) and healthy human CD34$^+$ blood progenitor cells (**D**) treated using an

ADAM10 inhibitor at the indicated concentration or the solvent were compared. Adapted from (Bahrami, Schmid et al., 2023).

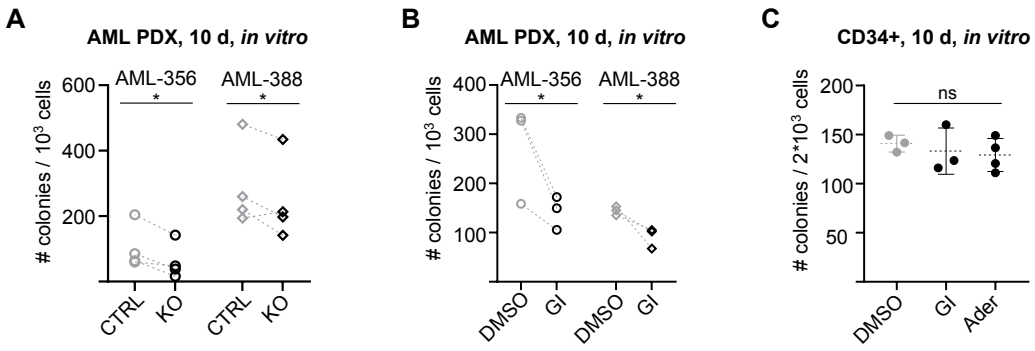

Figure 31: ADAM10 loss or reduction decreased the CFU potential of AML PDX models without affecting healthy human CD34+ blood progenitor cells. A Quantification of the ADAM10 KO CFU assays performed in AML PDX models as described in **Figure 29A** with each doth representing an independent replicate. **p*<0.05 by paired t-test. **B** Quantification of the ADAM10 Inhibitor CFU assays performed in AML PDX models as described in **Figure 30A** with each doth representing an independent replicate. * *p*<0.05 by paired t-test. **C** Quantification of the ADAM10 inhibitor CFU assays performed in healthy human CD34+ blood progenitor cells as described in **Figure 30B** with each doth representing an independent replicate. (GI254023X: GI, 100 µM; Aderbasib: Ader, 10 µM). ns by Holm-Sidak's multiple comparisons test compared to DMSO. Adapted from (Bahrami, Schmid et al., 2023).

Together with the diminished LSC frequencies after ADAM10 loss observed in the *in vivo* competitive LDTA assays, these data suggest that targeting of ADAM10 might be a promising concept to decrease the relapse-inducing LSCs.

4.7 ADAM10 loss renders PDX models of acute leukemia susceptible towards routinely used chemotherapeutic agents *in vivo*

ADAM10 reduction hampered the interaction between PDX cells and the BM microenvironment as shown in the early engraftment assays. Additionally, ADAM10 loss led to a decreased frequency of LSCs and a diminished CFU potential indicated by the competitive LDTA and the CFU assay after chemical inhibition or lentivirally mediated ADAM10 KO, respectively. Therefore, our next aim was to investigate ADAM10's importance during routine chemotherapy and to elucidate if its targeting might be beneficial for the treatment of acute leukemia patients.

Both *in vivo* and *in vitro* experiments were employed to address this question. For the *in vivo* experiments, a competitive approach was used, in which ADAM10 KO cells and PDX cells transduced with a control sgRNA were mixed (see 3.2.10). In contrast to the competitive validation assays, the cells were not mixed in a 1:1 ratio, but rather in a 3:1 to 4:1 surplus for the KO cells, in order to achieve a close to 1:1 ratio after three weeks of growth, when treatment was started. Using this competitive approach with both tested populations within the same animals guaranteed identical conditions for both cell populations during the treatment using chemotherapeutic agents (**Figure 32**).

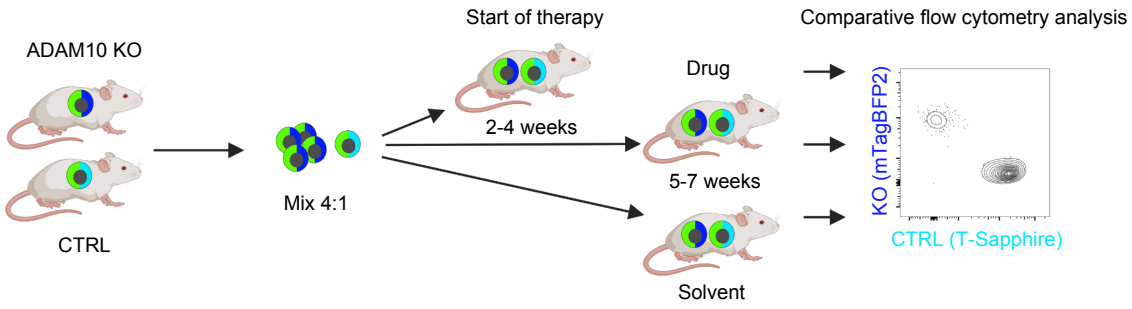

Figure 32: Scheme depicting the procedure of the competitive *in vivo* treatment trial. Control and ADAM10 KO PDX AML-661 cells were mixed in a 1:4 ratio aiming to counterbalance ADAM10 KO cells' engraftment and proliferation disadvantage before the start of therapy (SOT). Repeated *in vivo* imaging was utilized to track growth of the leukemic cells. One group of animals was sacrificed at the SOT, the drug or solvent treated groups after three consecutive weeks of the respective treatment. PDX cells were re-isolated from the BM and the spleen and analyzed via flow cytometry. Adapted from (Bahrami, Schmid et al., 2023).

In vivo bioluminescence imaging was used to monitor PDX cell engraftment, proliferation and potential response towards treatment, if luciferase-positive cells of the respective PDX model were available. AML-661 PDX cells were treated using cytarabine (AraC) or its solvent for three consecutive weeks. **Figure 33** shows the imaging data for the treated animals of the experiment along with its quantification and representative flow cytometry data. Leukemia

growth could be observed in the solvent-treated animals, while the AraC-treated mice displayed a rather constant, plateau-like leukemic burden.

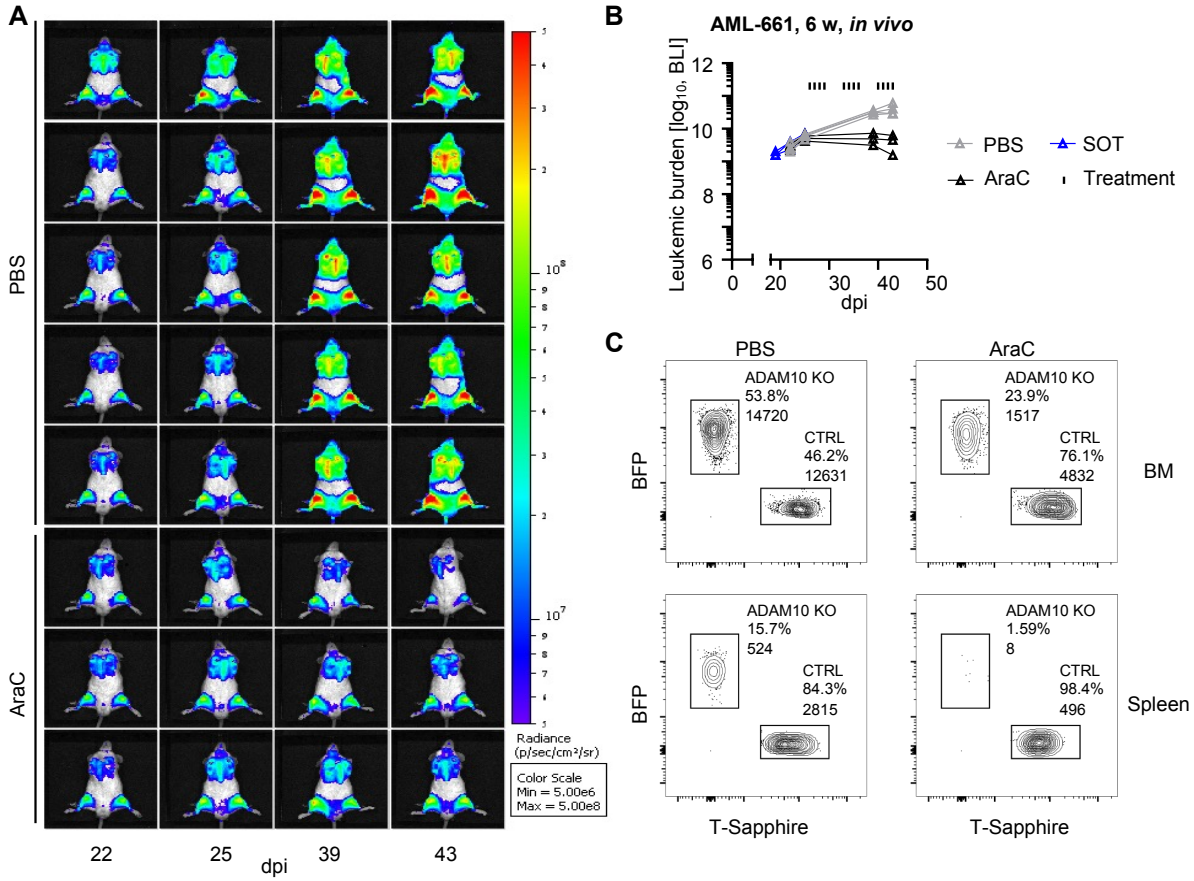

Figure 33: Quality controls of the competitive *in vivo* AraC treatment trial in PDX AML-661. A *In vivo* bioluminescence imaging of the animals of both treatment groups at the indicated days post transplantation. **B** Quantification of the imaging data of all animals of the trial including the start of therapy group. **C** Representative flow cytometry plots of the distribution of the control and ADAM10 KO population after treatment with AraC or PBS in the BM and spleen samples of the respective animals. Adapted from (Bahrami, Schmid et al., 2023).

When solvent-treated mice reached an advanced stage of leukemia, animals of both groups were sacrificed and PDX cells isolated from BM and spleen. Comparing the percentages as well as the absolute values of ADAM10 KO cells after three weeks of treatment between the PBS and AraC-treated animals displays a clear reduction KO cells in the AraC-treated animals, both in BM and spleen. This effect is especially striking in the spleen measurements, where almost no ADAM10 KO cells could be detected in the AraC-treated animals (**Figure 33C**).
In agreement with the *in vivo* imaging data, the AraC-treated mice showed lower percentages of human PDX cells, underlining AraC's anti-leukemic activity (**Figure 34A**). Within the human cells, the composition of the ADAM10 KO and control population was discriminated via flow cytometry, displaying a significant reduction of the ADAM10 KO population compared to the

control PDX cells upon treatment with AraC (**Figure 34BC**). This effect was present in both tested organs although reduction was more pronounced in the spleen.

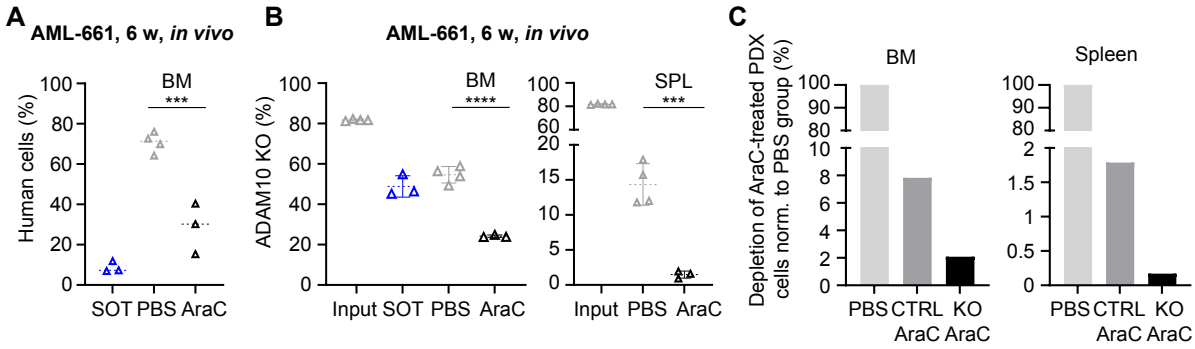

Figure 34: ADAM10 loss sensitizes towards AraC treatment in a competitive *in vivo* treatment trial in PDX AML-661. A Percentage of human PDX cells in the BM of mice from the start of therapy (n=3, SOT), PBS-treated (n=4, 1 animal with an extreme value was removed) and cytarabine (AraC)-treated (n=3, 2 animals were lost because of AraC-related toxicity) group of animals measured by flow cytometry. *** p<0.001 by unpaired t-test. **B** Percentage of AML-661 ADAM10 KO cells at transplantation, at SOT and after three consecutive weeks of treatment with AraC or PBS. **** p<0.0001, *** p<0.001 by unpaired t-test. **C** Percentage of remaining AraC-treated ADAM10 KO and control cells compared to the depletion of the control population treated with PBS in both measured organs. Adapted from (Bahrami, Schmid et al., 2023).

In a second *in vivo* experiment, ALL-265 PDX cells were treated using vincristine (VCR), cyclophosphamide (Cyclo) or their solvent for three consecutive weeks. As for AML-661, animals were sacrificed at the same time and PDX cells were isolated from BM and spleen. Exemplary flow cytometry plots of the BM of a Cyclo- and a PBS- treated animals are shown in **Figure 35A**, indicating a stable ADAM10 KO throughout the trial. Similar to the results in the AML PDX model, treatment with Cyclo or VCR significantly reduced the percentage of ADAM10 KO cells, with Cyclo displaying a stronger reduction of the KO population (**Figure 35B**).

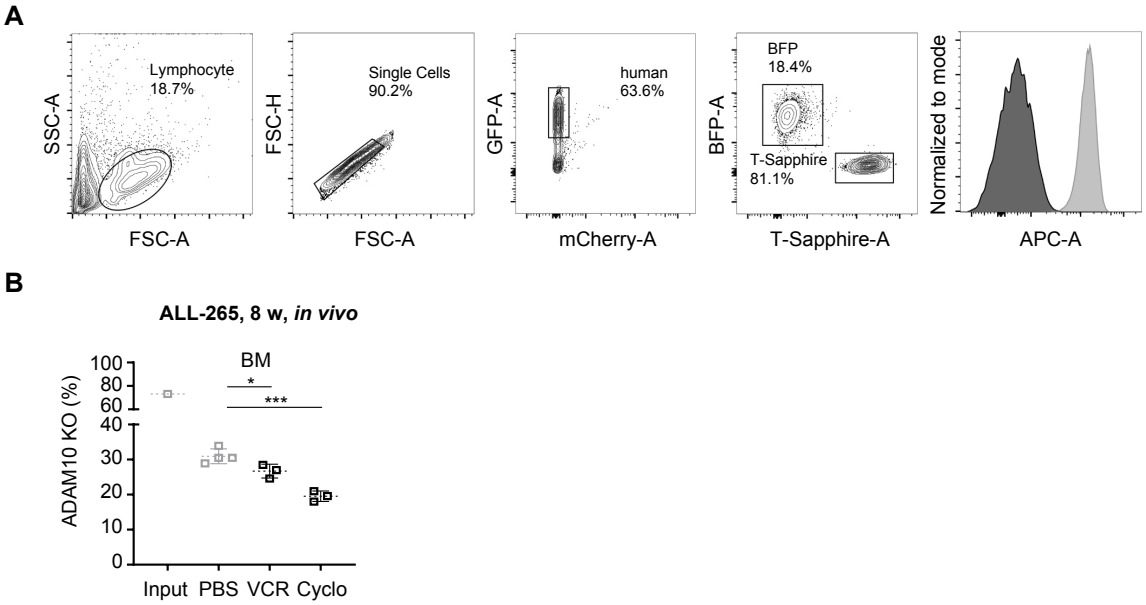

Figure 35: ADAM10 loss sensitizes towards vincristine and cyclophosphamide treatment as discovered by competitive *in vivo* treatment trial in PDX ALL-265. A Representative flow cytometry gating of BM samples of mice of the PBS-, VCR- or Cyclo- treated group stained for ADAM10. **B** Percentage of ALL-265 ADAM10 KO cells at the transplantation and after three consecutive weeks of treatment with VCR (n=3), Cyclo (n=3) or PBS (n=4). *** $p<0.001$, * $p<0.05$ by unpaired t-test. Adapted from (Bahrami, Schmid et al., 2023).

Furthermore, *in vitro* competitive chemotherapy trials were conducted with AML-356 and AML-661 PDX cells using AraC, Daunorubicine (Dauno) and Doxorubicine (Doxo) in concentrations within the clinically relevant range (see 3.6.6). In both tested AML models, the three chemotherapeutic agents led to a dose-dependent, significant decrease of the ADAM10 KO population compared to the control cells (**Figure 36**).

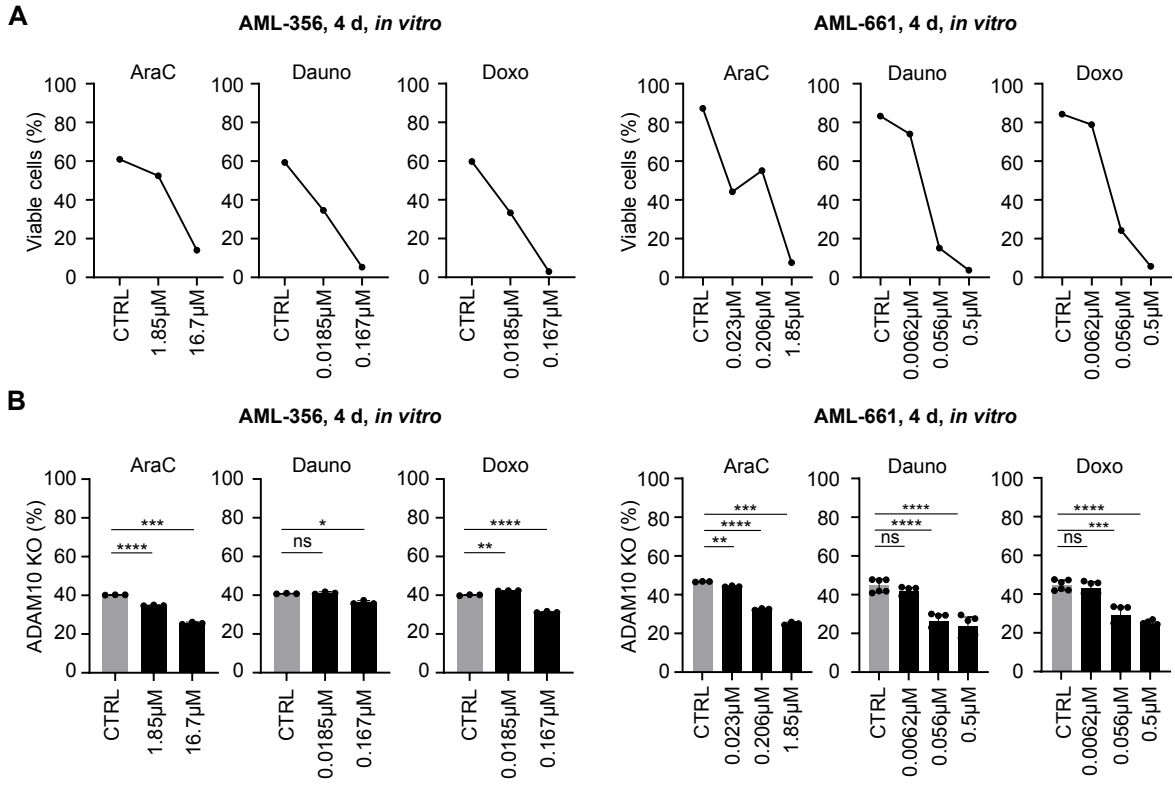

Figure 36: ADAM10 loss sensitizes towards cytarabine, daunorubicine and doxorubicine treatment as discovered by competitive *in vitro* treatment trial in PDX AML-356 and AML-661. AML PDX models RNP electroporated with either an ADAM10-targeting sgRNA mix or a non-targeting control sgRNA were mixed in a 1:1 ratio. Clinically relevant concentrations of the respective chemotherapeutic agents were added to the PDX samples in triplicates. Analysis of the ADAM10 KO and control population via flow cytometry 96 hours post induction. **A** Viability of the AML PDX cells at the indicated drug concentrations compared to the DMSO-treated controls. **B** Percentage of the ADAM10 KO population at the indicated drug concentrations compared to the DMSO-treated controls. **** p<0.0001, *** p<0.001, ** p<0.01, * p<0.05 by Brown-Forsythe and Welch ANOVA tests using multiple comparisons. Adapted from (Bahrami, Schmid et al., 2023).

In summary, both *in vivo* and *in vitro*, ADAM10 loss sensitized the tested AML and ALL PDX cells towards routine chemotherapy. Therefore, targeting of ADAM10 might add a valuable treatment tool to the currently available, routinely used chemotherapy regimen.

In conclusion, we were able to establish a pipeline of functional CRISPR/Cas9 dropout screens in PDX models of acute leukemia. This enabled elucidation of several shared as well as sample specific vulnerabilities which might be potential candidates for new therapeutic targets of ALL. Among those, this project identified ADAM10 as a fascinating novel target for the treatment of acute leukemia by delineating the detrimental effects of ADAM10 loss on broad cellular processes, such as cell cycle, apoptosis, metabolism and OXPHOS, but also functionally on essential properties of leukemic cells, such as the early engraftment potential, the frequency of leukemic stem cells, the CFU potential and the sensitivity towards chemotherapeutic agents *in vivo* and *in vitro*.

5. Discussion

Treatment outcome of acute leukemia patients has drastically improved during the last decades. Nevertheless, many challenges remain, especially regarding the treatment of patients belonging to difficult-to-treat subgroups and patients with relapsed disease. In order to better stratify patients to risk groups and specific treatment options, and to identify the mechanisms underlying relapse development, in the last years, a vast amount of data has been collected with the rise of multi-omics and single cell approaches. Still, most of these data have been acquired using cell line systems, which hardly resemble the disease, or are purely descriptive. Without demeaning the value of these findings, functional data are often sorely missed. For this project, we employed CRISPR/Cas9 KO screens to elucidate potential vulnerabilities of acute leukemias *in vivo* utilizing PDX models, which best mimic the patient's disease while at the same time enabling genetic engineering along with functional assays.

5.1 The pipeline for CRISPR/Cas9 KO screens in PDX models allows identification of potential AL vulnerabilities *in vivo*

Functional assays can promote a better understanding of disease development and progression. Choosing the most appropriate model system is often a trade-off between feasibility and clinical relevance. On the one side, primary patient material directly resembles the disease, but its availability is often limited and genetic manipulation is highly restricted; on the other side, cell lines are easy to genetically engineer and cell numbers are basically unlimited. Yet, they frequently acquire non-physiological mutations and thus fail to mimic the properties of the initial disease (Ben-David et al., 2018; Downing et al., 2012; Gillet et al., 2011; Ma et al., 2018; Pan et al., 2009; van Galen et al., 2019; Waanders et al., 2020). PDX models represent a good compromise, allowing amplification and manipulation of the cellular material, while maintaining many characteristics of the patient's leukemia throughout several passages (Richter-Pechańska et al., 2018; Vick et al., 2015).

Using the PDX model, we developed a pipeline for functional CRISPR/Cas9 KO screens, enabling the identification of vulnerabilities of the patient's acute leukemias *in vivo*. The interaction of leukemic cells with their respective microenvironment in the BM niche is essential, and we and others could show that this site represents a protective niche for LSCs, which give rise to relapses and are only insufficiently eradicated by routine chemotherapy (Delahaye et al., 2020; Menter & Tzankov, 2022; Phan & Croucher, 2020; Schepers et al., 2015; Zhou et al., 2016). Therefore, we aimed at finding novel candidates which can serve as potential targets to weaken this interaction, release the LSCs from the BM niche and re-sensitize them towards chemotherapy (Ebinger et al., 2016; Ebinger et al., 2020).

We employed our CRISPR/Cas9 KO screen pipeline using a customized surface molecule library of around 100 genes, which were selected from previous proteomic and transcriptomic results and supplemented with candidates from the literature. Comparing the sgRNA distribution between the input and the output samples using NGS, we found our quality controls to be met. While the non-cutting control sgRNAs serving as negative controls were unaltered in their abundance (**Figure 7B**), indicating the absence of an effect due to their expression, the sgRNAs targeting our positive control genes *CXCR4* and *ITGB1* were reduced in the output samples of both tested ALL PDX models (**Figure 7B**). This confirmed the potential of our pipeline to identify known essential genes in the *in vivo* setting. Apart from the controls, we elucidated both commonly depleted and sample specific candidates, reinforcing the idea to pinpoint individual patient's vulnerabilities as well as broader essentialities in leukemia patients. Sample specific dropouts were *NCSTN*, *CD81*, *CD79A*, *TRPM7* and *POTEI* in ALL-199 and *TFRC* in ALL-265. Commonly depleted candidates were the solute carrier (SLC) family members *SLC19A1*, which acts as a folate transporter and was connected to

methotrexate metabolism in ALL (Kotur et al., 2020; Ramalingam et al., 2022); and *SLC3A2*, the 4F2 heavy chain subunit of the amino acid transporter LAT1 (CD98), that has been connected to ferroptosis in several disease settings (Li et al., 2021; Ma et al., 2021; Wang et al., 2019).

The fifth gene depleted in both PDX models was ADAM10, which was of special interest for us due to its function as an extracellular sheddase and its involvement in processes like adhesion, migration, cytokine and intracellular signaling both in the context of healthy hematopoiesis as well as in diverse disease settings including T-ALL (Atapattu et al., 2016; Lambrecht et al., 2018; Mullooly et al., 2016; Smith et al., 2020). Additionally, ADAM10 displayed significantly higher mRNA expression levels in all tested acute leukemia subtypes except complex karyotype AML, identified by data mining of the publicly available MILE study dataset (202603_at; GSE13159) at the Bloodspot databank (**Figure 8A**). Along the same line, we found the surface protein levels of ADAM10 to be significantly elevated in our cohort of PDX models compared to healthy donor's BM cells isolated from patients with hip replacement. The higher expression levels of ADAM10 confirmed both on mRNA and protein level suggested a potentially higher dependency of acute leukemia cells on ADAM10. Furthermore, the disparate ADAM10 levels might open a therapeutic window, which allows targeting of ADAM10 without affecting normal hematopoiesis. Moreover, data mining of the Bloodspot databank (Human AML cells; 202603_at; GSE13159) and the Human protein atlas suggests that in fact higher mRNA expression levels of ADAM10 were correlated with worse overall survival. While this was a clear although statistically non-significant trend in primary material of AML patients, the effect was highly significant in other tumor entities, such as lung and pancreatic cancer. These data further emphasize ADAM10's potential role as a vulnerability of acute leukemias. Based on (i) the combined data of our CRISPR/Cas9 KO screen, (ii) ADAM10's function as an ectodomain sheddase, (iii) the connected pathways and biological processes as well as (iv) its expression data and association with poorer overall survival, we decided to continue with *ADAM10* as our candidate and to molecularly validate the screens results using competitive *in vivo* and *in vitro* assays.

5.2 Competitive *in vivo* validation assays confirm ADAM10 as an essentiality in AL

For the validation of candidates from the functional CRISPR/Cas9 KO screen, we performed competitive *in vivo* and *in vitro* assays. In the *in vivo* setting, this approach enabled us to track the engraftment and proliferation of the leukemic cells with and without the KO of the gene of interest within the same animal. As the conditions for both cell populations are therefore equal, this represents a highly reliable and very sensitive approach for detecting differences in the growth kinetics of the two cell populations, while at the same time reducing the number of animals. For the *in vitro* assays, cultivation of the two cell populations in the same well of the culturing vessel eliminates variability, allowing the detection of minute differences between the KO and control cell population in proliferation and survival.

Prerequisite for both assays is a high KO efficiency of the gene of interest. For the validation of ADAM10, we stably integrated three distinct sgRNAs targeting ADAM by lentiviral transduction and controlled KO efficiency via surface staining and subsequent flow cytometry. Both in the ALL cell lines NALM-6 and SEM (data not shown) as well as in one ALL and AML PDX model each (**Figure 10**), we observed strong reduction of ADAM10 protein levels, which are comparable to the signal of the cells stained with the antibody's isotype control. This confirms a very high KO efficiency and serves as reliable quality control for following competitive assays.

We used the three sgRNAs targeting ADAM10 from the CRISPR screens, which had shown the strongest depletion. Testing each of them against a control population in three separate mice enabled us to rule out potential off-target effects of one of the sgRNAs, which might have been overlooked if a mix of different sgRNAs had been used. Performing competitive validation assays in ALL and AML PDX models *in vivo*, we found the ADAM10 KO population to be depleted in seven out of eight tested ALL and PDX models (**Figure 12A**). This proves on the one hand a broad essentiality of acute leukemia PDX models on ADAM10 regardless of the underlying driver mutations and cytogenetic backgrounds. On the other hand, the results of the ALL-502 PDX model (**Figure 12B**), where no difference between the KO and the control population could be observed, eliminates the possibility of an unspecific depletion of the KO population for example due to the CRISPR/Cas9-induced DSBs and thereby strongly suggests a specific phenotype of ADAM10 loss in the other tested PDX models. Surprisingly, the level of depletion was mildly increased in the analyzed spleen samples compared to the BM samples in many PDX models (**Figure 12D**). This might indicate that the PDX cells rely on ADAM10 to disseminate from the BM and successfully engraft at a new tumor site, although further experiments would be needed to decipher the exact reason for the detected disparity. Sacrificing animals at earlier timepoints in addition to the routinely performed sacrificing at an

advanced stage of leukemia shed a light on the proliferation kinetics of ADAM10 KO cells compared to controls. Our data suggest a dual effect of ADAM10 loss. Firstly, early engraftment to the orthotopic BM niche shortly after transplantation seems to be severely hampered by the ADAM10 loss. Furthermore, also after homing to their respective niche, the KO cell population continuously displays a proliferation disadvantage in comparison to the control cells, as seen by the correlation of longer *in vivo* passages with stronger depletion, with most pronounced effects at an advanced stage of leukemia (**Figure 12E**).

In stark contrast to the results of the *in vivo* competitive assays, *in vitro* competitive assays displayed no dependency on ADAM10 in four out of five tested PDX models, with the exception of ALL-199, which showed a mild reduction of the ADAM10 KO population (**Figure 12C**). The discrepancy between the *in vivo* and *in vitro* data implies that ADAM10 is mainly essential for the interaction with the surrounding stroma cells and microenvironment rather than acting cell autonomously. Of note, previously, we showed also *WT1* and *DNMT3A* to be essential *in vivo*, but not *in vitro* (Ghalandary et al., 2023) underlining the importance of appropriate model systems such as the PDX model, which include the tumor microenvironment. Thereby, the situation in the patient is resembled as closely as possible which facilitates the identification of clinically relevant candidates.

5.3 *In vivo* ADAM10 reconstitution assays prove its importance by rescuing the observed phenotype

To confirm the specificity of the observed depletion phenotype upon ADAM10 KO and to further elucidate the role of distinct ADAM10 domains, we conducted rescue assays using different variants of the ADAM10 protein (**Figure 13**). Physiologically, ADAM10 gains its activity in a step-wise process during its trafficking from the ER via the Golgi to the plasma membrane and the removal of the inhibitory pro-domain, which is removed by furin and PC7 (Lambrecht et al., 2018). We removed the pro-domain from our ADAM10 variants to facilitate overexpression of the respective proteins and utilized both a catalytically active version of ADAM10 (ACT) and a variant lacking the metalloproteinase domain, which carries out ADAM10's enzymatic activity. We could confirm the successful expression and correct localization of the ACT variant by two independent proof-of-concept experiments in the H293T cell line (**Figure 14**). Western blot analysis comparing whole cell lysates with protein lysates enriched for membrane compartments in the KO setting displayed the presence of the ADAM10 variant in both fractions with increased protein levels in the membrane fraction (**Figure 14B**), suggesting correct trafficking. Furthermore, comparing confocal microscopy images of wild-type, ADAM10 KO and ACT-re-expressing H293T cells verified the localization of the ACT variant of ADAM10 at the cell membrane, resembling the localization of the endogenous ADAM10 in the wild-type situation (**Figure 14A**).

Passing these quality controls, we applied our generated ADAM10 variants to our *in vivo* competitive assay pipeline and compared ADAM10 KO cells re-expressing an ADAM10 variant with KO cells re-expressing a color construct at the time of transplantation and after sacrificing animals at an advanced stage of leukemia (**Figure 15A**). Flow cytometry analysis of the isolated cells showed comparable expression levels of the ACT and ∆MP variant based on the MFI of T-Sapphire, which is expressed at equimolar ratios with each of the variants (**Figure 15B**). Additionally, comparison of mRNA levels of the ADAM10 wild-type and the variant transcripts by qRT-PCR demonstrated that mRNA levels were significantly increased juxtapose ADAM10 KO cells and similar to the wild-type transcript's mRNA levels for both ADAM10 variant transcripts (**Figure 15C**). This proved that our experimental set-up was appropriate to investigate the different engraftment and proliferation characteristics of ADAM10 KO cells vs. ADAM10 variant re-expressing cells as well as analyzing differences between the two variants. ADAM10 KO cells with the re-expression of the catalytically active ACT variant were significantly enriched compared to ADAM10 KO control cells, while KO cells expressing the ∆MP variant of ADAM10 did not show any growth advantage. Together these data point out, that only the catalytically active variant of ADAM10 was able to at least partially rescue the phenotype of the ADAM10 loss, while the ∆MP failed to do so (**Figure 15D**). Thus,

ADAM10's function and essentiality seem to be mainly mediated by its enzymatic activity as a sheddase, which is executed by its metalloproteinase domain.
In line with these findings, so far mainly ADAM10's enzymatic activity as a metalloproteinase was described to be associated with development and progression of diverse tumors, such as T-ALL, colon cancers, breast cancer cells, or in glioblastoma (Gavert et al., 2007; Lambrecht et al., 2018; Liu et al., 2006; Smith et al., 2020; Venkatesh et al., 2017). Furthermore, as regulation of ADAM10 activity is crucial for several biological processes, mutations in its prodomain, which is part of the controlling mechanism by acting as an inhibitor of ADAM10's catalytic activity, were connected to Alzheimer's disease or the rare skin disease reticulate acropigmentation of Kitamura (Kim et al., 2009; Kono et al., 2013; Suh et al., 2013).
Additional experiments are needed to further elucidate the importance of ADAM10's prodomain in acute leukemia. Moreover, performing additional assays, such as a competitive reconstitution assay including an ADAM10 variant lacking the disintegrin domain instead of the metalloproteinase domain to control for potentially negative effects on protein stability induced by the removal of a domain might further strengthen the findings of the performed reconstitution assay.

5.4 Multi-omics analysis uncovers OXPHOS, metabolism, cell cycle and apoptosis as major pathways affected by ADAM10 loss

We next aimed to elucidate altered biological processes and pathways in ADAM10 KO cells compared to their respective controls by performing multi-omics experiments.

Firstly, we performed a mass-spec-based experiment in the ALL cell lines NALM-6 and SEM. Here, we cultured the cell lines with and without ADAM10 KO in serum deprived medium for three days to induce cellular stress. As ADAM10 is an ectodomain sheddase, we strived to compare not only the changes in the proteome, but also the secretome, enabling to track the differentially secreted proteins upon ADAM10 loss (**Figure 16**). This goal was achieved by separating the cell pellet from the supernatant upon harvesting of the cells. Unsupervised hierarchical clustering of SEM ADAM10 KO and control samples resulted in a clear separation of the two groups (**Figure 17A**). GSEA pathway analysis revealed apoptosis and cell death related pathways to be most significantly enriched in the KO cells compared to the controls, with the pathways cell death, apoptosis, Fas ligand, apoptotic cleavage and p53 network being the top five most significantly enriched (**Figure 17B**). This clearly indicates a pro-survival role of ADAM10 in the SEM cell line upon the induction of cellular stress such as serum deprivation. Furthermore, this might indicate a higher sensitivity towards other stressors such as chemotherapeutic agents upon ADAM10 loss. Grouping the differentially regulated pathways into functional groups, in addition to the apoptosis / cell death cluster, cell cycle, cellular metabolism as well as plasma membrane and adhesion associated pathways were altered following loss of ADAM10 (**Figure 17C**). These results emphasize the broad involvement of ADAM10 in various cellular processes. This can be explained by its role as an ectodomain sheddase with a high number of target proteins through which ADAM10 acts both directly as well as indirectly via its multiple substrates (Edwards et al., 2008).

Moreover, we performed mass-spec analysis of the secretome samples to identify differentially secreted proteins upon KO of ADAM10. ADAM10 KO and control samples could be divided by unsupervised hierarchical clustering as for the proteome, suggesting a clearly detectable difference between the two groups (**Figure 18A**, **B**). Among the detected proteins, 44 and 62 proteins were differentially secreted in SEM and NALM-6 cells, respectively, with five proteins being shared between both (**Figure 18C**, **D**). These five include the *bona fide* target of ADAM10, APP, which is very well described for its role in Alzheimer's disease (AD), where its cleavage by α-secretases including ADAM10 prevent formation of β-amyloid, a main constituent of senile plaques and important hallmark of AD (Murphy, 2008; Rovelet-Lecrux et al., 2006; Wilson et al., 1999; Zhang et al., 2011). Another shared protein is the heat shock protein 90 α (HSP90α), which not only is highly expressed in acute leukemia patients but its function as a 'cancer chaperone' was connected to several tumor entities including acute

leukemias (Kanyan et al., 1996; Solit & Rosen, 2006; Song et al., 2020; Sreedhar et al., 2004; Trepel et al., 2010; Whitesell & Dai, 2005; Workman, 2004; Yufu et al., 1992). The other three proteins are the histone associated proteins H2AFX and HIST1H4A together with the GGH, although this is significantly downregulated in SEM cells and upregulated in the NALM-6 cells. Significantly differentially regulated proteins found in one of the cell lines include ADAM10 itself, H2AFY, an additional protein connected to histones, and FLT3, a well-studied tyrosine kinase in the cancer and especially AML field. Patients harboring a FLT3-ITD mutated disease bear an intermediate clinical prognosis, which has been ameliorated during the last years by the usage of tyrosine inhibitors such as midostaurin or gilteritinib (Antar et al., 2020; Daver et al., 2021; Döhner et al., 2022; Kennedy & Smith, 2020; Maiti et al., 2021; Zhao et al., 2022).

In summary, proteome and secretome analysis of the ALL cell lines SEM and NALM-6 upon ADAM10 loss identified important cellular processes to be affected including cell death, cell cycle, metabolism and adhesion. Moreover, secretome analysis allowed us to shed light at differentially secreted proteins. Their dysregulation might contribute to the observed phenotype upon ADAM10 loss and therefore to the essentiality of ADAM10 in PDX models of acute leukemia.

As a next step, transcriptome analysis of the two ALL PDX models ALL-199 and ALL-265 was performed comparing ADAM10 KO and control cells. Using unsupervised hierarchical clustering, KO and control groups were separated instead of the respective PDX model, underlining the marked alterations in the transcriptomes of the ADAM10 KO samples (**Figure 19A**). Pathway analysis of the differentially regulated transcripts among others identified processes, such as the KEGG terms cell cycle, cell adhesion and OXPHOS (**Figure 19C**). These results are in line with our findings from the proteome and secretome analysis of the cell lines, further emphasizing ADAM10's importance for the enumerated pathways and biological processes.

Thirdly, we performed proteome analysis of ALL-199 and ALL-265 PDX models. As for the other experiments, ADAM10 KO and control samples were separated by unsupervised hierarchical clustering (**Figure 20A**). Analysis of the most significantly affected pathways revealed new pathways including nucleotide and ribonucleotide binding along with membrane associated processes and OXPHOS, which could also be detected in transcriptome analysis (**Figure 20B**).

Combining cell line proteome and secretome with PDX transcriptome and proteome data, interesting pathways and candidates affected by the loss of ADAM10 could be identified. This includes the differentially secreted proteins FLT3 and HSP90α as well as cell death, cell cycle, metabolism and cell adhesion, pathways detected repeatedly using independent experimental set ups. In order to confirm some of these commonly altered pathways in proof-of-concept

experiments, we performed functional experiments, testing changes in cell cycle and cell death as a consequence of ADAM10 inhibition or KO.

For the evaluation of the effect of ADAM10 loss on the cell cycle of PDX cells, we treated ALL-199 cells directly after isolation from the sacrificed donor animals using either the ADAM10 inhibitor or its solvent *in vitro* for three days (**Figure 21A**). Daily cell cycle analysis after DAPI staining discovered the percentage of cells in the G1 phase to progressively increase in the ADAM10 inhibitor treated cells while cells in S phase diminished with time and the cells in G2/M phase were mildly reduced in both groups, although with a steeper decrease in the inhibitor treated cells (**Figure 21D**). These data strongly suggest a G1 arrest of the ALL-199 PDX cells as a consequence of inhibiting ADAM10 and thus functionally prove the connection of ADAM10 loss and cell cycle, which was previously found both in proteome and transcriptome analysis. In line with our findings, higher expression levels of ADAM10 was associated with increased cell cycle activity, while inhibition or loss of ADAM decreased the rate of proliferation in different tumor entities, including T-ALL, triple negative breast and bladder cancer cells as well as in renal cell and hepatocellular carcinoma cells (Cheng et al., 2021; Doberstein et al., 2011; Fu et al., 2014; Liu et al., 2015; Ma et al., 2015; Zheng et al., 2020).

ADAM10's influence on the level of cell death was investigated using PDX cells performing an ADAM10 KO in freshly isolated cells via electroporation of RNPs containing either crRNAs targeting ADAM10 or a non-targeting control crRNA (**Figure 22A**). Three days post electroporation, apoptosis rates were determined by Annexin V and DAPI double staining. KO of ADAM10 significantly increased the percentage of Annexin V-positive cells both in the ALL-199 PDX model and three AML PDX models roughly by a factor two (**Figure 22C**, **D**). Of note, the rate of apoptotic cells was generally increased in the ALL model compared to the AML models, which is in line with the higher feasibility of culturing AML PDX cells *in vitro*. Similar to the experiments conducted for analyzing the effect of ADAM10 inhibition on the cell cycle, also for evaluation of the apoptosis rates, chemical inhibition of ADAM10 using GI254023X was performed. Here, we obtained highly comparable data to the KO experiments (**Figure 22C**, **D**), showing an increase in the percentage of Annexin V-positive cells by the same factor two in the AML models, while it was a little less pronounced in ALL-199 with a factor of 1.5. Together, these assays functionally support data from our proteome analysis, indicating that loss or inhibition of ADAM10 in fact results in higher levels of apoptosis in PDX models of acute leukemia. In agreement with these results, elevated ADAM10 expression levels were described to increase resistance towards chemotherapy and attenuate apoptosis rates, while inhibition of ADAM10 increased chemosensitivity and induced apoptosis in breast, bladder and prostate cancer cells along with hepatocellular and nasopharyngeal carcinoma cells (Fu et al.,

2014; Liu et al., 2015; Ma et al., 2015; Yang et al., 2012; You et al., 2015; Zhang et al., 2014; Zhu et al., 2014).

In summary, the multi-omics results comparing ADAM10 KO and control cells combined with the proof-of-concept experiments, indicate a cell autonomous effect of ADAM10 loss on cell cycle, the rate of cell death and metabolism including OXPHOS. Recently, OXPHOS has gained a lot of attention in the acute leukemia field with new mitochondrial complex I inhibitors being tested in translational research as well as in clinical trials (Baccelli et al., 2019; Yap et al., 2023). Dependency on OXPHOS was described in ALL and AML cell lines, PDX models and primary patient material, often in combination with higher resistance towards chemotherapy, thus underlining the potential of targeting this pathway (Chen et al., 2021; Farge et al., 2017).

In order to further strengthen the generated -omics data, additional proof-of-concept experiments investigating cellular respiration utilizing e.g., Seahorse equipment or performing adhesion assays might be conducted. Moreover, ADAM10's role within the described pathways might be further characterized by pinpointing the affected target proteins using functional and molecular assays.

5.5 Loss of ADAM10 impairs early engraftment, reduces the LSC frequency, diminishes the CFU potential, and sensitizes towards chemotherapy

To further functionally characterize the effects of ADAM10 loss, we performed assays examining properties such as the engraftment potential, the stem cell frequency, the CFU potential as well as sensitivity towards chemotherapeutic agents.

Firstly, we tested ADAM10's effect on the early engraftment capacity of ALL PDX cells. To this end, chemical inhibition was used as approach to reduce ADAM10 surface levels. Two commercially available small molecule ADAM10 inhibitors GI254023X and Aderbasib were titrated to find an optimal concentration. Inhibiting ADAM10's catalytic activity results in its removal from the cell surface and subsequent degradation. This has been previously described and we could reproduce these data (**Figure 23**) (Seifert et al., 2021). We aimed at finding an inhibitor concentration which markedly reduces ADAM10's surface levels without affecting the cells' viability. 100 µM was established as the best concentration fulfilling both prerequisites for both tested inhibitors. Alterations in the engraftment potential of the PDX cells were tested by pre-treating freshly isolated cells with one of the inhibitors at the described concentration or its corresponding solvent. Flow cytometry elucidated reduced ADAM10 surface levels, while cell viability was not affected (**Figure 24**). PDX cells were re-isolated from the BM of the mice and the percentage of human cells determined using flow cytometry. The inhibitor-treated group of animals showed a lower engraftment rate in each tested setting with a reduction ranging from around 35% to 60% (**Figure 25B**). This proves that reduction of ADAM10 hampers early engraftment and homing to the orthotopic niche, which results in the observed lower engraftment rates. Additionally, keeping a portion of cells *in vitro* after the pre-treatment and performing every handling step as for the transplanted cells did not lead to elevated levels of dying cells, thus ruling out any delayed toxicity related to the pre-treatment, which could have been a part of the observed *in vivo* phenotype (**Figure 24D**). This indicates that the detected engraftment differences are specific for the ADAM10 reduction in the *in vivo* situation.

In a next step, we aimed at characterizing the effects of ADAM10 loss on stem cells. The frequency of stem cells within a population of PDX cells is an important characteristic for the model's potential to engraft and thereby to induce leukemia. Likewise, in the patient's disease the LSCs are able to induce a disease relapse after initial remission. Thus, efficient targeting and removal of stem cells is a key factor for prolonged complete remission and eventually cure (Delahaye et al., 2020; Menter & Tzankov, 2022; Misaghian et al., 2009; Phan & Croucher, 2020; Pollyea & Jordan, 2017; Schepers et al., 2015; Zhou et al., 2016). We and others have shown that chemotherapeutic agents often only inefficiently target these dormant LSCs within their protective niche in the BM (Ebinger et al., 2016; Konopleva et al., 2002; Manabe et al., 1992; Mudry et al., 2000; Panayiotidis et al., 1996). Of note, ADAM10 levels were elevated in

the label retaining cells (LRCs) resembling LSCs in previous proteome analyses from our lab and collaborators (Bahrami et al., 2023). To functionally investigate ADAM10's importance for LSCs, LDTAs were performed, which represent the current gold standard for addressing LSCs (**Figure 26**). We utilized a slightly modified, competitive version, where the same number of ADAM10 KO and control cells were mixed in a 1:1 ratio within each animal. We determined a lower frequency of LIC in the ADAM10 KO population for both tested ALL PDX models, although to varying extent (**Figure 28**). While in ALL-199 the LIC frequency was roughly reduced by a factor of ten compared to the controls, only a threefold reduction was detected in ALL-265, still confirming the general trend of reduced LIC frequencies upon ADAM10 loss. These data strongly suggest an effect of ADAM10 loss on the stem cell compartment and therefore indicate a potential therapeutic opportunity to target LSCs by reducing ADAM10 levels.

In order to independently examine ADAM10's importance for stemness, we performed colony formation assays after lentiviral KO or chemical inhibition of ADAM10, respectively (**Figure 29** and **Figure 30**). For the KO approach, Cas9-transgenic PDX cells were lentivirally transduced with an sgRNA targeting ADAM10 or a non-targeting control sgRNA. After *in vitro* cultivation, allowing establishment of the KO, cells were enriched by FACS and seeded. The number and shape of colonies as well as the ADAM10 surface levels were evaluated after ten days. While colony number was reduced for each of the individual experiments and both tested AML PDX models, the general shape of the colonies was unaltered (**Figure 29B**, **C** and **Figure 31A**). As an important quality control, the harvested KO colonies still displayed an ADAM10 surface expression comparable to the isotype-stained controls, confirming the sorting and plating purity (**Figure 29D**). We used both Cas9-transgenic PDX cells and commercially available healthy human CD34+ progenitor cells for the experiments and reduced ADAM10 levels with chemical inhibitors (**Figure 30**). Each inhibitor in both experimental settings successfully reduced ADAM10 surface levels before the plating of the CFUs as seen for the PDX cells in previous experiments and in line with the literature (**Figure 30C**, **D**) (Seifert et al., 2021). After removal of the inhibitor at the timepoint of plating, ADAM10 levels recovered and were indistinguishable from that of the control cells (**Figure 30C**). Nevertheless, pre-treatment of both tested AML PDX models with GI254023X was sufficient to significantly reduce the number of colonies to a similar extent as observed for the cells with ADAM10 KO (**Figure 31B**). In contrast, colony numbers of the healthy CD34+ progenitors were unaffected by inhibition with both inhibitors at the same concentrations that affected PDX cells in the CFU assay and the early engraftment assays, respectively (**Figure 31C**). This strongly supports the notion that PDX models of acute leukemia are more sensitive towards inhibition of ADAM10 compared to healthy progenitor cells, thus opening a potential therapeutic window for targeting ADAM10 in leukemia patients.

Lastly, we conducted competitive chemotherapy trials *in vivo* and *in vitro* to compare ADAM10 KO and control cells upon treatment with routinely used chemotherapeutic agents.

For the *in vivo* trials, we mixed ADAM10 KO and controls cells with a 4:1 advantage for the KOs due to their depletion over time as observed in the competitive validation assays. After initial engraftment, monitored by bioluminescent imaging or measurement of blasts in the peripheral blood, we evaluated the distribution of the ADAM10 KO and control population by sacrificing the "start of therapy" animals. After three consecutive weeks of treatment with the respective chemotherapeutic agent, all animals were sacrificed and the distribution of the ADAM10 KO compared to the control cells was evaluated in the treatment and control groups. In the AML-661 trial, as expected, AraC kept the leukemia in a steady-state disease as seen in the imaging data compared to the control animals, in which the leukemic cells continued to proliferate (**Figure 33**). This is in line with the flow cytometry data at the experimental endpoint, which showed only a mild increase in the percentage of PDX cells in the BM compared to the "start of therapy" animals, which is in stark contrast to the drastic increase from around 10% to 75% blasts in the BM of the solvent-treated animals (**Figure 34A**). More importantly, not only was the total number of PDX cells in the BM reduced upon AraC treatment, but strikingly the percentage of ADAM10 KO cells within in the total PDX cells was significantly decreased compared to the solvent-treated animals in the two tested organs BM and spleen by a factor of around 2.5 and eight, respectively (**Figure 34B**, **C**). This suggests that ADAM10 KO cells are significantly more sensitive towards AraC treatment than the control cells. Along the same line, in the ALL-265 trial treating the animals with either VCR or Cyclo, ADAM10 KO cells were significantly depleted upon treatment compared to the corresponding controls, although to a lesser extent of around 20% to 40%, respectively (**Figure 35B**).

For the *in vitro* competitive treatment assays PDX cells were electroporated with RNPs containing a mix of three crRNAs targeting ADAM10 or a non-targeting crRNA. ADAM10 KO and control cells were mixed in a 1:1 ratio and treated using different concentrations of the chemotherapeutic agents. Viability and distribution of the two populations after treatment was evaluated by flow cytometry (**Figure 36**). For each of the three chemotherapeutic agents, the ADAM10 KO cells showed a disadvantage compared to the corresponding controls at clinically relevant doses. While AML-661 ADAM10 KO cells responded to treatment with all three drugs in a dose-dependent manner, AML-356 ADAM10 KO cells were most sensitive towards AraC, sensitive towards Doxo at the higher dose and only mildly affected by Dauno.

The combined results of the *in vivo* and *in vitro* competitive treatment trials indicate an increased sensitivity towards chemotherapy of both ALL and AML PDX models. This further emphasizes the potential clinical benefit of targeting ADAM10 in leukemia patients, possibly as an addition to routinely used chemotherapeutic agents.

5.6 Conclusion and Outlook

In conclusion, we uncovered ADAM10 as a novel vulnerability in acute leukemia by combining multi-omics approaches and CRISPR/Cas9 screens. Based on previously identified surface molecules with higher expression in slowly cycling LSC-resembling LRC cells using ultra-sensitive proteomics and transcriptomics (Bahrami et al., 2023) complemented with candidates from the literature, we generated a customized surface molecule library. Our aim was to find surface molecule candidates which can be targeted to disrupt the interaction of leukemic cells including LSCs with the protective BM microenvironment, thereby releasing the cells from their niche and rendering them susceptible towards chemotherapy. Applying this customized library to our established pipeline for functional CRISPR/Cas9 KO screens, allowed us to identify ADAM10 as a potential candidate in two distinct ALL PDX models.

ADAM10's broad essentiality could be validated in several ALL and AML PDX models. The specificity of the observed phenotype was confirmed using rescue assays, which additionally unraveled a crucial role of the catalytically active metalloproteinase domain. Performing multi-omics analyses comparing ADAM10 KO and control cells identified changes in different cellular pathways including OXPHOS, membrane and adhesion, cell death and cell cycle related pathways. We could functionally confirm ADAM10's effect on the latter two by proof-of-concept experiments. Further functional experiments elucidated that chemical inhibition of ADAM10 significantly decreased the early engraftment capacity, ADAM10 KO or chemical inhibition significantly reduced the CFU potential and ADAM10 loss sensitized both ALL and AML PDX models towards chemotherapeutic agents.

Together these findings strongly indicate that ADAM10 is a vulnerability in acute leukemias (**Figure 37**). With its broad effect on many biological processes, such as cell death, metabolism and cell cycle, and its effects on stem cells and engraftment of leukemic cells in their orthotopic niche, ADAM10 clearly is a fascinating, novel candidate to be targeted in leukemia patients. Moreover, as ADAM10 loss sensitized towards chemotherapeutic agents, combination therapies with existing drugs might be considered as another promising therapeutic option. We therefore strongly suggest ADAM10 as a potential new candidate for the treatment of acute leukemia patients.

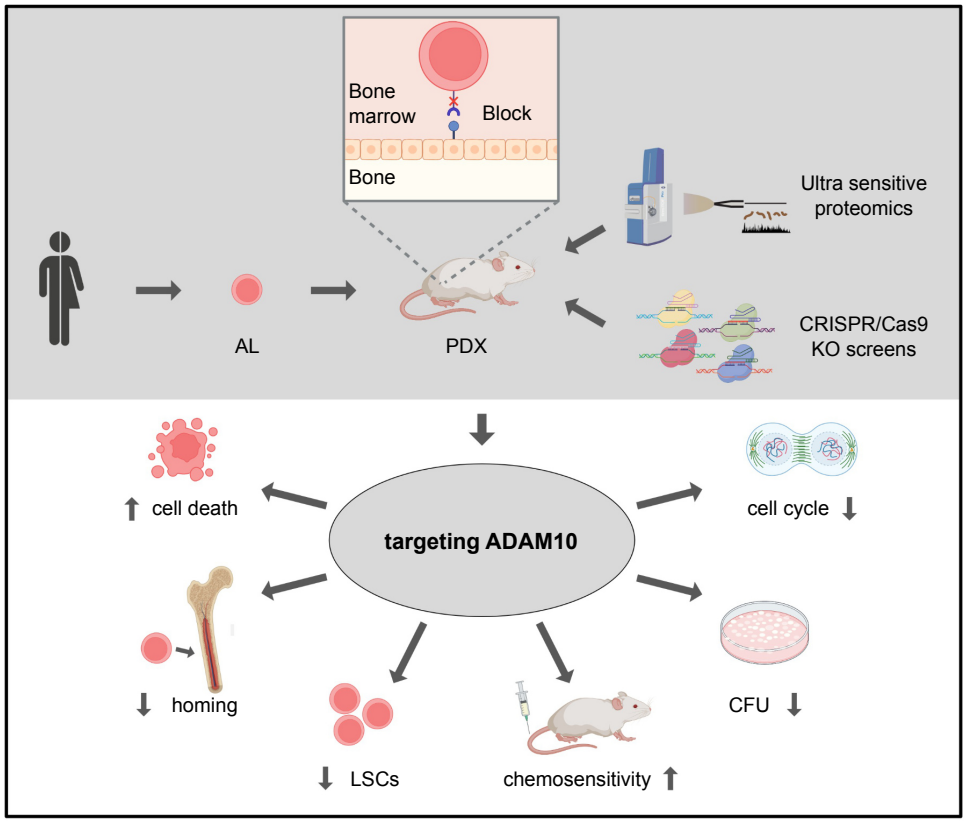

Figure 37: Summary of the identification of ADAM10 as vulnerability of acute leukemia. Ultra-sensitive proteomics combined with functional CRISPR/Cas9 KO screens were employed using patient-derived xenograft models of acute leukemia to identify potential vulnerabilities, which might disrupt the interaction between leukemic cells and their protective niche. Targeting of ADAM10 resulted in increased levels of cell death, decreased cell cycling, diminished early engraftment capacity, reduced CFU potential, lowered leukemia stem cell frequency and increased sensitivity towards chemotherapy.

To further validate ADAM10's potential as a new candidate for leukemia treatment possible next steps are among others performing pre-clinical chemotherapy trials combined with the inhibition of ADAM10 using chemical inhibitors or neutralizing antibodies, rather than lentiviral KO, in order to better reflect the options available in the clinics. Unfortunately, currently available inhibitors and antibodies are not suitable for these experiments due to insufficient reduction of ADAM10 and high off-target toxicities. Additionally, some of them are not yet available for such studies.

There is still a long way to go, and more translational research and eventually clinical trials are needed to fully establish ADAM10 as clinical therapeutic target. Nevertheless, ADAM10 has the potential to be a promising candidate for the treatment of acute leukemia patients in the future.

Bibliography

Antar, A. I., Otrock, Z. K., Jabbour, E., Mohty, M., & Bazarbachi, A. (2020). FLT3 inhibitors in acute myeloid leukemia: ten frequently asked questions. *Leukemia, 34*(3), 682-696.

Arber, D. A., Orazi, A., Hasserjian, R., Thiele, J., Borowitz, M. J., Le Beau, M. M., et al. (2016). The 2016 revision to the World Health Organization classification of myeloid neoplasms and acute leukemia. *Blood, 127*(20), 2391-2405.

Atapattu, L., Saha, N., Chheang, C., Eissman, M. F., Xu, K., Vail, M. E., et al. (2016). An activated form of ADAM10 is tumor selective and regulates cancer stem-like cells and tumor growth. *J Exp Med, 213*(9), 1741-1757.

Baccelli, I., Gareau, Y., Lehnertz, B., Gingras, S., Spinella, J.-F., Corneau, S., et al. (2019). Mubritinib targets the electron transport chain complex I and reveals the landscape of OXPHOS dependency in acute myeloid leukemia. *Cancer Cell, 36*(1), 84-99. e88.

Bagger, F. O., Kinalis, S., & Rapin, N. (2019). BloodSpot: a database of healthy and malignant haematopoiesis updated with purified and single cell mRNA sequencing profiles. *Nucleic acids research, 47*(D1), D881-D885.

Bahrami, E., Schmid, J. P., Jurinovic, V., Becker, M., Wirth, A.-K., Ludwig, R., et al. (2023). Combined proteomics and CRISPR–Cas9 screens in PDX identify ADAM10 as essential for leukemia in vivo. *Molecular Cancer, 22*(1), 107.

Baron, J., & Wang, E. S. (2018). Gemtuzumab ozogamicin for the treatment of acute myeloid leukemia. *Expert review of clinical pharmacology, 11*(6), 549-559.

Barrett, D. M., Seif, A. E., Carpenito, C., Teachey, D. T., Fish, J. D., June, C. H., et al. (2011). Noninvasive bioluminescent imaging of primary patient acute lymphoblastic leukemia: a strategy for preclinical modeling. *Blood, The Journal of the American Society of Hematology, 118*(15), e112-e117.

Ben-David, U., Beroukhim, R., & Golub, T. R. (2019). Genomic evolution of cancer models: perils and opportunities. *Nature Reviews Cancer, 19*(2), 97-109.

Ben-David, U., Siranosian, B., Ha, G., Tang, H., Oren, Y., Hinohara, K., et al. (2018). Genetic and transcriptional evolution alters cancer cell line drug response. *Nature, 560*(7718), 325-330.

Bernt, K. M., & Armstrong, S. A. (2009). Leukemia stem cells and human acute lymphoblastic leukemia. *Seminars in hematology, 46*(1), 33-38.

Bindea, G., Mlecnik, B., Hackl, H., Charoentong, P., Tosolini, M., Kirilovsky, A., et al. (2009). ClueGO: a Cytoscape plug-in to decipher functionally grouped gene ontology and pathway annotation networks. *Bioinformatics, 25*(8), 1091-1093.

Binger, K. J., & Wright, M. D. (2022). Seeing your partner: Structural elucidation of the first C8 tetraspanin protein. *Structure, 30*(2), 203-205.

Bomken, S., Buechler, L., Rehe, K., Ponthan, F., Elder, A., Blair, H., et al. (2013). Lentiviral marking of patient-derived acute lymphoblastic leukaemic cells allows in vivo tracking of disease progression. *Leukemia, 27*(3), 718-721.

Borgmann, A., Baldy, C., Stackelberg, A., Beyermann, B., Fichtner, I., Nürnberg, P., et al. (2000). Childhood all blasts retain phenotypic and genotypic characteristics upon long-term serial passage in NOD/SCID mice. *Pediatric hematology and oncology, 17*(8), 635-650.

Bosma, G. C., Custer, R. P., & Bosma, M. J. (1983). A severe combined immunodeficiency mutation in the mouse. *Nature, 301*(5900), 527-530.

Brinkman, E. K., Chen, T., Amendola, M., & van Steensel, B. (2014). Easy quantitative assessment of genome editing by sequence trace decomposition. *Nucleic Acids Res, 42*(22), e168.

Brown, P., Inaba, H., Annesley, C., Beck, J., Colace, S., Dallas, M., et al. (2020). Pediatric acute lymphoblastic leukemia, version 2.2020, NCCN clinical practice guidelines in oncology. *Journal of the National Comprehensive Cancer Network, 18*(1), 81-112.

Bukowski, K., Kciuk, M., & Kontek, R. (2020). Mechanisms of multidrug resistance in cancer chemotherapy. *International journal of molecular sciences, 21*(9), 3233.

Burd, A., Levine, R. L., Ruppert, A. S., Mims, A. S., Borate, U., Stein, E. M., et al. (2020). Precision medicine treatment in acute myeloid leukemia using prospective genomic profiling: feasibility and preliminary efficacy of the Beat AML Master Trial. *Nature Medicine, 26*(12), 1852-1858.

Byrne, A. T., Alferez, D. G., Amant, F., Annibali, D., Arribas, J., Biankin, A. V., et al. (2017). Interrogating open issues in cancer precision medicine with patient-derived xenografts. *Nat Rev Cancer, 17*(4), 254-268.

Carlet, M., Völse, K., Vergalli, J., Becker, M., Herold, T., Arner, A., et al. (2021). In vivo inducible reverse genetics in patients' tumors to identify individual therapeutic targets. *Nat Commun, 12*(1), 5655.

Cassidy, J. W., Caldas, C., & Bruna, A. (2015). Maintaining tumor heterogeneity in patient-derived tumor xenografts. *Cancer Research, 75*(15), 2963-2968.

Castaigne, S., Pautas, C., Terré, C., Raffoux, E., Bordessoule, D., Bastie, J.-N., et al. (2012). Effect of gemtuzumab ozogamicin on survival of adult patients with de-novo acute myeloid leukaemia (ALFA-0701): a randomised, open-label, phase 3 study. *The Lancet, 379*(9825), 1508-1516.

Chaimowitz, N. S., Martin, R. K., Cichy, J., Gibb, D. R., Patil, P., Kang, D.-J., et al. (2011). A disintegrin and metalloproteinase 10 regulates antibody production and maintenance of lymphoid architecture. *The Journal of Immunology, 187*(10), 5114-5122.

Chen, C., Hao, X., Lai, X., Liu, L., Zhu, J., Shao, H., et al. (2021). Oxidative phosphorylation enhances the leukemogenic capacity and resistance to chemotherapy of B cell acute lymphoblastic leukemia. *Science advances, 7*(11), eabd6280.

Cheng, Y., Lin, L., Li, X., Lu, A., Hou, C., Wu, Q., et al. (2021). ADAM10 is involved in the oncogenic process and chemo-resistance of triple-negative breast cancer via

regulating Notch1 signaling pathway, CD44 and PrPc. *Cancer Cell International, 21*(1), 1-15.

Chitadze, G., Lettau, M., Bhat, J., Wesch, D., Steinle, A., Fürst, D., et al. (2013). Shedding of endogenous MHC class I-related chain molecules A and B from different human tumor entities: heterogeneous involvement of the “a disintegrin and metalloproteases” 10 and 17. *International journal of cancer, 133*(7), 1557-1566.

Cissé, M., Duplan, E., Guillot-Sestier, M.-V., Rumigny, J., Bauer, C., Pages, G., et al. (2011). The extracellular regulated kinase-1 (ERK1) controls regulated α-secretase-mediated processing, promoter transactivation, and mRNA levels of the cellular prion protein. *Journal of Biological Chemistry, 286*(33), 29192-29206.

Clappier, E., Gerby, B., Sigaux, F., Delord, M., Touzri, F., Hernandez, L., et al. (2011). Clonal selection in xenografted human T cell acute lymphoblastic leukemia recapitulates gain of malignancy at relapse. *Journal of Experimental Medicine, 208*(4), 653-661.

Daver, N., Venugopal, S., & Ravandi, F. (2021). FLT3 mutated acute myeloid leukemia: 2021 treatment algorithm. *Blood cancer journal, 11*(5), 104.

De Kouchkovsky, I., & Abdul-Hay, M. (2016). Acute myeloid leukemia: a comprehensive review and 2016 update. *Blood cancer journal, 6*(7), e441-e441.

Delahaye, M. C., Salem, K. I., Pelletier, J., Aurrand-Lions, M., & Mancini, S. J. C. (2020). Toward Therapeutic Targeting of Bone Marrow Leukemic Niche Protective Signals in B-Cell Acute Lymphoblastic Leukemia. *Front Oncol, 10*, 606540.

Deng, W., Cho, S., Su, P.-C., Berger, B. W., & Li, R. (2014). Membrane-enabled dimerization of the intrinsically disordered cytoplasmic domain of ADAM10. *Proceedings of the National Academy of Sciences, 111*(45), 15987-15992.

Díaz-Rodríguez, E., Montero, J. C., Esparís-Ogando, A., Yuste, L., & Pandiella, A. (2002). Extracellular signal-regulated kinase phosphorylates tumor necrosis factor α-converting enzyme at threonine 735: a potential role in regulated shedding. *Molecular biology of the cell, 13*(6), 2031.

DiNardo, C. D., Pratz, K. W., Letai, A., Jonas, B. A., Wei, A. H., Thirman, M., et al. (2018). Safety and preliminary efficacy of venetoclax with decitabine or azacitidine in elderly patients with previously untreated acute myeloid leukaemia: a non-randomised, open-label, phase 1b study. *The lancet oncology, 19*(2), 216-228.

Doberstein, K., Pfeilschifter, J., & Gutwein, P. (2011). The transcription factor PAX2 regulates ADAM10 expression in renal cell carcinoma. *Carcinogenesis, 32*(11), 1713-1723.

Doench, J. G. (2018). Am I ready for CRISPR? A user's guide to genetic screens. *Nature Reviews Genetics, 19*(2), 67-80.

Doench, J. G., Fusi, N., Sullender, M., Hegde, M., Vaimberg, E. W., Donovan, K. F., et al. (2016). Optimized sgRNA design to maximize activity and minimize off-target effects of CRISPR-Cas9. *Nat Biotechnol, 34*(2), 184-191.

Döhner, H., Wei, A. H., Appelbaum, F. R., Craddock, C., DiNardo, C. D., Dombret, H., et al. (2022). Diagnosis and management of AML in adults: 2022 recommendations

from an international expert panel on behalf of the ELN. *Blood, The Journal of the American Society of Hematology, 140*(12), 1345-1377.

Dohner, H., Wei, A. H., & Lowenberg, B. (2021). Towards precision medicine for AML. *Nat Rev Clin Oncol, 18*(9), 577-590.

Doudna, J. A., & Charpentier, E. (2014). The new frontier of genome engineering with CRISPR-Cas9. *Science, 346*(6213), 1258096.

Downing, J. R., Wilson, R. K., Zhang, J., Mardis, E. R., Pui, C.-H., Ding, L., et al. (2012). The pediatric cancer genome project. *Nature Genetics, 44*(6), 619-622.

Duffy, M. J., McKiernan, E., O'Donovan, N., & McGowan, P. M. (2009). Role of ADAMs in cancer formation and progression. *Clin Cancer Res, 15*(4), 1140-1144.

Eaves, C. J. (2015). Hematopoietic stem cells: concepts, definitions, and the new reality. *Blood, 125*(17), 2605-2613.

Ebinger, S., Ozdemir, E. Z., Ziegenhain, C., Tiedt, S., Castro Alves, C., Grunert, M., et al. (2016). Characterization of Rare, Dormant, and Therapy-Resistant Cells in Acute Lymphoblastic Leukemia. *Cancer Cell, 30*(6), 849-862.

Ebinger, S., Zeller, C., Carlet, M., Senft, D., Bagnoli, J. W., Liu, W. H., et al. (2020). Plasticity in growth behavior of patients' acute myeloid leukemia stem cells growing in mice. *Haematologica, 105*(12), 2855-2860.

Ebsen, H., Lettau, M., Kabelitz, D., & Janssen, O. (2014). Identification of SH3 domain proteins interacting with the cytoplasmic tail of the a disintegrin and metalloprotease 10 (ADAM10). *PLoS One, 9*(7), e102899.

Edwards, D. R., Handsley, M. M., & Pennington, C. J. (2008). The ADAM metalloproteinases. *Molecular aspects of medicine, 29*(5), 258-289.

Eschenbrenner, E., Jouannet, S., Clay, D., Chaker, J., Boucheix, C., Brou, C., et al. (2020). TspanC8 tetraspanins differentially regulate ADAM10 endocytosis and half-life. *Life Science Alliance, 3*(1), e201900444.

Estey, E. (2016). Acute myeloid leukemia: 2016 Update on risk-stratification and management. *American journal of hematology, 91*(8), 824-846.

Estey, E. H. (2020). Acute myeloid leukemia: 2021 update on risk-stratification and management. *American journal of hematology, 95*(11), 1368-1398.

Farge, T., Saland, E., De Toni, F., Aroua, N., Hosseini, M., Perry, R., et al. (2017). Chemotherapy-resistant human acute myeloid leukemia cells are not enriched for leukemic stem cells but require oxidative metabolism. *Cancer discovery, 7*(7), 716-735.

Feldinger, K., Generali, D., Kramer-Marek, G., Gijsen, M., Ng, T. B., Wong, J. H., et al. (2014). ADAM10 mediates trastuzumab resistance and is correlated with survival in HER2 positive breast cancer. *Oncotarget, 5*(16), 6633-6646.

Fu, L., Liu, N., Han, Y., Xie, C., Li, Q., & Wang, E. (2014). ADAM10 regulates proliferation, invasion, and chemoresistance of bladder cancer cells. *Tumor Biology, 35*, 9263-9268.

Galmarini, C., Mackey, J., & Dumontet, C. (2001). Nucleoside analogues: mechanisms of drug resistance and reversal strategies. *Leukemia, 15*(6), 875-890.

Gavert, N., Sheffer, M., Raveh, S., Spaderna, S., Shtutman, M., Brabletz, T., et al. (2007). Expression of L1-CAM and ADAM10 in human colon cancer cells induces metastasis. *Cancer Research, 67*(16), 7703-7712.

Ghalandary, M., Gao, Y., Amend, D., Kutkaite, G., Vick, B., Spiekermann, K., et al. (2023). WT1 and DNMT3A play essential roles in the growth of certain patient AML cells in mice. *Blood, 141*(8), 955-960.

Gibb, D. R., El Shikh, M., Kang, D.-J., Rowe, W. J., El Sayed, R., Cichy, J., et al. (2010). ADAM10 is essential for Notch2-dependent marginal zone B cell development and CD23 cleavage in vivo. *Journal of Experimental Medicine, 207*(3), 623-635.

Gillet, J.-P., Calcagno, A. M., Varma, S., Marino, M., Green, L. J., Vora, M. I., et al. (2011). Redefining the relevance of established cancer cell lines to the study of mechanisms of clinical anti-cancer drug resistance. *Proceedings of the National Academy of Sciences, 108*(46), 18708-18713.

Guo, S., Qian, W., Cai, J., Zhang, L., Wery, J. P., & Li, Q. X. (2016). Molecular Pathology of Patient Tumors, Patient-Derived Xenografts, and Cancer Cell Lines. *Cancer Res, 76*(16), 4619-4626.

Habringer, S., Lapa, C., Herhaus, P., Schottelius, M., Istvanffy, R., Steiger, K., et al. (2018). Dual targeting of acute leukemia and supporting niche by CXCR4-directed theranostics. *Theranostics, 8*(2), 369.

Harrison, N., Koo, C. Z., & Tomlinson, M. G. (2021). Regulation of ADAM10 by the TspanC8 family of tetraspanins and their therapeutic potential. *International journal of molecular sciences, 22*(13), 6707.

Hartmann, D., de Strooper, B., Serneels, L., Craessaerts, K., Herreman, A., Annaert, W., et al. (2002). The disintegrin/metalloprotease ADAM 10 is essential for Notch signalling but not for alpha-secretase activity in fibroblasts. *Hum Mol Genet, 11*(21), 2615-2624.

Hidalgo, M., Amant, F., Biankin, A. V., Budinska, E., Byrne, A. T., Caldas, C., et al. (2014). Patient-derived xenograft models: an emerging platform for translational cancer research. *Cancer Discov, 4*(9), 998-1013.

Ho, D., Quake, S. R., McCabe, E. R., Chng, W. J., Chow, E. K., Ding, X., et al. (2020). Enabling technologies for personalized and precision medicine. *Trends in biotechnology, 38*(5), 497-518.

Holohan, C., Van Schaeybroeck, S., Longley, D. B., & Johnston, P. G. (2013). Cancer drug resistance: an evolving paradigm. *Nature Reviews Cancer, 13*(10), 714-726.

Hope, K. J., Jin, L., & Dick, J. E. (2003). Human acute myeloid leukemia stem cells. *Archives of medical research, 34*(6), 507-514.

Hortobagyi, G. (1997). Anthracyclines in the treatment of cancer: an overview. *Drugs, 54*, 1-7.

Hu, C. D., & Kerppola, T. K. (2003). Simultaneous visualization of multiple protein interactions in living cells using multicolor fluorescence complementation analysis. *Nat Biotechnol, 21*(5), 539-545.

Hundhausen, C., Schulte, A., Schulz, B., Andrzejewski, M. G., Schwarz, N., von Hundelshausen, P., et al. (2007). Regulated shedding of transmembrane chemokines by the disintegrin and metalloproteinase 10 facilitates detachment of adherent leukocytes. *The Journal of Immunology, 178*(12), 8064-8072.

Hunger, S. P., & Mullighan, C. G. (2015). Redefining ALL classification: toward detecting high-risk ALL and implementing precision medicine. *Blood, The Journal of the American Society of Hematology, 125*(26), 3977-3987.

Jayavelu, A. K., Wolf, S., Buettner, F., Alexe, G., Häupl, B., Comoglio, F., et al. (2022). The proteogenomic subtypes of acute myeloid leukemia. *Cancer Cell, 40*(3), 301-317.e312.

Juarez, J., Dela Pena, A., Baraz, R., Hewson, J., Khoo, M., Cisterne, A., et al. (2007). CXCR4 antagonists mobilize childhood acute lymphoblastic leukemia cells into the peripheral blood and inhibit engraftment. *Leukemia, 21*(6), 1249-1257.

Kamel-Reid, S., Letarte, M., Doedens, M., Greaves, A., Murdoch, B., Grunberger, T., et al. (1991). Bone marrow from children in relapse with pre-B acute lymphoblastic leukemia proliferates and disseminates rapidly in scid mice. *Blood, 78*(11), 2973-2981.

Kamel-Reid, S., Letarte, M., Sirard, C., Doedens, M., Grunberger, T., Fulop, G., et al. (1989). A model of human acute lymphoblastic leukemia in immune-deficient SCID mice. *Science, 246*(4937), 1597-1600.

Kansal, R. (2016). Acute myeloid leukemia in the era of precision medicine: recent advances in diagnostic classification and risk stratification. *Cancer biology & medicine, 13*(1), 41.

Kanyan, X., Wenli, L., Shen, Q., Hanying, S., & Jinzhi, T. (1996). Study of heat shock protein HSP90α, HSP70, HSP27 mRNA expression in human acute leukemia cells. *Journal of Tongji Medical University, 16*, 212-216.

Kennedy, V. E., & Smith, C. C. (2020). FLT3 mutations in acute myeloid leukemia: key concepts and emerging controversies. *Frontiers in oncology, 10*, 612880.

Khoury, J. D., Solary, E., Abla, O., Akkari, Y., Alaggio, R., Apperley, J. F., et al. (2022). The 5th edition of the World Health Organization classification of haematolymphoid tumours: myeloid and histiocytic/dendritic neoplasms. *Leukemia, 36*(7), 1703-1719.

Khwaja, A., Bjorkholm, M., Gale, R. E., Levine, R. L., Jordan, C. T., Ehninger, G., et al. (2016). Acute myeloid leukaemia. *Nature reviews Disease primers, 2*(1), 1-22.

Kikutani, H., & Makino, S. (1992). The murine autoimmune diabetes model: NOD and related strains. *Advances in immunology, 51*, 285-322.

Kim, M., Suh, J., Romano, D., Truong, M. H., Mullin, K., Hooli, B., et al. (2009). Potential late-onset Alzheimer's disease-associated mutations in the ADAM10 gene attenuate α-secretase activity. *Human molecular genetics, 18*(20), 3987-3996.

Kirtonia, A., Pandya, G., Sethi, G., Pandey, A. K., Das, B. C., & Garg, M. (2020). A comprehensive review of genetic alterations and molecular targeted therapies for the implementation of personalized medicine in acute myeloid leukemia. *Journal of molecular medicine, 98*, 1069-1091.

Kohga, K., Takehara, T., Tatsumi, T., Miyagi, T., Ishida, H., Ohkawa, K., et al. (2009). Anticancer chemotherapy inhibits MHC class I–related chain a ectodomain shedding by downregulating ADAM10 expression in hepatocellular carcinoma. *Cancer Research, 69*(20), 8050-8057.

Kono, M., Sugiura, K., Suganuma, M., Hayashi, M., Takama, H., Suzuki, T., et al. (2013). Whole-exome sequencing identifies ADAM10 mutations as a cause of reticulate acropigmentation of Kitamura, a clinical entity distinct from Dowling-Degos disease. *Human molecular genetics, 22*(17), 3524-3533.

Konopleva, M., Konoplev, S., Hu, W., Zaritskey, A., Afanasiev, B., & Andreeff, M. (2002). Stromal cells prevent apoptosis of AML cells by up-regulation of anti-apoptotic proteins. *Leukemia, 16*(9), 1713-1724.

Konopleva, M. Y., & Jordan, C. T. (2011). Leukemia stem cells and microenvironment: biology and therapeutic targeting. *Journal of Clinical Oncology, 29*(5), 591.

Kotur, N., Lazic, J., Ristivojevic, B., Stankovic, B., Gasic, V., Dokmanovic, L., et al. (2020). Pharmacogenomic markers of methotrexate response in the consolidation phase of pediatric acute lymphoblastic leukemia treatment. *Genes, 11*(4), 468.

Lambrecht, B. N., Vanderkerken, M., & Hammad, H. (2018). The emerging role of ADAM metalloproteinases in immunity. *Nat Rev Immunol, 18*(12), 745-758.

Li, N., Jiang, W., Wang, W., Xiong, R., Wu, X., & Geng, Q. (2021). Ferroptosis and its emerging roles in cardiovascular diseases. *Pharmacological Research, 166*, 105466.

Li, W., Xu, H., Xiao, T., Cong, L., Love, M. I., Zhang, F., et al. (2014). MAGeCK enables robust identification of essential genes from genome-scale CRISPR/Cas9 knockout screens. *Genome Biol, 15*(12), 554.

Liu, G., Lin, Q., Jin, S., & Gao, C. (2022). The CRISPR-Cas toolbox and gene editing technologies. *Molecular cell, 82*(2), 333–347.

Liu, P. C., Liu, X., Li, Y., Covington, M., Wynn, R., Huber, R., et al. (2006). Identification of ADAM10 as a major source of HER2 ectodomain sheddase activity in HER2 overexpressing breast cancer cells. *Cancer biology & therapy, 5*(6), 657-664.

Liu, S., Zhang, W., Liu, K., Ji, B., & Wang, G. (2015). Silencing ADAM10 inhibits the in vitro and in vivo growth of hepatocellular carcinoma cancer cells. *Molecular Medicine Reports, 11*(1), 597-602.

Liu, W. H., Mrozek-Gorska, P., Wirth, A. K., Herold, T., Schwarzkopf, L., Pich, D., et al. (2020). Inducible transgene expression in PDX models in vivo identifies KLF4 as a therapeutic target for B-ALL. *Biomark Res, 8*, 46.

Liu, Y., Mi, Y., Mueller, T., Kreibich, S., Williams, E. G., Van Drogen, A., et al. (2019). Multi-omic measurements of heterogeneity in HeLa cells across laboratories. *Nature biotechnology, 37*(3), 314-322.

Londino, J. D., Gulick, D., Isenberg, J. S., & Mallampalli, R. K. (2015). Cleavage of signal regulatory protein α (SIRPα) enhances inflammatory signaling. *Journal of Biological Chemistry, 290*(52), 31113-31125.

Lownik, J. C., Luker, A. J., Damle, S. R., Cooley, L. F., El Sayed, R., Hutloff, A., et al. (2017). ADAM10-mediated ICOS ligand shedding on B cells is necessary for proper T cell ICOS regulation and T follicular helper responses. *The Journal of Immunology, 199*(7), 2305-2315.

Ma, L., Zhang, X., Yu, K., Xu, X., Chen, T., Shi, Y., et al. (2021). Targeting SLC3A2 subunit of system XC− is essential for m6A reader YTHDC2 to be an endogenous ferroptosis inducer in lung adenocarcinoma. *Free Radical Biology and Medicine, 168*, 25-43.

Ma, S., Xu, J., Wang, X., Wu, Q.-Y., Cao, J., Li, Z.-Y., et al. (2015). Effect of ADAM10 inhibitor GI254023X on proliferation and apoptosis of acute T-lymphoblastic leukemia Jurkat cells in vitro and its possible mechanisms. *Zhongguo shi yan xue ye xue za zhi, 23*(4), 950-955.

Ma, X., Liu, Y., Liu, Y., Alexandrov, L. B., Edmonson, M. N., Gawad, C., et al. (2018). Pan-cancer genome and transcriptome analyses of 1,699 paediatric leukaemias and solid tumours. *Nature, 555*(7696), 371-376.

Maetzig, T., Ruschmann, J., Sanchez Milde, L., Lai, C. K., von Krosigk, N., & Humphries, R. K. (2017). Lentiviral Fluorescent Genetic Barcoding for Multiplex Fate Tracking of Leukemic Cells. *Mol Ther Methods Clin Dev, 6*, 54-65.

Maiti, A., DiNardo, C. D., Daver, N. G., Rausch, C. R., Ravandi, F., Kadia, T. M., et al. (2021). Triplet therapy with venetoclax, FLT3 inhibitor and decitabine for FLT3-mutated acute myeloid leukemia. *Blood cancer journal, 11*(2), 25.

Malani, D., Kumar, A., Brück, O., Kontro, M., Yadav, B., Hellesøy, M., et al. (2022). Implementing a functional precision medicine tumor board for acute myeloid leukemia. *Cancer discovery, 12*(2), 388-401.

Malard, F., & Mohty, M. (2020). Acute lymphoblastic leukaemia. *Lancet, 395*(10230), 1146-1162.

Manabe, A., Coustan-Smith, E., Behm, F. G., Raimondi, S. C., & Campana, D. (1992). Bone marrow-derived stromal cells prevent apoptotic cell death in B-lineage acute lymphoblastic leukemia. *Blood, 79*(9), 2370–2377.

Matthews, A. L., Szyroka, J., Collier, R., Noy, P. J., & Tomlinson, M. G. (2017). Scissor sisters: regulation of ADAM10 by the TspanC8 tetraspanins. *Biochemical Society Transactions, 45*(3), 719-730.

McDermott, S. P., Eppert, K., Lechman, E. R., Doedens, M., & Dick, J. E. (2010). Comparison of human cord blood engraftment between immunocompromised mouse strains. *Blood, The Journal of the American Society of Hematology, 116*(2), 193-200.

Menter, T., & Tzankov, A. (2022). Tumor Microenvironment in Acute Myeloid Leukemia: Adjusting Niches. *Front Immunol, 13*, 811144.

Miletti-González, K. E., Murphy, K., Kumaran, M. N., Ravindranath, A. K., Wernyj, R. P., Kaur, S., et al. (2012). Identification of function for CD44 intracytoplasmic domain

(CD44-ICD): modulation of matrix metalloproteinase 9 (MMP-9) transcription via novel promoter response element. *Journal of Biological Chemistry, 287*(23), 18995-19007.

Minond, D. (2020). Novel Approaches and Challenges of Discovery of Exosite Modulators of a Disintegrin and Metalloprotease 10. *Front Mol Biosci, 7*, 75.

Misaghian, N., Ligresti, G., Steelman, L. S., Bertrand, F. E., Bäsecke, J., Libra, M., et al. (2009). Targeting the leukemic stem cell: the Holy Grail of leukemia therapy. *Leukemia, 23*(1), 25-42.

Moore, J. D. (2015). The impact of CRISPR–Cas9 on target identification and validation. *Drug discovery today, 20*(4), 450-457.

Mootha, V. K., Lindgren, C. M., Eriksson, K.-F., Subramanian, A., Sihag, S., Lehar, J., et al. (2003). PGC-1α-responsive genes involved in oxidative phosphorylation are coordinately downregulated in human diabetes. *Nature Genetics, 34*(3), 267-273.

Mudry, R. E., Fortney, J. E., York, T., Hall, B. M., & Gibson, L. F. (2000). Stromal cells regulate survival of B-lineage leukemic cells during chemotherapy. *Blood, The Journal of the American Society of Hematology, 96*(5), 1926-1932.

Mueller, A. C., Piper, M., Goodspeed, A., Bhuvane, S., Williams, J. S., Bhatia, S., et al. (2021). Induction of ADAM10 by Radiation Therapy Drives Fibrosis, Resistance, and Epithelial-to-Mesenchyal Transition in Pancreatic Cancer. *Cancer Res, 81*(12), 3255-3269.

Mullighan, C. G., Phillips, L. A., Su, X., Ma, J., Miller, C. B., Shurtleff, S. A., et al. (2008). Genomic analysis of the clonal origins of relapsed acute lymphoblastic leukemia. *Science, 322*(5906), 1377-1380.

Mullooly, M., McGowan, P. M., Crown, J., & Duffy, M. J. (2016). The ADAMs family of proteases as targets for the treatment of cancer. *Cancer Biol Ther, 17*(8), 870-880.

Murphy, G. (2008). The ADAMs: signalling scissors in the tumour microenvironment. *Nature Reviews Cancer, 8*(12), 932-941.

Nagano, O., & Saya, H. (2004). Mechanism and biological significance of CD44 cleavage. *Cancer science, 95*(12), 930-935.

Nervi, B., Ramirez, P., Rettig, M. P., Uy, G. L., Holt, M. S., Ritchey, J. K., et al. (2009). Chemosensitization of acute myeloid leukemia (AML) following mobilization by the CXCR4 antagonist AMD3100. *Blood, The Journal of the American Society of Hematology, 113*(24), 6206-6214.

Niewiarowski, S., McLane, M. A., Kloczewiak, M., & Stewart, G. J. (1994). Disintegrins and other naturally occurring antagonists of platelet fibrinogen receptors. *Seminars in hematology, 31*(4), 289-300.

Nückel, H., Switala, M., Sellmann, L., Horn, P., Dürig, J., Dührsen, U., et al. (2010). The prognostic significance of soluble NKG2D ligands in B-cell chronic lymphocytic leukemia. *Leukemia, 24*(6), 1152-1159.

Pan, C., Kumar, C., Bohl, S., Klingmueller, U., & Mann, M. (2009). Comparative proteomic phenotyping of cell lines and primary cells to assess preservation of cell type-specific functions. *Molecular & cellular proteomics, 8*(3), 443-450.

Panayiotidis, P., Jones, D., Ganeshaguru, K., Foroni, L., & Hoffbrand, A. (1996). Human bone marrow stromal cells prevent apoptosis and support the survival of chronic lymphocytic leukaemia cells in vitro. *British journal of haematology, 92*(1), 97-103.

Passaro, D., Irigoyen, M., Catherinet, C., Gachet, S., De Jesus, C. D. C., Lasgi, C., et al. (2015). CXCR4 is required for leukemia-initiating cell activity in T cell acute lymphoblastic leukemia. *Cancer Cell, 27*(6), 769-779.

Patel, B., Dey, A., Castleton, A. Z., Schwab, C., Samuel, E., Sivakumaran, J., et al. (2014). Mouse xenograft modeling of human adult acute lymphoblastic leukemia provides mechanistic insights into adult LIC biology. *Blood, The Journal of the American Society of Hematology, 124*(1), 96-105.

Patro, R., Duggal, G., Love, M. I., Irizarry, R. A., & Kingsford, C. (2017). Salmon provides fast and bias-aware quantification of transcript expression. *Nat Methods, 14*(4), 417-419.

Pavlaki, M., & Zucker, S. (2003). Matrix metalloproteinase inhibitors (MMPIs): the beginning of phase I or the termination of phase III clinical trials. *Cancer and metastasis reviews, 22*, 177-203.

Petit, I., Szyper-Kravitz, M., Nagler, A., Lahav, M., Peled, A., Habler, L., et al. (2002). G-CSF induces stem cell mobilization by decreasing bone marrow SDF-1 and up-regulating CXCR4. *Nat Immunol, 3*(7), 687-694.

Phan, T. G., & Croucher, P. I. (2020). The dormant cancer cell life cycle. *Nat Rev Cancer, 20*(7), 398-411.

Pickar-Oliver, A., & Gersbach, C. A. (2019). The next generation of CRISPR–Cas technologies and applications. *Nature reviews Molecular cell biology, 20*(8), 490-507.

Pollyea, D. A., & Jordan, C. T. (2017). Therapeutic targeting of acute myeloid leukemia stem cells. *Blood, The Journal of the American Society of Hematology, 129*(12), 1627-1635.

Pruessmeyer, J., Hess, F. M., Alert, H., Groth, E., Pasqualon, T., Schwarz, N., et al. (2014). Leukocytes require ADAM10 but not ADAM17 for their migration and inflammatory recruitment into the alveolar space. *Blood, The Journal of the American Society of Hematology, 123*(26), 4077-4088.

Pui, C.-H. (2020). Precision medicine in acute lymphoblastic leukemia. *Frontiers of medicine, 14*, 689-700.

Pulte, D., Gondos, A., & Brenner, H. (2009). Improvement in survival in younger patients with acute lymphoblastic leukemia from the 1980s to the early 21st century. *Blood, The Journal of the American Society of Hematology, 113*(7), 1408-1411.

Pulte, D., Jansen, L., Gondos, A., Katalinic, A., Barnes, B., Ressing, M., et al. (2014). Survival of adults with acute lymphoblastic leukemia in Germany and the United States. *PLoS One, 9*(1), e85554.

Rabinovich, B. A., Ye, Y., Etto, T., Chen, J. Q., Levitsky, H. I., Overwijk, W. W., et al. (2008). Visualizing fewer than 10 mouse T cells with an enhanced firefly luciferase in immunocompetent mouse models of cancer. *Proceedings of the National Academy of Sciences, 105*(38), 14342-14346.

Rad, E. R., Foeng, J., McPeak, D., Tyllis, T., Abbott, C., bandara, V., et al. (2022). Abstract 5505: ADAM10-targeting CAR-T cells inhibit colon cancer cell growth in vivo. *Cancer Research, 82*(12_Supplement), 5505-5505.

Ramalingam, R., Kaur, H., Scott, J. X., Sneha, L. M., Arunkumar, G., Srinivasan, A., et al. (2022). Evaluation of cytogenetic and molecular markers with MTX-mediated toxicity in pediatric acute lymphoblastic leukemia patients. *Cancer Chemotherapy and Pharmacology, 89*(3), 393-400.

Reyat, J. S., Chimen, M., Noy, P. J., Szyroka, J., Rainger, G., & Tomlinson, M. G. (2017). ADAM10-interacting tetraspanins Tspan5 and Tspan17 regulate VE-cadherin expression and promote T lymphocyte transmigration. *The Journal of Immunology, 199*(2), 666-676.

Richter-Pechańska, P., Kunz, J. B., Bornhauser, B., von Knebel Doeberitz, C., Rausch, T., Erarslan-Uysal, B., et al. (2018). PDX models recapitulate the genetic and epigenetic landscape of pediatric T-cell leukemia. *EMBO molecular medicine, 10*(12), e9443.

Roberts, K. G., & Mullighan, C. G. (2015). Genomics in acute lymphoblastic leukaemia: insights and treatment implications. *Nature reviews Clinical oncology, 12*(6), 344-357.

Rovelet-Lecrux, A., Hannequin, D., Raux, G., Meur, N. L., Laquerrière, A., Vital, A., et al. (2006). APP locus duplication causes autosomal dominant early-onset Alzheimer disease with cerebral amyloid angiopathy. *Nature Genetics, 38*(1), 24-26.

Schepers, K., Campbell, T. B., & Passegué, E. (2015). Normal and leukemic stem cell niches: insights and therapeutic opportunities. *Cell stem cell, 16*(3), 254-267.

Schindelin, J., Arganda-Carreras, I., Frise, E., Kaynig, V., Longair, M., Pietzsch, T., et al. (2012). Fiji: an open-source platform for biological-image analysis. *Nature methods, 9*(7), 676-682.

Schulz, B., Pruessmeyer, J., Maretzky, T., Ludwig, A., Blobel, C. P., Saftig, P., et al. (2008). ADAM10 regulates endothelial permeability and T-Cell transmigration by proteolysis of vascular endothelial cadherin. *Circulation research, 102*(10), 1192-1201.

Seifert, A., Düsterhöft, S., Wozniak, J., Koo, C. Z., Tomlinson, M. G., Nuti, E., et al. (2021). The metalloproteinase ADAM10 requires its activity to sustain surface expression. *Cell Mol Life Sci, 78*(2), 715-732.

Shalem, O., Sanjana, N. E., Hartenian, E., Shi, X., Scott, D. A., Mikkelson, T., et al. (2014). Genome-scale CRISPR-Cas9 knockout screening in human cells. *Science, 343*(6166), 84-87.

Shannon, P., Markiel, A., Ozier, O., Baliga, N. S., Wang, J. T., Ramage, D., et al. (2003). Cytoscape: a software environment for integrated models of biomolecular interaction networks. *Genome research, 13*(11), 2498-2504.

Shultz, L. D., Lyons, B. L., Burzenski, L. M., Gott, B., Chen, X., Chaleff, S., et al. (2005). Human lymphoid and myeloid cell development in NOD/LtSz-scid IL2R gamma null mice engrafted with mobilized human hemopoietic stem cells. *J Immunol, 174*(10), 6477-6489.

Shultz, L. D., Schweitzer, P. A., Christianson, S. W., Gott, B., Schweitzer, I. B., Tennent, B., et al. (1995). Multiple defects in innate and adaptive immunologic function in NOD/LtSz-scid mice. *Journal of Immunology (Baltimore, Md.: 1950), 154*(1), 180-191.

Siegel, R. L., Miller, K. D., Wagle, N. S., & Jemal, A. (2023). Cancer statistics, 2023. *Ca Cancer J Clin, 73*(1), 17-48.

Smith, T. M., Jr., Tharakan, A., & Martin, R. K. (2020). Targeting ADAM10 in Cancer and Autoimmunity. *Front Immunol, 11*, 499.

Solit, D. B., & Rosen, N. (2006). Hsp90: a novel target for cancer therapy. *Current topics in medicinal chemistry, 6*(11), 1205-1214.

Song, K.-H., Oh, S. J., Kim, S., Cho, H., Lee, H.-J., Song, J. S., et al. (2020). HSP90A inhibition promotes anti-tumor immunity by reversing multi-modal resistance and stem-like property of immune-refractory tumors. *Nature communications, 11*(1), 562.

Soond, S. M., Everson, B., Riches, D. W., & Murphy, G. (2005). ERK-mediated phosphorylation of Thr735 in TNFα-converting enzyme and its potential role in TACE protein trafficking. *Journal of cell science, 118*(11), 2371-2380.

Sreedhar, A. S., Söti, C., & Csermely, P. (2004). Inhibition of Hsp90: a new strategy for inhibiting protein kinases. *Biochimica et Biophysica Acta (BBA)-Proteins and Proteomics, 1697*(1-2), 233-242.

Stone, R. M., Mandrekar, S. J., Sanford, B. L., Laumann, K., Geyer, S., Bloomfield, C. D., et al. (2017). Midostaurin plus chemotherapy for acute myeloid leukemia with a FLT3 mutation. *New England Journal of Medicine, 377*(5), 454-464.

Subramanian, A., Tamayo, P., Mootha, V. K., Mukherjee, S., Ebert, B. L., Gillette, M. A., et al. (2005). Gene set enrichment analysis: a knowledge-based approach for interpreting genome-wide expression profiles. *Proceedings of the National Academy of Sciences, 102*(43), 15545-15550.

Suh, J., Choi, S. H., Romano, D. M., Gannon, M. A., Lesinski, A. N., Kim, D. Y., et al. (2013). ADAM10 missense mutations potentiate β-amyloid accumulation by impairing prodomain chaperone function. *Neuron, 80*(2), 385-401.

Sulis, M. L., Saftig, P., & Ferrando, A. A. (2011). Redundancy and specificity of the metalloprotease system mediating oncogenic NOTCH1 activation in T-ALL. *Leukemia, 25*(10), 1564-1569. doi:10.1038/leu.2011.130

Tanaka, M., Nanba, D., Mori, S., Shiba, F., Ishiguro, H., Yoshino, K., et al. (2004). ADAM binding protein Eve-1 is required for ectodomain shedding of epidermal growth factor receptor ligands. *Journal of Biological Chemistry, 279*(40), 41950-41959.

Tavor, S., Petit, I., Porozov, S., Avigdor, A., Dar, A., Leider-Trejo, L., et al. (2004). CXCR4 regulates migration and development of human acute myelogenous leukemia stem cells in transplanted NOD/SCID mice. *Cancer Res, 64*(8), 2817-2824.

Terwilliger, T., & Abdul-Hay, M. (2017). Acute lymphoblastic leukemia: a comprehensive review and 2017 update. *Blood cancer journal, 7*(6), e577-e577.

Terziyska, N., Castro Alves, C., Groiss, V., Schneider, K., Farkasova, K., Ogris, M., et al. (2012). In vivo imaging enables high resolution preclinical trials on patients' leukemia cells growing in mice. *PLoS One, 7*(12), e52798.

Tian, L., Wu, X., Chi, C., Han, M., Xu, T., & Zhuang, Y. (2008). ADAM10 is essential for proteolytic activation of Notch during thymocyte development. *International immunology, 20*(9), 1181-1187.

Townsend, E. C., Murakami, M. A., Christodoulou, A., Christie, A. L., Koster, J., DeSouza, T. A., et al. (2016). The Public Repository of Xenografts Enables Discovery and Randomized Phase II-like Trials in Mice. *Cancer Cell, 29*(4), 574-586.

Trepel, J., Mollapour, M., Giaccone, G., & Neckers, L. (2010). Targeting the dynamic HSP90 complex in cancer. *Nature Reviews Cancer, 10*(8), 537-549.

Truong, D. J., Kuhner, K., Kuhn, R., Werfel, S., Engelhardt, S., Wurst, W., et al. (2015). Development of an intein-mediated split-Cas9 system for gene therapy. *Nucleic acids research, 43*(13), 6450-6458.

Tsimberidou, A. M., Fountzilas, E., Nikanjam, M., & Kurzrock, R. (2020). Review of precision cancer medicine: Evolution of the treatment paradigm. *Cancer treatment reviews, 86*, 102019.

Uhlén, M., Fagerberg, L., Hallström, B. M., Lindskog, C., Oksvold, P., Mardinoglu, A., et al. (2015). Tissue-based map of the human proteome. *Science, 347*(6220), 1260419.

Uy, G. L., Rettig, M. P., Motabi, I. H., McFarland, K., Trinkaus, K. M., Hladnik, L. M., et al. (2012). A phase 1/2 study of chemosensitization with the CXCR4 antagonist plerixafor in relapsed or refractory acute myeloid leukemia. *Blood, 119*(17), 3917-3924.

van Galen, P., Hovestadt, V., Wadsworth II, M. H., Hughes, T. K., Griffin, G. K., Battaglia, S., et al. (2019). Single-cell RNA-seq reveals AML hierarchies relevant to disease progression and immunity. *Cell, 176*(6), 1265-1281. e1224.

Venkatesh, H. S., Tam, L. T., Woo, P. J., Lennon, J., Nagaraja, S., Gillespie, S. M., et al. (2017). Targeting neuronal activity-regulated neuroligin-3 dependency in high-grade glioma. *Nature, 549*(7673), 533-537.

Vick, B., Rothenberg, M., Sandhöfer, N., Carlet, M., Finkenzeller, C., Krupka, C., et al. (2015). An advanced preclinical mouse model for acute myeloid leukemia using patients' cells of various genetic subgroups and in vivo bioluminescence imaging. *PLoS One, 10*(3), e0120925.

Waanders, E., Gu, Z., Dobson, S. M., Antić, Ž., Crawford, J. C., Ma, X., et al. (2020). Mutational landscape and patterns of clonal evolution in relapsed pediatric acute lymphoblastic leukemia. *Blood cancer discovery, 1*(1), 96-111.

Wang, H., La Russa, M., & Qi, L. S. (2016). CRISPR/Cas9 in genome editing and beyond. *Annual review of biochemistry, 85*, 227-264.

Wang, Q.-s., Wang, Y., Lv, H.-y., Han, Q.-w., Fan, H., Guo, B., et al. (2015). Treatment of CD33-directed chimeric antigen receptor-modified T cells in one patient with relapsed and refractory acute myeloid leukemia. *Molecular therapy, 23*(1), 184-191.

Wang, T., Wei, J. J., Sabatini, D. M., & Lander, E. S. (2014). Genetic screens in human cells using the CRISPR-Cas9 system. *Science, 343*(6166), 80-84.

Wang, W., Green, M., Choi, J. E., Gijón, M., Kennedy, P. D., Johnson, J. K., et al. (2019). CD8+ T cells regulate tumour ferroptosis during cancer immunotherapy. *Nature, 569*(7755), 270-274.

Wei, A., Strickland, S. A., Hou, J.-Z., Fiedler, W., Lin, T. L., Walter, R. B., et al. (2018). Venetoclax with low-dose cytarabine induces rapid, deep, and durable responses in previously untreated older adults with AML ineligible for intensive chemotherapy. *Blood, 132*, 284.

Whitesell, L., & Dai, C. (2005). HSP90: a rising star on the horizon of anticancer targets. *Future Oncology, 1*(4), 529–540.

Wilson, C. A., Doms, R. W., & Lee, V. M. (1999). Intracellular APP processing and Aβ production in Alzheimer disease. *Journal of neuropathology and experimental neurology, 58*(8), 787-794.

Woiterski, J., Ebinger, M., Witte, K. E., Goecke, B., Heininger, V., Philippek, M., et al. (2013). Engraftment of low numbers of pediatric acute lymphoid and myeloid leukemias into NOD/SCID/IL2Rcγnull mice reflects individual leukemogenecity and highly correlates with clinical outcome. *International journal of cancer, 133*(7), 1547-1556.

Wong, N. C., Bhadri, V. A., Maksimovic, J., Parkinson-Bates, M., Ng, J., Craig, J. M., et al. (2014). Stability of gene expression and epigenetic profiles highlights the utility of patient-derived paediatric acute lymphoblastic leukaemia xenografts for investigating molecular mechanisms of drug resistance. *BMC genomics, 15*(1), 1-13.

Workman, P. (2004). Altered states: selectively drugging the Hsp90 cancer chaperone. *Trends in molecular medicine, 10*(2), 47-51.

Wu, E., Croucher, P. I., & McKie, N. (1997). Expression of members of the novel membrane linked metalloproteinase family ADAM in cells derived from a range of haematological malignancies. *Biochem Biophys Res Commun, 235*(2), 437-442.

Xu, P., Liu, J., Sakaki-Yumoto, M., & Derynck, R. (2012). TACE activation by MAPK-mediated regulation of cell surface dimerization and TIMP3 association. *Science signaling, 5*(222), ra34.

Yang, C.-l., Jiang, F.-q., Xu, F., & Jiang, G.-x. (2012). ADAM10 overexpression confers resistance to doxorubicin-induced apoptosis in hepatocellular carcinoma. *Tumor Biology, 33*, 1535-1541.

Yap, T. A., Daver, N., Mahendra, M., Zhang, J., Kamiya-Matsuoka, C., Meric-Bernstam, F., et al. (2023). Complex I inhibitor of oxidative phosphorylation in advanced solid tumors and acute myeloid leukemia: phase I trials. *Nature Medicine, 29*(1), 115-126.

Yin, H., Xue, W., & Anderson, D. G. (2019). CRISPR-Cas: a tool for cancer research and therapeutics. *Nat Rev Clin Oncol, 16*(5), 281-295.

Yoda, M., Kimura, T., Tohmonda, T., Uchikawa, S., Koba, T., Takito, J., et al. (2011). Dual functions of cell-autonomous and non-cell-autonomous ADAM10 activity in granulopoiesis. *Blood, 118*(26), 6939-6942.

You, B., Shan, Y., Shi, S., Li, X., & You, Y. (2015). Effects of ADAM 10 upregulation on progression, migration, and prognosis of nasopharyngeal carcinoma. *Cancer science, 106*(11), 1506-1514.

Yufu, Y., Nishimura, J., & Nawata, H. (1992). High constitutive expression of heat shock protein 90α in human acute leukemia cells. *Leukemia research, 16*(6-7), 597-605.

Zeng, Z., Samudio, I. J., Munsell, M., An, J., Huang, Z., Estey, E., et al. (2006). Inhibition of CXCR4 with the novel RCP168 peptide overcomes stroma-mediated chemoresistance in chronic and acute leukemias. *Molecular cancer therapeutics, 5*(12), 3113-3121.

Zhang, W., Liu, S., Liu, K., Ji, B., Wang, Y., & Liu, Y. (2014). Knockout of ADAM10 enhances sorafenib antitumor activity of hepatocellular carcinoma in vitro and in vivo. *Oncology reports, 32*(5), 1913-1922.

Zhang, Y.-w., Thompson, R., Zhang, H., & Xu, H. (2011). APP processing in Alzheimer's disease. *Molecular brain, 4*, 1-13.

Zhao, J. C., Agarwal, S., Ahmad, H., Amin, K., Bewersdorf, J. P., & Zeidan, A. M. (2022). A review of FLT3 inhibitors in acute myeloid leukemia. *Blood reviews, 52*, 100905.

Zheng, R., Li, M., Wang, S., & Liu, Y. (2020). Advances of target therapy on NOTCH1 signaling pathway in T-cell acute lymphoblastic leukemia. *Exp Hematol Oncol, 9*(1), 31.

Zhou, H.-S., Carter, B. Z., & Andreeff, M. (2016). Bone marrow niche-mediated survival of leukemia stem cells in acute myeloid leukemia: Yin and Yang. *Cancer biology & medicine, 13*(2), 248.

Zhu, L. B., Zhao, S. T., Xu, T. Z., & Wang, H. (2014). Tumor necrosis factor-α-induced a disintegrin and metalloprotease 10 increases apoptosis resistance in prostate cancer cells. *Oncology Letters, 7*(3), 897-901.

Zong, H., Sen, S., Zhang, G., Mu, C., Albayati, Z. F., Gorenstein, D. G., et al. (2016). In vivo targeting of leukemia stem cells by directing parthenolide-loaded nanoparticles to the bone marrow niche. *Leukemia, 30*(7), 1582-1586.

List of Publications

Combined proteomics and CRISPR–Cas9 screens in PDX identify ADAM10 as essential for leukemia in vivo.

Bahrami E[*], **Schmid JP**[*], Jurinovic V, Becker M, Wirth AK, Ludwig R, Kreissig S, Duque Angel TV, Amend D, Hunt K, Öllinger R, Rad R, Frenz JM, Solovey M, Ziemann F, Mann M, Vick B, Wichmann C, Herold T, Jayavelu AK[#], Jeremias I[#].

Mol Cancer. 2023 Jul 8;22(1):107. doi: 10.1186/s12943-023-01803-0. PMID: 37422628; PMCID: PMC10329331.

In vivo inducible reverse genetics in patients' tumors to identify individual therapeutic targets.

Carlet M, Völse K, Vergalli J, Becker M, Herold T, Arner A, Senft D, Jurinovic V, Liu WH, Gao Y, Dill V, Fehse B, Baldus CD, Bastian L, Lenk L, Schewe DM, Bagnoli JW, Vick B, **Schmid JP**, Wilhelm A, Marschalek R, Jost PJ, Miething C, Riecken K, Schmidt-Supprian M, Binder V, Jeremias I.

Nat Commun. 2021 Sep 27;12(1):5655. doi: 10.1038/s41467-021-25963-z. PMID: 34580292; PMCID: PMC8476619.